Von Herzen, R.P., Robinson, P.T., et al., 1991
Proceedings of the Ocean Drilling Program, Scientific Results, Vol. 118

21. TECTONIC EVOLUTION OF THE ATLANTIS II FRACTURE ZONE[1]

Henry J.B. Dick,[2] Hans Schouten,[2] Peter S. Meyer,[2] David G. Gallo,[2] Hugh Bergh,[3] Robert Tyce,[4] Phillipe Patriat,[5] Kevin T.M. Johnson,[2] Jon Snow,[2] and Andrew Fisher[6]

ABSTRACT

SeaBeam echo sounding, seismic reflection, magnetics, and gravity profiles were run along closely spaced tracks (5 km) parallel to the Atlantis II Fracture Zone on the Southwest Indian Ridge, giving 80% bathymetric coverage of a 30- × 170-nmi strip centered over the fracture zone. The southern and northern rift valleys of the ridge were clearly defined and offset north-south by 199 km. The rift valleys are typical of those found elsewhere on the Southwest Indian Ridge, with relief of more than 2200 m and widths from 22 to 38 km. The ridge-transform intersections are marked by deep nodal basins lying on the transform side of the neovolcanic zone that defines the present-day spreading axis. The walls of the transform generally are steep (25°–40°), although locally, they can be more subdued. The deepest point in the transform is 6480 m in the southern nodal basin, and the shallowest is an uplifted wave-cut terrace that exposes plutonic rocks from the deepest layer of the ocean crust at 700 m. The transform valley is bisected by a 1.5-km-high median tectonic ridge that extends from the northern ridge-transform intersection to the midpoint of the active transform. The seismic survey showed that the floor of the transform contains up to 0.5 km of sediment. Piston-coring at two locations on the transform floor recovered more than 1 m of sand and gravel, which appears to be turbidites shed from the walls of the fracture zone. Extensive dredging showed that more than two-thirds of the crust exposed in the transform valley and its walls were plutonic rocks, principally gabbros and residual mantle peridotites. In contrast, based on dredging and seafloor morphology, only relatively undisrupted pillow basalt flows have been exposed on crust of the same age spreading away from the transform.

Magnetic anomalies are well defined out to 11 m.y. over the flanking transverse ridges and transform valley, even where layer 2 appears to be absent. The total opening rate is 1.6 cm/yr, but the arrangement of the anomalies indicates that the spreading for each ridge is asymmetric, with the ridge flanks facing the transform spreading at a rate of 1.0 cm/yr. Such an asymmetric spreading pattern requires that both the northern and southern ridges migrate away from each other at 0.2 cm/yr, thus lengthening the transform at 0.4 cm/yr for the last 11 m.y.

To the north, the fracture zone valley is oriented differently from the present-day transform, indicating a paleospreading direction change at 17 m.y. from N10°E to due north-south. This change placed the transform into extension for the 11-m.y. period required for simple orthogonal ridge-transform geometry to be reestablished and produced a large transtensional basin within the transform valley. This basin was split by continued transform slip after 11 m.y., with the larger half moving to the north with the African Plate.

INTRODUCTION

Here, we report the preliminary results of a geological and geophysical survey of the Atlantis II Fracture Zone on the Southwest Indian Ridge by the *Robert D. Conrad* that was conducted for Leg 118 drilling. The survey included concurrent SeaBeam echo-sounding; single-channel, seismic-reflection; magnetic; and gravity profiles along closely spaced tracks (5 km) parallel to the strike of the Atlantis II Fracture Zone (Fig. 1). The survey gave bathymetric coverage of 80% for about 14,500 km² of seafloor across a 30- × 170-nmi strip centered over the fracture zone valley. Thirty-five locations were dredged along the walls of the active transform, its inactive extensions, and the adjacent rift valleys (1) to obtain a representative sampling of the different morphologic features encountered during the survey and (2) to attempt a systematic sampling of the transform valley walls, both with depth and along a lithospheric flow line.

The Atlantis II Fracture Zone is a major left-lateral, large-offset transform that cuts the Southwest Indian Ridge at 31°S, 57°E. It was named by Engel and Fisher (1975), who mapped and dredged the transform, recovering peridotite, gabbro, and basalt in five dredge hauls from the transform walls. Although their data represented only a preliminary survey, the fracture zone was clearly physiographically representative of the numerous large offset high-relief fracture zones on the Southwest Indian Ridge.

The principal goals of Leg 118 were (1) to utilize a major Southwest Indian Ridge fracture zone as a tectonic window into the uppermost mantle or lower ocean crust and (2) to test the feasibility of drilling plutonic rocks formed at ocean ridges. A Southwest Indian Ridge fracture zone was selected as these have consistently produced the highest proportion of altered mantle peridotite during dredging, and thus most often have exposed the deepest levels of the lower crust and mantle of any fracture zones found on accessible ocean ridges. Weather is a critical consideration for ship operations in the southern oceans, and the Atlantis II Fracture Zone was selected as it is the northernmost of the major high-relief Southwest Indian Ridge fracture zones and therefore has the best weather window.

SUMMARY OF PRINCIPAL RESULTS

Physiographically, we found that the Atlantis II Fracture Zone is similar to other large offset fracture zones in the Atlantic and Indian oceans, with approximately 6 km of

[1] Von Herzen, R. P., Robinson, P. T., et al., 1991. *Proc. ODP, Sci. Results*, 118: College Station, TX (Ocean Drilling Program).

[2] Woods Hole Oceanographic Institution, Woods Hole, MA 02543, U.S.A.
[3] Bernard Price Institute, Johannesburg, South Africa.
[4] School of Oceanography, University of Rhode Island, Narragansett, RI, U.S.A.
[5] Laboratoire de Géophysique Marine, Institute de Physique du Globe de Paris, Paris, France.
[6] Ocean Drilling Program, Texas A&M University, College Station, TX 77843, U.S.A.

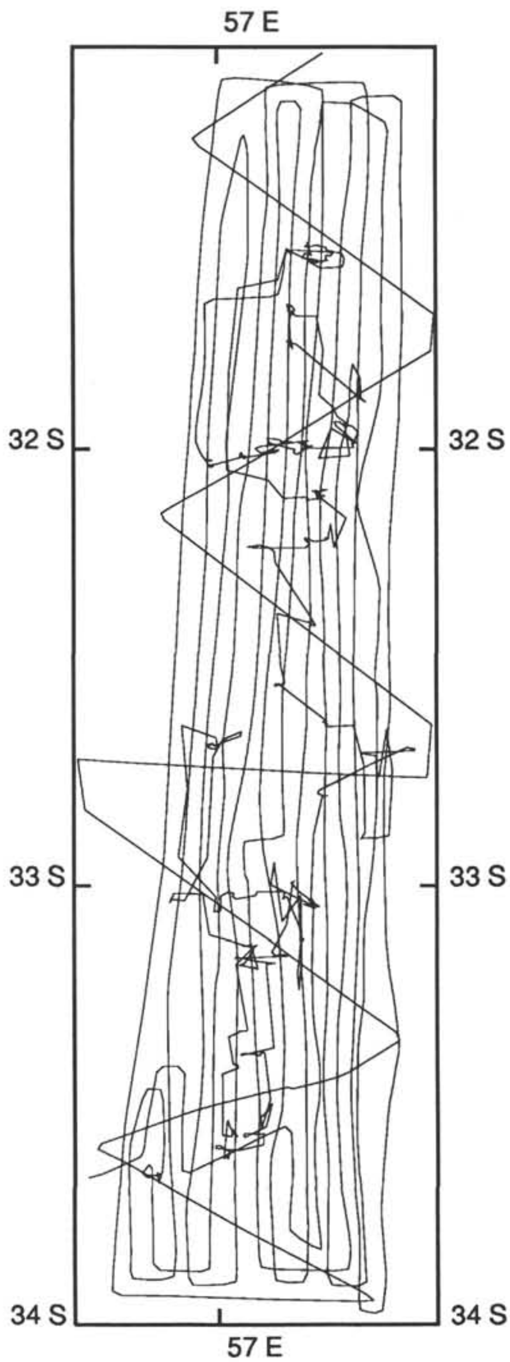

Figure 1. Track plot for Leg 9 Cruise 27 of the *Robert Conrad*.

vertical relief and a deep transform valley. Each of its intersections with the Southwest Indian Ridge is marked by a deep nodal basin that lies on the transform side of the neovolcanic zone. These basins extend for some distance from the transform floor up the rift valleys, lying on the transform side between the neovolcanic zone and the base of the rift valley wall. The walls of the fracture zone valley that pass through the transform tectonic zone differ greatly from the walls formed of crust which spread from the neovolcanic zones away from the transform directly into its aseismic extensions. The transform walls are largely made up of great transverse ridges, are often very steep, and expose abundant plutonic rocks and a smaller proportion of basalt. Conversely, where the crust spreads in the opposite direction away from the transform tectonic zone to form the nontransform wall along the inactive trace of the fracture zone, only pillow basalt is exposed, and the crust is only slightly uplifted above the valley floor. This disparity in physiography and geology between crust spreading away from and into the transform tectonic zone at ridge-transform intersections suggests a major transform edge effect at slow-spreading ridges, which causes the deeper levels of the ocean crust to become unroofed and exposed preferentially along the walls of the transform valley.

Gravity data show that the high transverse ridge flanking the transform to the east is largely isostatically unsupported and is composed of high-density material, ruling out an origin as an isostatically compensated serpentinite diapir (J. Snow et al., unpubl. data, 1990). Along the transverse ridge, the highest density crust occurs at the most elevated points along the ridge, and the lowest density crust at topographic lows.

The magnetic data allow us to identify and to map confidently anomalies out to about anomaly 5 (roughly 11 Ma), and to identify somewhat more tentatively out to anomaly 10 (roughly 30 Ma). The anomalies are well developed over large regions, where only plutonic rocks were dredged, providing convincing evidence that the plutonic crust can act as a source layer for marine magnetic anomalies, which is consistent with the drilling results at Hole 735B (Pariso et al., this volume) and with shore-based studies of gabbros and metagabbros (e.g., Kent et al., 1978). In addition, the spreading rates determined from the anomalies on either side of the transform show that both northern and southern ridge axes have been spreading asymmetrically at a rate of 1 cm/yr in the direction of the transform and 0.6 cm/yr away from the transform for at least the last 11 m.y. Because the total spreading rate on the Southwest Indian Ridge has been relatively constant at 1.6 cm/yr for the last 34 m.y. (Fisher and Sclater, 1983), rigid plate geometry required the active transform to grow at approximately 0.4 cm/yr over the last 11 m.y., increasing the total offset by about 44 km.

In plan view, the physiography of the fracture zone is dominated by a major change in spreading direction at about 17 Ma. This is indicated by a 10° shift in the orientation of the northern fracture zone trace from N10°E to approximately north-south and a complementary shift in the ridge-parallel topographic grain of the rift mountain topography. The change in spreading direction placed the transform tectonic zone into oblique extension (transtension), which lasted until 17 Ma, when a simple orthogonal ridge-transform geometry was recreated by propagation of the northern and southern ridge axes across the old transform valley. This prolonged period of transtension across the transform created an unusually broad fracture zone valley. The absence of coherent magnetic anomalies within the postulated zone of extension and the chaotic mixture of shattered altered basalt, diabase, gabbro, and peridotite in dredge hauls from the median tectonic ridge that projects from the floor of the valley suggest that the transtensional spreading was amagmatic and must have drastically thinned and tectonized the crust within the transform. After 17 Ma, this broad basin was split by continued spreading, with two-thirds moving to the north with the African Plate, and a smaller proportion to the south with the Antarctic Plate, creating a remarkable asymmetry to the transform physiography.

The large median tectonic ridge, which bisects the transform valley, is thought to have formed by serpentine diapirism that accompanied faulting and alteration of the shallow mantle beneath crust drastically thinned by the period of extension along the transform. This ridge also was split after 17 m.y., when extension stopped, with a small proportion moving to the south with the Antarctic Plate, and a larger proportion to the north with the African Plate.

As it turned out, the site survey revealed an atypical abundance of gabbroic rocks exposed along the walls of the Atlantis II Fracture Zone, in contrast to what has been dredged from other Southwest Indian Ridge transforms that rarely includes gabbro. The volume of gabbros dredged at the Atlantis II Fracture Zone is large and nearly equal to the volume of peridotite recovered. We do not think that this represents a sampling anomaly, as the difficulty in dredging these features was greater than we have encountered at numerous other fracture zones on the Southwest Indian Ridge, where we have predominantly dredged peridotite (Dick, 1989; Fisher et al., 1986; Whitehead et al., 1984; Dick et al., 1984; Sclater et al., 1978). Similar difficulties have been encountered in dredging regions, such as the Kane Fracture Zone on the Mid-Atlantic Ridge where abundant gabbros have been observed by submersible (Karson and Dick, 1983, 1984). At this time, we do not have an explanation for the unusual abundance of gabbro at the Atlantis II Fracture Zone, compared to similar transforms along the Southwest Indian Ridge.

TECTONIC SETTING OF THE ATLANTIS II FRACTURE ZONE

The Southwest Indian Ridge, where the Atlantis II Fracture Zone is situated, has existed from the initial breakup of Gondwanaland in the Mesozoic (e.g., Norton and Sclater, 1979). Shortly before 80 Ma, the ridge axis, which previously existed north of Madagascar, jumped south, changed direction, and started the separation of Madagascar and India (Fisher and Sclater, 1983). This connected the newly formed Central Indian Ridge to the preexisting Southwest Indian and Southeast Indian ridges to form the Indian Ocean Triple Junction in its present ridge-ridge-ridge configuration. Since 80 Ma, the Indian Ocean Triple Junction has migrated steadily to the northeast. This required extension of the Southwest Indian Ridge, creating a series of new ridge segments and fracture zones (including the Atlantis II Fracture Zone) and produced a triangular wedge of rough topography (Fig. 2) that penetrated into smoother crust formed at the faster spreading Southeast and Central Indian ridges (Fisher and Sclater, 1983; Tapscott et al., 1980; Sclater et al., 1981). As these Southwest Indian Ridge fracture zones nucleated at or near the Triple Junction during ridge extension within existing ocean crust, they have the important characteristic of being entirely oceanic, without inherited features or geologic complications from early continental breakup.

The spreading rate along the Southwest Indian Ridge has varied with time, with changes from 3.3 to 1.2 cm/yr (half-rate) at anomaly 28 (roughly 63 Ma) and from 1.2 to 0.8 cm/yr at anomaly 13 (about 34 Ma) (Fisher and Sclater, 1983). The Atlantis II Fracture Zone formed during ridge extension at about 58 Ma (Fig. 2). All the area covered by this survey, however, is younger than anomaly 13, and therefore, the seafloor surveyed was generated at 0.8 cm/yr at the very-slow end of the spreading rate spectrum (Fig. 3). Consistent with this, all the features characteristic of slow-spreading ridges, including rough topography, deep rift valleys, and abundant tectonic exposures of plutonic and mantle rocks, are greatly accentuated.

Dick (1989) recently described the geology of this and the similar American-Antarctic Ridge in some detail, and pointed out that in the transforms, two-thirds of the rocks dredged are altered residual mantle peridotites, while most of the remainder are pillow basalts. This extraordinary exposure of mantle peridotites on the seafloor suggests that the crust must be unusually thin near Southwest Indian Ridge transforms. In addition, the small amount of gabbro recovered relative to basalt and peridotite, compared to dredge programs of similar size at north Atlantic transforms, suggests that a gabbroic layer 3 may be commonly absent or attenuated near Southwest Indian Ridge transforms. This is thought to reflect extreme segmented volcanism (e.g., Whitehead et al., 1984) caused by an unusually low rate of magma supply and crustal formation.

A low rate of magma supply for the very slow-spreading Southwest Indian Ridge also is indicated by thermal modeling and seismic measurements of crustal thickness at the very slow-spreading Arctic Ridge (Reid and Jackson, 1981). Reid and Jackson's work suggested that at half rates of less than 1 cm/yr, crustal formation is inhibited by conductive heat loss from the mantle, producing lower degrees of melting in the underlying mantle. They suggested that this might explain the anomalously thin 4-km-thick crust at the Arctic Ridge (Reid and Jackson, 1981).

We should point out that while the Southwest Indian Ridge lies at the extreme end of the spreading spectrum, this class of ridge, in terms of length, is the most common variety of major ocean ridge (Solomon, 1989) (Fig. 3). Thus, the Southwest Indian Ridge, rather than being anomalous, represents one of the two principal end-members for crustal formation at ocean ridges.

Ridge basalts and peridotites from this section of the ridge have been extensively studied (Dick et al., 1984; le Roex et al., 1988; Hamelin and Allegre, 1985; Snow et al., 1987; Johnson et al., 1990). Isotopically and in terms of trace elements, the basalts dredged in the vicinity of the Atlantis II Fracture Zone are near end-member depleted MORBs (Hamelin and Allegre, 1985; Snow et al., 1987; le Roex et al., 1988). The major element characteristics of the basalts indicate that they are the products of some of the lowest degrees of mantle melting anywhere along the Southwest Indian Ridge, with basalts having characteristically high normative plagioclase relative to pyroxene, and high sodium and titanium at a given ratio of Mg/(Mg + Fe) or constant MgO content (Dick et al., 1984; Schouten et al., 1987; Klein and Langmuir, 1987). These chemical characteristics are typical of ridge basalts that erupted far from hot spots.

Abyssal peridotites dredged along the Southwest Indian Ridge have a large systematic change in composition along the ridge (Dick et al., 1984; Dick and Bullen, 1984; Dick, 1989; Johnson et al., 1990). Although significant local variations exist, peridotites dredged from the ridge away from the Bouvet and Marion Island hot spots are less depleted, with more aluminous and sodic minerals and less modal olivine and more diopside. These variations require a factor of two variation in the degree of melting, with the highest degrees near the hot spots (Dick et al., 1984; Dick, 1989; Johnson and Dick, 1990; see also Michael and Bonatti, 1985). Assuming a model starting bulk composition of a light rare earth element-depleted lherzolite (1.5 to 2.5 times chondritic) requires that the Atlantis II peridotites be the residues of roughly 12% melting, compared with 22% melting for Bouvet Fracture Zone peridotites (Johnson et al., 1990).

Following the rationale of Mckenzie (1984) and Klein and Langmuir (1987), the low degree of melting indicated for basalts and peridotites in the vicinity of the Atlantis II Fracture Zone implies a relatively thin crust, assuming that the major element mantle source beneath the ridge is of roughly constant composition. Such a uniform mantle composition is indicated by the linear trend of Southwest Indian Ridge peridotites in the modal olivine-diopside-enstatite ter-

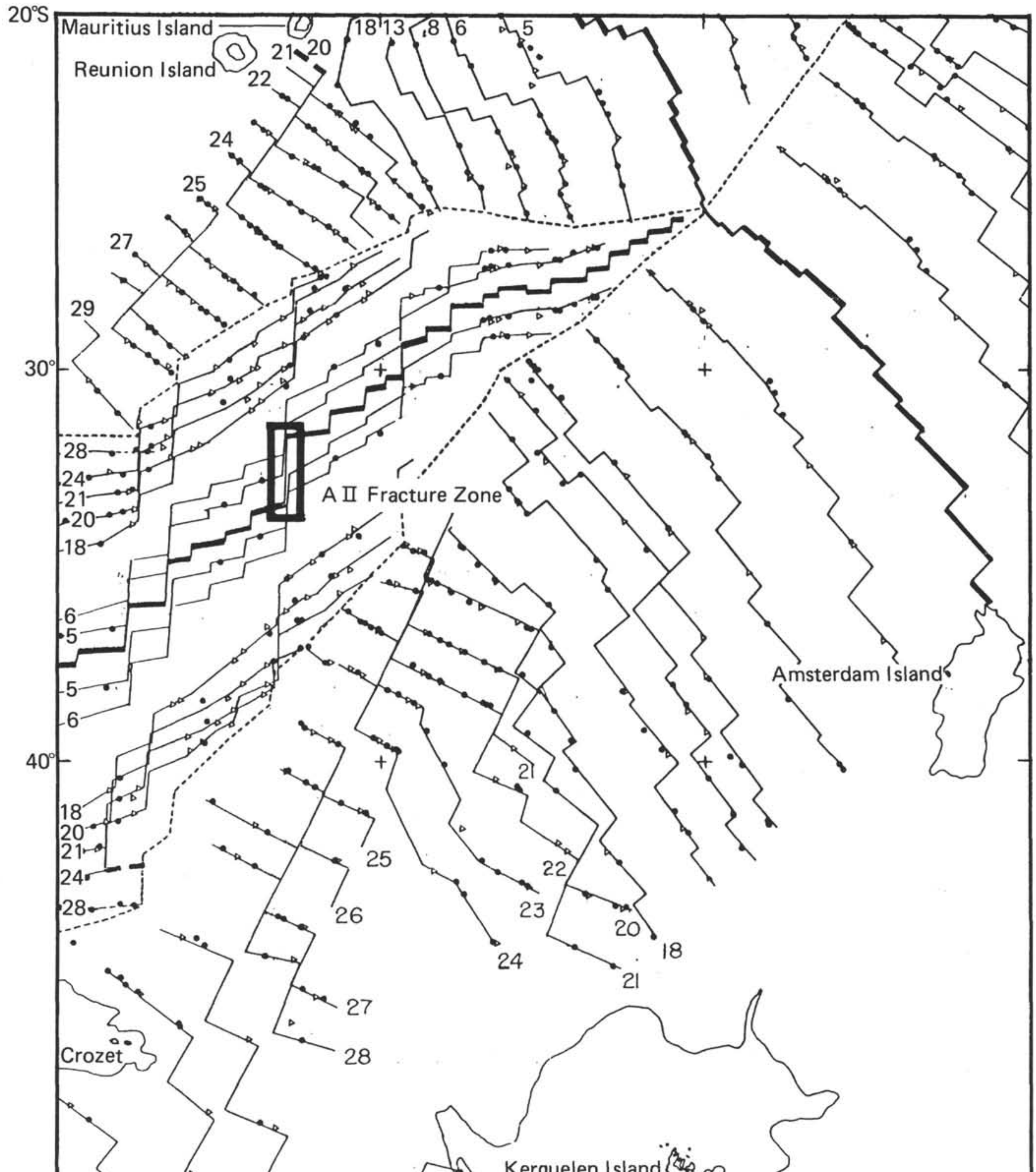

Figure 2. Tectonic map of the Southwest Indian Ridge (from Patriat, 1986).

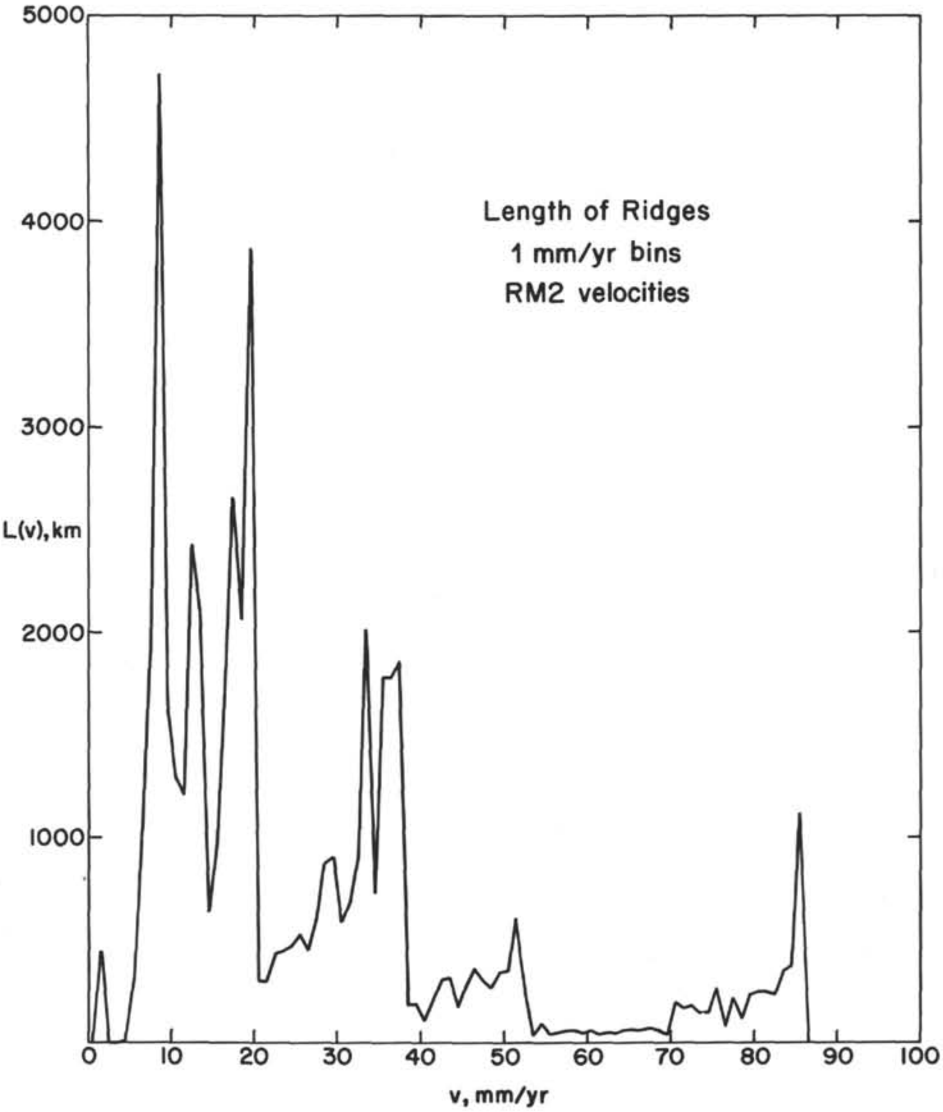

Figure 3. Total length of mid-ocean ridges plotted vs. one-half spreading rate in 1 mm/yr bins (from Solomon, 1989).

nary. Such a trend may be explained only if the mantle major element source region is nearly uniform.

On the basis of seismic crustal thickness measurements at the western end of the Arctic Ridge, where the spreading rate is approximately the same as that of the Southwest Indian Ridge, we infer that the crust drilled and surveyed in the vicinity of the Atlantis II Fracture Zone is thin compared with that at other ocean ridges. Moreover, the petrologic data also suggest that the crustal section should be thinnest along the Southwest Indian Ridge, in the vicinity of the Atlantis II Fracture Zone. A crustal thickness of 4 km might be a reasonable guess for the region.

PHYSIOGRAPHY OF THE ATLANTIS II FRACTURE ZONE

SeaBeam Survey

The survey was conducted on a 5-km spacing on north-south lines parallel to the strike of the transform, with nine zigzag crossings down the fracture zone to provide tie lines (Fig. 1). One of these lines was run orthogonal to the transform across its midpoint and extended well out into the rift mountains of the Southwest Indian Ridge to either side to provide a long gravity line and to establish the relative depth of the transform floor and transverse ridges to the adjacent seafloor. Navigation was done primarily by dead reckoning between transit satellites, aided daily by the 2 to 3 hr of available Global Positioning System satellite navigation. Gaps in transit satellite coverage averaged about 1 hr, although periods up to 3 hr occurred when no good satellite positions were available.

The final navigation of the ship's track was determined by reconciling the long north-south lines with the preliminary survey lines that crossed the fracture zone (Appendix, back-pocket). Higher resolution maps (presented as figures in the text) were made by reconciling the details of overlapping SeaBeam bathymetric swaths and by making final track shifts visually. These local maps were then contoured by hand between SeaBeam swaths to produce final bathymetry for the subarea.

The resolution of the SeaBeam system varies with the relative roughness of the topography being surveyed (e.g.,

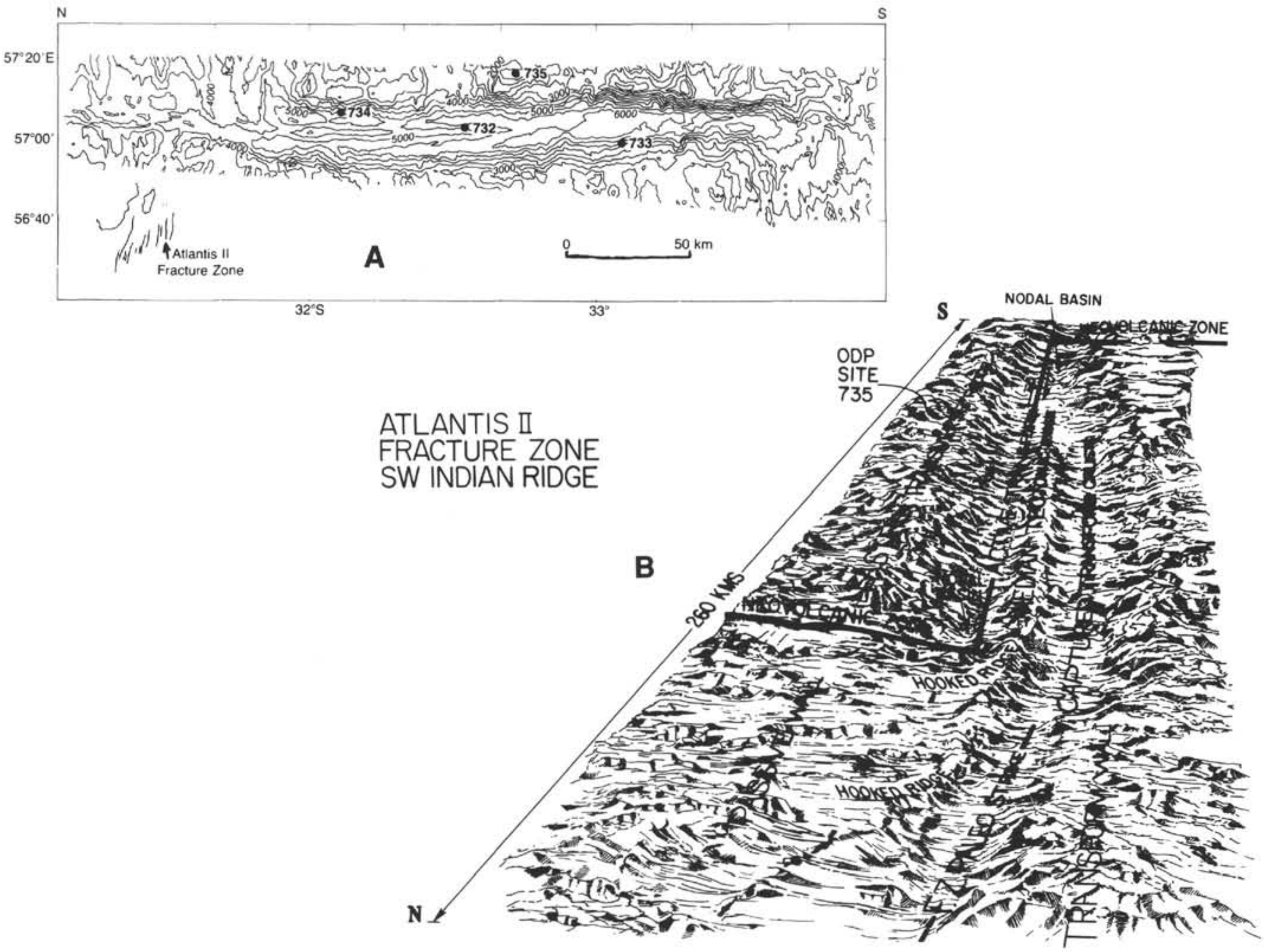

Figure 4. **A.** Bathymetric map of the Atlantis II Fracture Zone; 500 m contour interval. Hand-contoured from ungridded Seabeam swaths by the senior author. Locations of drill sites shown for reference. **B.** Physiographic map of the Atlantis II Fracture Zone with the spreading axes and transform plate boundary shown by solid line. Paleostrike of the fracture zone shown by dashed line. Note the sharp contrast in physiography of crust spreading in the direction of the transform to that of crust spreading in the opposite direction.

Pockalny et al., 1988). Where the seafloor is comparatively flat, the vertical resolution is 1 to 5 m and the horizontal resolution is approximately the same. For rough topography, the resolution of the system is substantially degraded, and the vertical and horizontal resolution decrease to about 10 m. Thus, in areas of rough topography, features having a relief of less than 10 m or less than 100 m wide may not be detected.

Rift Valleys

The Southwest Indian Ridge is marked by deep rift valleys at both its northern and southern intersections with the Atlantis II Fracture Zone (Figs. 4A and 4B). These rift valleys are similar to those described at other slow-spreading ridges and may have well-developed axial symmetry, except near ridge-transform intersections. The rift valley walls (where they intersect the transform valley walls) are much higher and steeper than the facing walls that are spreading away from the transform. The northern and southern rift valley walls near the transform rise 2.4 and 2.8 km, respectively, above the rift valley floor and are abruptly terminated by the transform valley. In contrast, the rift valley walls, which intersect the nontransform walls of the fracture zone, are only 1200 m high and can be traced across the fracture zone valley.

Southern Rift Valley

The southern rift valley of the Southwest Indian Ridge is broad and V-shaped in plan view, measuring approximately 35 km across from the crests of the rift valley walls, with 2.5 km total relief. The rift valley walls are irregular in cross section and consist of a series of successively elevated parallel ridges. Presumably, these represent a series of normal faults that have uplifted the crust into the adjoining rift mountains. The ridgelike structures may be horst and graben structures, or may represent a series of rifted volcanic ridges. There is a narrow, well-defined inner-rift valley, which consists of an axial ridge having a flanking deep on either side. These deeps define the extent of the inner-rift valley floor, which is 6.7 km wide. The northern of the two flanking deeps runs down into the fracture zone valley, where it intersects the nodal deep to form a deep L-shaped basin at the ridge-transform intersection. In contrast, the southern flanking deep is poorly defined where the neovolcanic zone crosses the fracture zone valley.

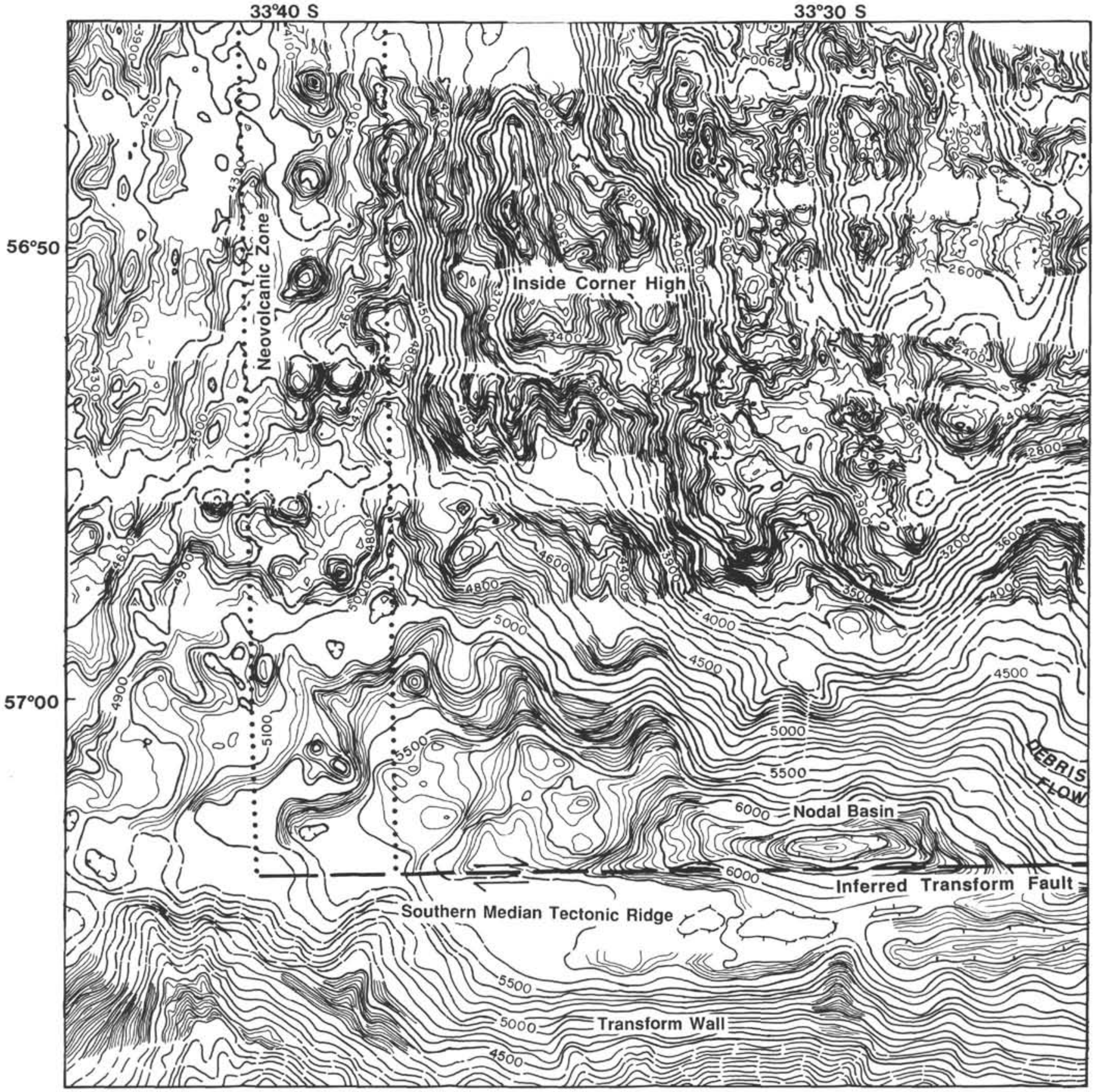

Figure 5. High-resolution bathymetric map of the southern ridge-transform intersection of the Atlantis II Fracture Zone. SeaBeam tracks shifted by eye to eliminate conflicts in the data and hand-contoured. Contour interval = 25 m. Only 100 m contours (heavy lines) shown where contour density is high. Solid lines show actual data, and hatched lines show inferred contours. Limits of the inferred neovolcanic zone shown by dotted lines; the inferred present-day transform slip zone is indicated by the dashed line. The present-day inside corner high appears to have only recently developed as it is much less pronounced than the rift mountains immediately to the north. Similarly, note that the nodal deep is relatively shallow just north of the present-day neovolcanic zone. A large debris flow (and matching land-slip scar) can be seen on the northern edge of the transform valley in the figure covering the zone of inferred transform slip.

The present-day axis of accretion in the southern rift valley has been inferred from a well-developed 32-km-long linear chain of 12 regularly spaced, intact, small seamounts that lie along a 500-m-high east-west axial ridge (Fig. 5). These are typically 1 to 2 km wide at their base and rise 75 to 250 m above the crest of the ridge. Similar physiographic features define neovolcanic zones at many rift valleys and have been mapped by submersible and deep-towed camera as small volcanic cones at slow-spreading ridges, such as the FAMOUS region at 36°N on the Mid-Atlantic Ridge (Ballard and van Andel, 1977; Karson et al., 1987). Similar seamounts have also been mapped that extend across the fracture zone valley floor at the Kane (Karson and Dick, 1983) and Oceanographer (OTTER, 1984) ridge-transform intersections. Thus, the east-west ridge and seamount chain probably represent constructional volcanism above an axial fissure system analogous to the localized eruptions found along the Hawaiian Kileau Rift and the Icelandic fissure systems (e.g., Ryan, 1987; Wolfe, 1988; Gronvold, 1988). Because prolonged rifting during amagmatic periods might disrupt this morphology, it is reasonable to assume that this zone, which is also the locus of the central magnetic high, represents the axis of recent volcanism.

The axial ridge that defines the southern neovolcanic zone slopes downward at 3° from a water depth of 3700 m over about 35 km to its inferred terminus at 5500 m on the fracture zone valley floor. No clear evidence of local volcanic segmentation can be seen along this zone. As the floor of the fracture zone is reached, the neovolcanic zone becomes indistinct and the topography gentler. Projecting the neovolcanic zone across the valley, where small volcanic cones appear, indicates that it extends in a straight line and lies along a bench at about 5450 m at the top of the southern wall of the nodal basin. There is no evidence that this zone extends past the nodal basin, which is flanked to the east by a perched sediment pond.

Northern Rift Valley

The northern rift valley is morphologically distinct from the southern one. It is narrower (23.4 km measured between the peaks of the rift mountains), has greater relief (2.8 km), and is distinctly L-shaped in plan view. The rift-valley walls are steeper and more regular than those of the southern rift valley and consist of a series of uplifted benches, rather than ridges, that are presumed, on the basis of submersible observations and camera tows over similar features at other slow-spreading ridges, to represent a series of blocks of crust originally formed within the inner-rift valley, uplifted on normal faults (e.g., Atwater and Mudie, 1968; Macdonald, 1977; Macdonald and Atwater, 1978). There is a well-developed, inner-rift valley about 4.3 km wide consisting of a poorly developed axial ridge with two flanking deeps. The northern of these deeps is well defined and is 350 m deeper than the axial ridge. Its northern wall is straight and runs across the fracture zone valley floor, then curves abruptly to the south to meet the northern flank of the median tectonic ridge. This northern rift wall is steep and high (600 m) where it crosses the fracture zone valley, giving the ridge-transform intersection its L-shape. The southern flanking deep is locally indistinct, particularly along the easternmost 11 km in the rift valley, and is unusually broad and much shallower than the northern flanking deep. It slopes down to the transform, where it dies out on a broad, curved bench that forms part of the northern wall of the nodal basin.

The neovolcanic zone in the northern rift valley is less distinct than along the southern axis. A small axial ridge having a string of small volcanic cones lies along the inferred magnetic axis and extends to a bench at 4925 m, where it merges with the series of curved benches defining the northern wall of the nodal basin (Fig. 6).

Ridge-Transform Intersections

The ridge-transform intersections are complex regions having a number of distinct physiographic elements. These include (1) the extensions of the active neovolcanic zones from the rift valleys across the fracture zone floor described above; (2) the nodal basins that lie on the transform side of the neovolcanic zone in the fracture zone valley and comprise the deepest points in the entire transform; (3) the inside corner highs at the junctions of the transform and rift valley walls; (4) the extensions of the rift valley walls across the fracture zone valley on the nontransform side of the neovolcanic zone; and (5) the old transform wall abutting the neovolcanic zone and facing the rift valley, where old ocean crust has been welded to new crust.

Nodal Basins

Nodal basins are a key tectonic element of the ridge-transform intersections. The northern basin is the deepest point in the northern one-third of the survey area, while the southern basin, nearly 6500 m deep, is the deepest point that was found during the entire survey. In both cases, the neovolcanic zone crosses the fracture zone on the nontransform side of the nodal basin, and there is no indication that the neovolcanic zone is splitting either basin.

The northern nodal basin is L-shaped, curves around the transform corner, and connects to the southern, flanking deep of the rift valley axial high. This basin is bounded to the north by a series of steep slopes and benches that extend down from the northern rift mountains, cross the fracture zone valley, and curve into the western wall of the transform valley. The neovolcanic zone extends down the rift valley and onto the middle of the three benches, while two large, joined volcanic cones lie on the bench immediately above the floor of the nodal basin. The deepest point in the basin is just south of the intersection of the two valleys and lies north of the crest of the large inside corner high on the eastern transform wall. To the west, the basin is bounded by the steep wall of the northern median tectonic ridge, where it joins the southern end of a large hooked ridge extending down from the northern rift mountains of the rift valley. This geometry is remarkable similar to that at the eastern nodal basins of the Kane and Vema fracture zones (e.g.: Karson and Dick, 1983, 1984; Pockalny et al., 1988; Macdonald et al., 1986; Auzende et al., 1990).

The southern nodal basin is morphologically very different and consists of a linear deep whose lowest point lies along the transform axis 10.7 km from the neovolcanic zone. This basin is relatively shallow adjacent to the neovolcanic zone, where the northern nodal basin is deepest, and slopes relatively gently downward to the north, across two 1-km-long flat benches. To the east, it is bounded by a large, flat, perched sediment pond on the floor of the fracture zone. While the transform valley wall adjacent to the deepest point of the southern nodal basin is high, as it is to the north, the transform valley wall at the present-day ridge-transform corner has a much gentler slope and the inside-corner high is 1 km lower than the crest of the rift mountains on strike with the bottom of the nodal deep. Thus, the poor development of the nodal basin immediately adjacent to the neovolcanic zone and the intersection of the rift and transform valley walls are accompanied by a depressed transform-corner high. The striking difference in the northern and southern basins suggests that the nodal basin is not a steady-state feature of the ridge-transform intersection, but one whose development and position vary with time.

Transform Volcano

On the southern side of the northern nodal basin is a half ring structure of volcanic cones that have merged to form a half circle about 1 km in diameter. This structure extends up the side of the transform wall (Fig. 6). The largest of these volcanic cones has a well-developed, local, collapse caldera structure on its summit. Relatively fresh glassy pillow basalts were dredged from this feature. However, gabbro was recovered by dredging the transform wall adjacent to the volcanic structures, and it is evident that the volcanic edifice on plutonic rocks that have been exposed by earlier faulting and formation of the transform wall. This intact volcanic struc-

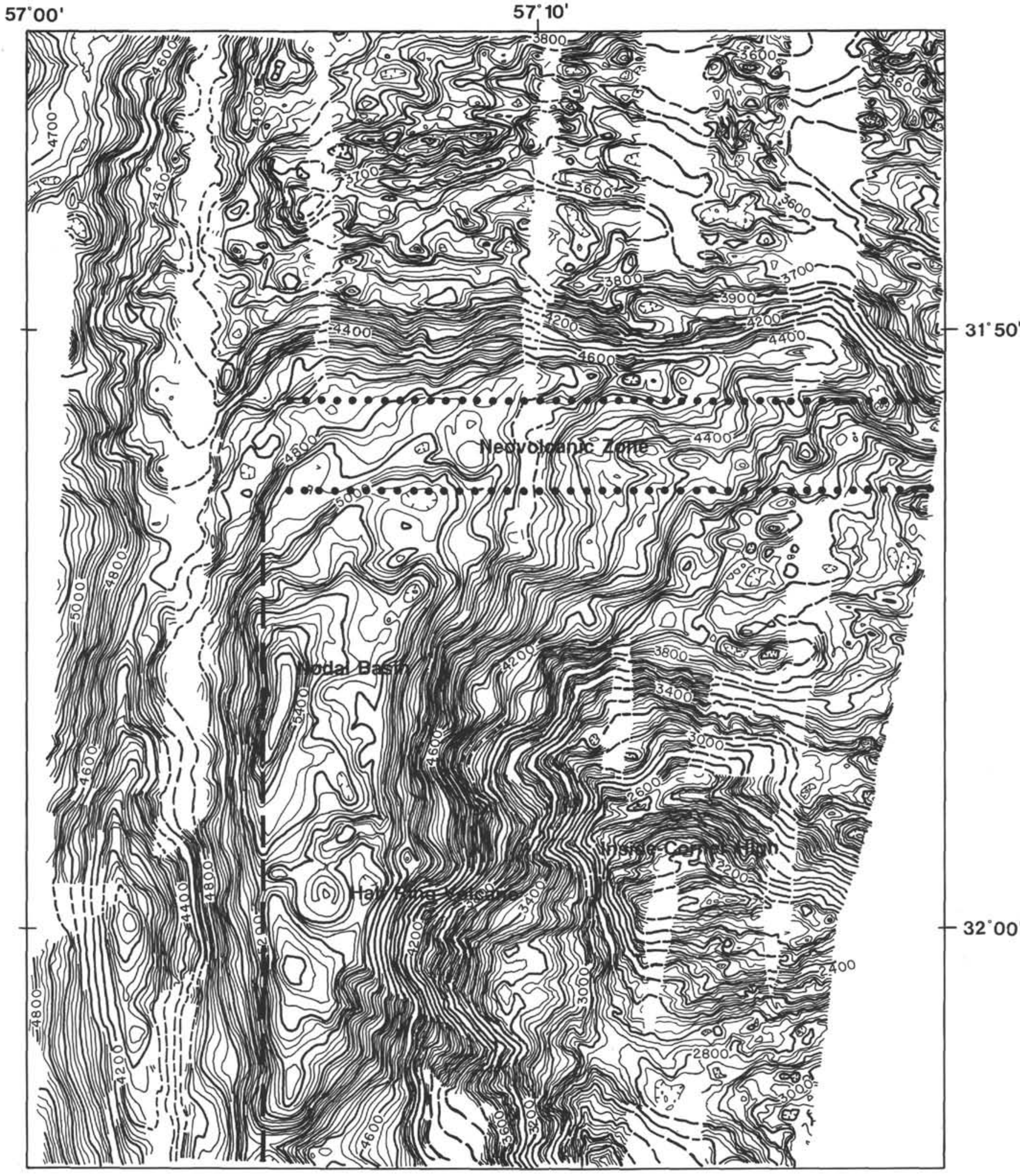

Figure 6. High-resolution bathymetric map of the northern ridge-transform intersection of the Atlantis II Fracture Zone. SeaBeam tracks shifted to eliminate conflicts in the data by eye and contoured by hand. Contour interval = 25 m, except where contour densities are high (100 m). Solid lines show actual data, and hatched lines show inferred contours. Dotted lines show approximate location of the present-day neovolcanic zone. Heavy dashed lines show the inferred position of the active transform fault. Note the prominent volcanic edifice consisting of a half-ring structure of small seamounts on the floor of the transform at 31°59.5′S. Such a structure should be expected because of volcanic venting along a ring dike above a magma chamber and implies an entirely different stress regime than exists within the neovolcanic zone at the spreading axis.

ture, sitting in the middle of the transform tectonic zone on plutonic rocks, is unlikely to pre-date formation of the nodal basin and transform wall and, therefore, most likely represents a true transform volcano.

Outside Corners

The outside corners of the ridge-transform intersections are defined by the intersection of the rift valley walls with the inactive fracture zone valleys. At these locations, the rift mountains of the Southwest Indian Ridge slope gently downward, across the floor of the fracture zone valley. At the northern ridge-transform intersection, the wall of the inner rift valley extends across the fracture zone valley, is about 700 m high, and has a steep slope. It is striking that crust of the same age as the crest of this wall, spreading into the transform valley, has been down-dropped about 500 m into the nodal basin. At the southern ridge-transform intersection, the rift valley wall on the nontransform side of the neovolcanic zone also extends across the fracture zone valley floor, but has a much gentler slope, although the overall relief is greater–approximately 1000 m. Crust of the same age as the crest of this wall in the transform valley is nearly 1000 m deeper.

Inside Corner Highs

Inside corner highs, shoaling to approximately 1900 m, are present at both the northern and southern ridge-transform intersections. At these locations, the crust has undergone 1700 to 1800 m of excess uplift relative to crust of the same age on the opposing rift valley wall. The steep slopes bounding these inside corner highs are probably the product of the normal faulting that accompanied block uplift, similar to those at other slow-slipping transforms (e.g., Severinghaus and Macdonald, 1988). Locally, lineaments oblique to the regional structural fabric of these two walls may represent oblique faults similar to those reported at the Kane (Karson and Dick, 1983) and Oceanographer fracture zones (OTTER, 1984).

Topographic Asymmetry at the Ridge-Transform Intersections

A striking feature of the ridge-transform intersections is that crust spreading away from the transform has been uplifted to form rift mountains, while that spreading into the transform is greatly depressed. Crust of the same age as the 5500-m-deep floor of the northern nodal basin, which is spreading in the opposite direction, has been uplifted to 3800 m to form rift mountains. Crust of the same age as that in the 6500-m-deep southern nodal basin is only 4800 m deep. This contrast in elevation is reversed when the inside corner highs are examined. Whereas the northern, inside corner high shoals to less than 2000 m, crust of the same age that is spreading in the opposite direction is 3400 m deep. At the southern ridge-transform intersection, crust on the transverse ridge of the same age as the nodal basin sits at less than 2000 m, while that of the same age, spreading in the opposite direction, is 3600 m deep. This pronounced asymmetry of topography for the inside and outside (nontransform) corners at the intersection of the rift and transform valleys is a characteristic feature of slow-spreading ridge-transforms (e.g., Searle and Laughton, 1977; Karson and Dick, 1983; Fox and Gallo, 1984; Parmentier and Forsyth, 1985; Collette, 1986; Severinghaus and Macdonald, 1988).

Transform Tectonic Zone

The Atlantis II transform valley is 199 km long and about 37 km wide, measured from the crests of the flanking transverse ridges. Unlike many large offset transforms in the North Atlantic (e.g., the Kane–Pockalny et al., 1988), the Atlantis II transform valley walls are uniformly steep and high and range from 2 to 5 km, with an average relief of 4 km. The valley has a forklike morphology that divides into a double valley in its northern half, where it is bisected by a high, 110-km-long, median tectonic ridge. The eastern branch of this valley, where we postulate that the presently active transform fault is located, terminates at the northern ridge-transform intersection, where it abuts the spreading center and the northern rift mountains. By contrast, the western valley curves gently northward from its junction with the eastern valley into the inactive trace of the fracture zone, defining a distinctive crescent-shaped basin. In the southern half of the fracture zone, only a very subdued median tectonic ridge appears, and the transform valley floor is relatively wide and flat. The large, relatively straight, southern transform valley abuts the southern spreading center and the relatively low rift mountains to the south, where they extend across the fracture zone valley.

Transverse Ridges

Both transform walls are capped by remarkable transverse ridges. The crests of these ridges are greatly elevated, not only with respect to the transform valley, but with respect to the nontransform crust outside the transform tectonic zone. As our survey did not extend much beyond the fracture zone, it was difficult to estimate this excess elevation above normal seafloor of the same age, but we think that it exceeds 1 km. Locally, this excess elevation can be extreme. We conducted a long profile across the transform out onto crust well away from the fracture zone across the largest high, where Hole 735B was drilled, which allowed us to determine the elevation of the transverse ridges above normal seafloor in this region. The seafloor is about 2 km deeper west of the crest of the western transverse ridge, while it is 4 km deeper to the east of the eastern transverse ridge. The excess elevation of the transverse ridges, with respect to normal seafloor far from the fracture zone, indicates that the seafloor was upturned and locally block-faulted upward adjacent to the fracture zone.

A series of alternating highs and lows appears along the crests of these ridges that provides as much as 2.5 km of additional relief along them (e.g., Fig. 7). This suggests that the major highs along the crest of the transverse ridges are large local horsts. One of the curious features of these tectonic blocks sitting on top the transverse ridges is that they are very irregularly shaped. Often, they are bounded by steep planar slopes that have orientations at variance with the trend of the ridge axes, or the trend of the transform. A good example of this is the triangular block situated astride the eastern transverse ridge at 30°20′S. This suggests to us that a major component of the excess local uplift of these blocks was not directly related to simple extensional or strike slip tectonics of the ridge-transform intersection, but was a subsequent response to other dynamic forces. Morphologically, the seafloor on the side of the transverse ridge facing away from the transform adjacent to these highs can be steep, suggesting the existence of major sets of high-angle normal faults that face away from the fracture zone.

Preliminary analysis of the long gravity lines along these ridges is being published elsewhere, but this indicates that the saddle points along the transverse ridge are underlain by crust having a normal density, while the highs are underlain by crust having anomalously high densities, which in some cases, indicates near-zero crustal thickness (J. Snow et al., unpubl. data, 1990). Morphologically, the terrain in the saddles frequently contains ridge parallel lineations and closely resembles volcanic terrain. A good example of this can be seen just south of the triangular tectonic block mentioned above. In contrast, the crests of some of the tectonic blocks are anomalously smooth compared to seafloor volcanic terrain, and

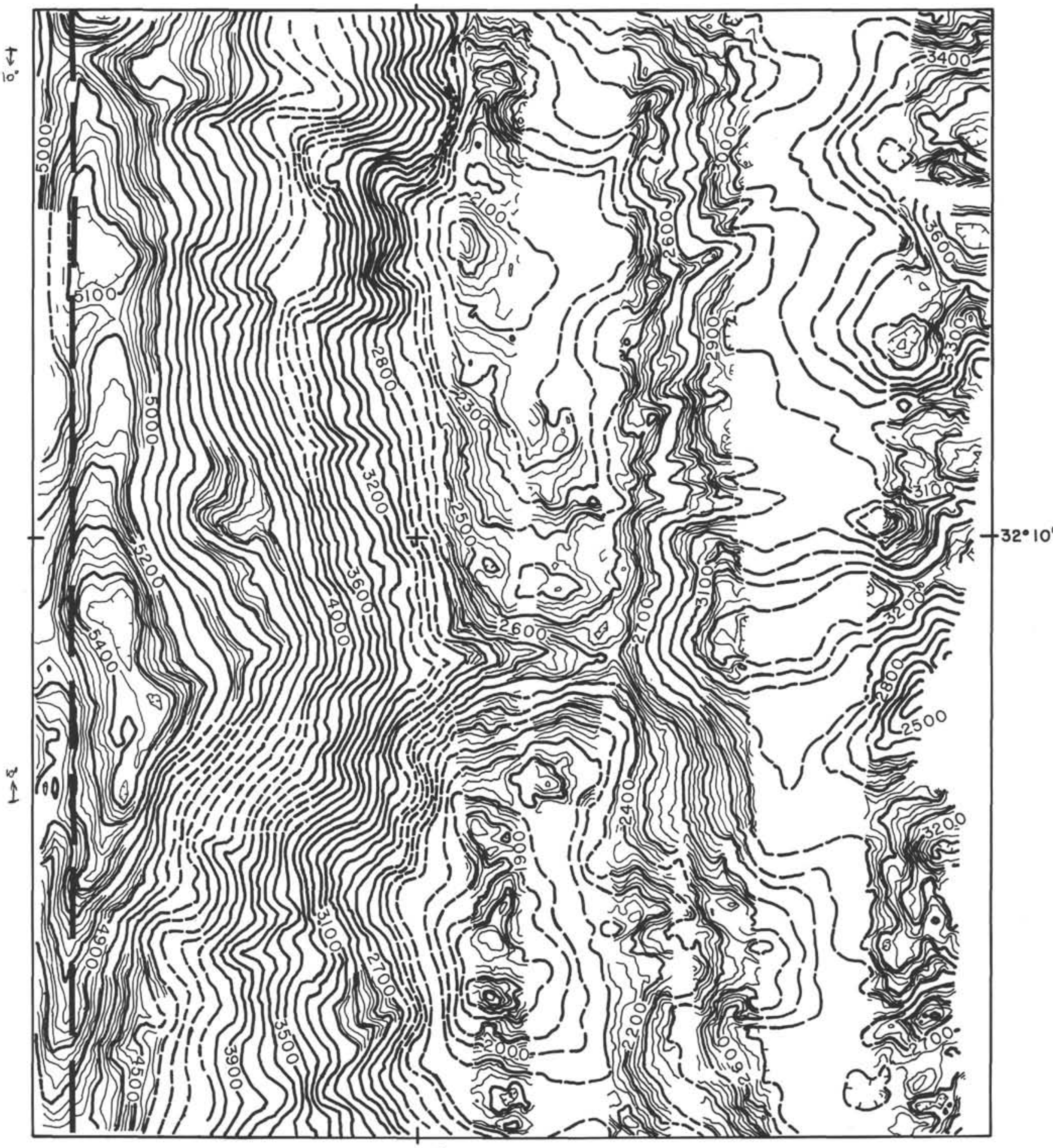

Figure 7. Hand-contoured bathymetric map of the eastern transverse ridge, showing local tectonic blocks situated along the crest of the ridge. SeaBeam tracks hand shifted by eye to eliminate conflicts in the data. Solid lines indicate actual data, while hatched lines show inferred contours. Contour intervals include 100 m (heavy lines) and 25 m (light lines) where contour density permits. Heavy dashed line shows the present day inferred transform fault axis.

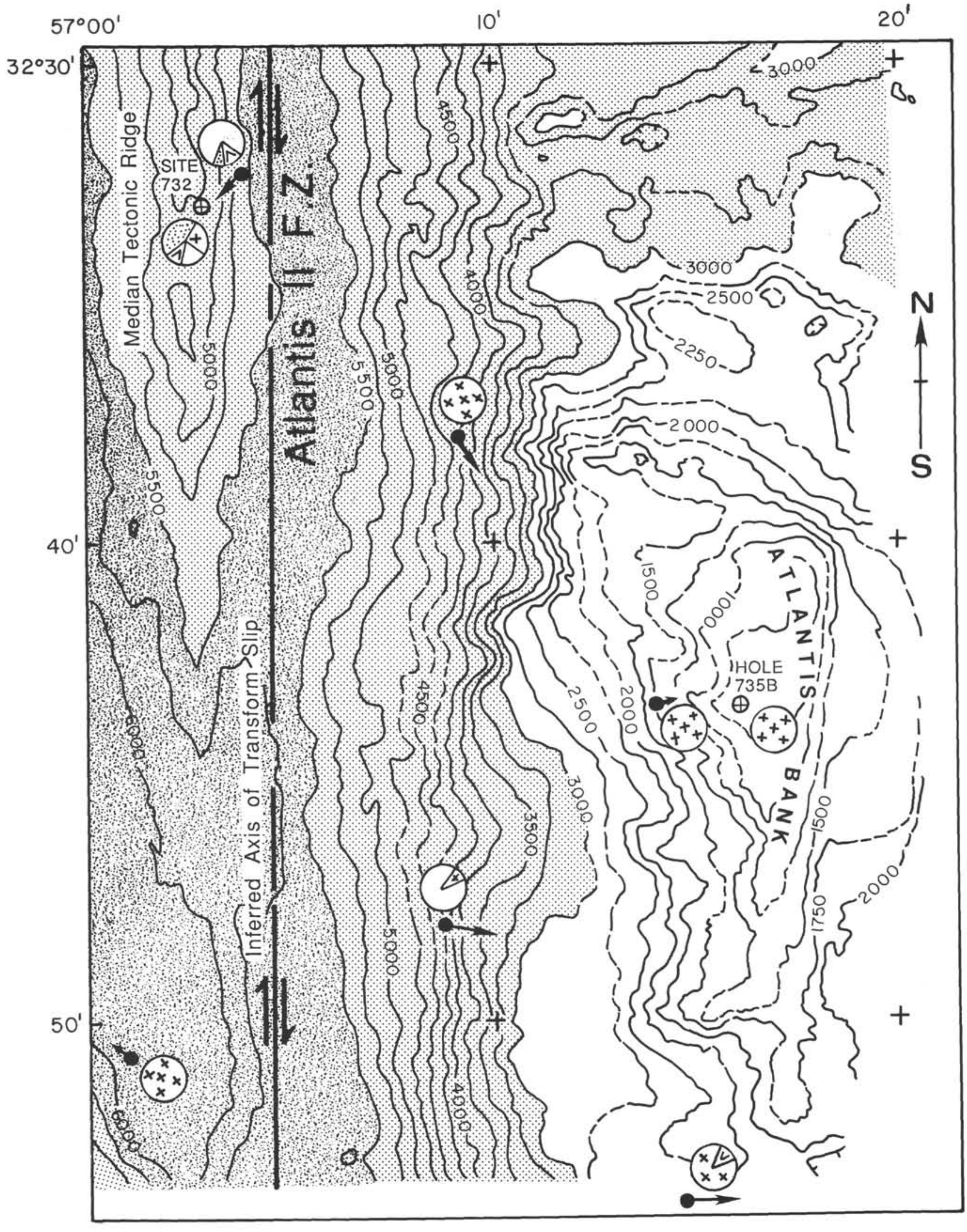

Figure 8. Hand-contoured bathymetric map of the eastern transverse ridge, showing the location of Site 732 and Hole 735B. SeaBeam tracks hand-shifted by eye to eliminate conflicts in the data. Solid lines indicate actual data, while hatched lines show inferred contours. Contour interval = 250 m. Solid dots and arrows indicate the starting point and approximate track of dredge hauls. Filled circles indicate the approximate proportions of rock types recovered in each dredge: white = altered peridotite, + = gabbro, v = basalt and diabase, stippled greenstone.

peridotite and gabbro have been dredged near their summits. The most notorious example is the block on which Hole 735B was drilled, which consists of a flat gabbro pavement exposed on a wave-cut terrace and is figuratively as smooth as a billiard table (compared with normal basement relief) with less than 10-m local relief over a 30-km^2 area (Fig. 8). Thus fitting the gravity data, dense plutonic rocks are commonly found at the highs, while lower density basalts, inferred from seafloor morphology and dredging, are found at the lows.

Transform Walls

There is a significant morphologic difference between the two walls of the transform valley. The eastern wall is generally steeper and higher than the western wall, with slopes ranging from a relatively "gentle" 11° to a maximum of 32°, with an average slope of about 23°. The western wall is generally less steep and ranges from 11° to 24°, with an average slope of about 19°. In addition to the gentler slope of the western wall, the opposing transform walls have significantly different shapes. The eastern wall consists of three relatively straight segments that step progressively westward as the crust becomes younger. In contrast, the western wall is curved and trends N10°E at its northernmost extension outside the transform zone, then curves to north-south at the midpoint of the survey region and trends N5°W to the south.

The walls of the Atlantis II transform have a marked sutured appearance due to numerous land-slip or slump scars. These have a characteristic arcuate, spoon-shaped depression that resembles a glacial cirque, with (in many instances) a toe of debris at their foot. The most spectacular example is located at 33°24′S on the western wall of the transform valley, near the southern ridge-transform intersection. There, a cirque-shaped scar is 14 km wide on the transform valley wall and has a huge, cone-shaped slump deposit at its foot that extends out about 4.5 km onto the floor of the fracture zone. Typically, slump scars are smaller, averaging around 3 to 4 km wide, but generally run the full length of the wall from its top down to its base. Slump morphologies, where the hillside starts at the top as a bowl-shaped depression, which reverses downward at a bench to a bulge, characterizes large areas, particularly along the western wall. These irregular scars provide evidence of major mass wasting along the entire length of the transform and lend support to the idea that mass wasting and slope modification are very important processes in the evolution of the terrain along and within the transform valley (OTTER, 1985).

Transform Valley Floors

The floor of the transform valley contains numerous flat sediment ponds along its entire length. The largest of these are three linear ponds, from 100 to 150 km^2 each, in the southern half of the transform valley. We conducted a mini-survey down the axes of these ponds and across the intervening southern median tectonic ridge with the single-channel seismic profiler (Fig. 9) and found reflections that extended down to approximately 0.25 s in the western two ponds and almost 0.5 s in the eastern pond.

From piston cores in both ponds, we recovered approximately 1 m of coarse sand and gravel, which on inspection proved to consist of clasts of peridotite, gabbro, greenstone, and basalt. This material is similar to the coarser debris that was dredged from the transform walls. These cores contained very different proportions of clasts, with the eastern core consisting of a mix of peridotite, gabbro, greenstone, and basalt, while the western core was mostly greenstone and basalt, suggesting that these sediments were derived from different sources: presumably the eastern and western walls of the transform, respectively.

Thus, we interpret the sediment reflectors (which are peculiar compared to reflections from normal pelagic sequences) as alternating pelagic sediment and gravel turbidites derived by debris flow from the transform walls. Assuming a slightly higher seismic velocity for such deposits compared to ordinary pelagic ooze, the western pond may contain a minimum of 350 m of turbiditic sands and gravels, and the eastern basin may contain in excess of 700 m of similar material.

Local sediment ponds persist along the western branch of the transform valley, between the old transform wall and the northern median tectonic ridge and into the inactive trace of the fracture zone. To the south, the large, relatively broad, western sediment pond pinches out between the southern median tectonic ridge and the western wall of the fracture zone about 50 km north of the ridge-transform intersection. Disconnected sediment ponds also occur along the length of the eastern transform valley in the northern half of the transform. In the southern half of the transform, a 3-km-wide, 100-km-long sediment pond occurs between the eastern wall and the discontinuous southern median tectonic ridge. This pond extends down the transform past the eastern margin of the nodal basin and the ridge-transform intersection and ends at an abutment of the eastern transform wall just south of the neovolcanic zone. A few isolated ponds occur to the south of the ridge-transform intersection and are co-linear with it.

Median Tectonic Ridges

The transform valley is split down its axis by two median tectonic ridges, which we infer as lying on either side of the present-day transform slip zone. In the northern half of the fracture zone, a 1.5-km-high median tectonic ridge extends 110 km down the middle of the transform valley. This ridge terminates in the north at 31°54′S at a saddle, where it joins the end of a hooked ridge that extends down from the northern rift mountains across the fracture zone valley. The neovolcanic zone, defined geomorphologically, terminates against the northern extension of this hooked ridge and does not cross it or exist west of the median tectonic ridge. Thus, the western fork of the Atlantis II transform valley may be inactive, with no neovolcanic zone, and the present locus of transform faulting may lie near the axis of the eastern transform valley floor against the foot of the northern median tectonic ridge. The axis of the northern median tectonic ridge slopes gently at about 1.4° downward to 32°37.7′S, where the slope of the ridge steepens and plunges down to the floor of the transform valley, disappearing completely at 32°47′S. Morphologically, the northern median tectonic ridge is complex. On a large scale, it is simply a long, linear, tapering ridge, but at the 50-m contour scale, the crest of the ridge has a series of elongate subparallel highs, which may be offset from one another by more than 1 km. Locally, at 32°16′S, there is a short 8-km parallel segment of tapered ridge that is offset 2 km to the east on the side of the median tectonic ridge. This and other similar features along the ridge indicate that this feature has a composite origin and may have been produced by a repetitive process over a long time.

A second, far more subdued, median tectonic ridge, parallel to the northern median tectonic ridge, appears within the transform valley at 33°38′S, near its intersection with the southern ridge axis, and extends 96 km to the north, where it merges with the eastern wall of the fracture zone. The maximum elevation along the ridge is only about 250 m, and it is discontinuous, disappearing intermittently. As a tectonic feature, it often exists only as a lineament, defined by a slope break, along much of its length. This ridge disappears in the

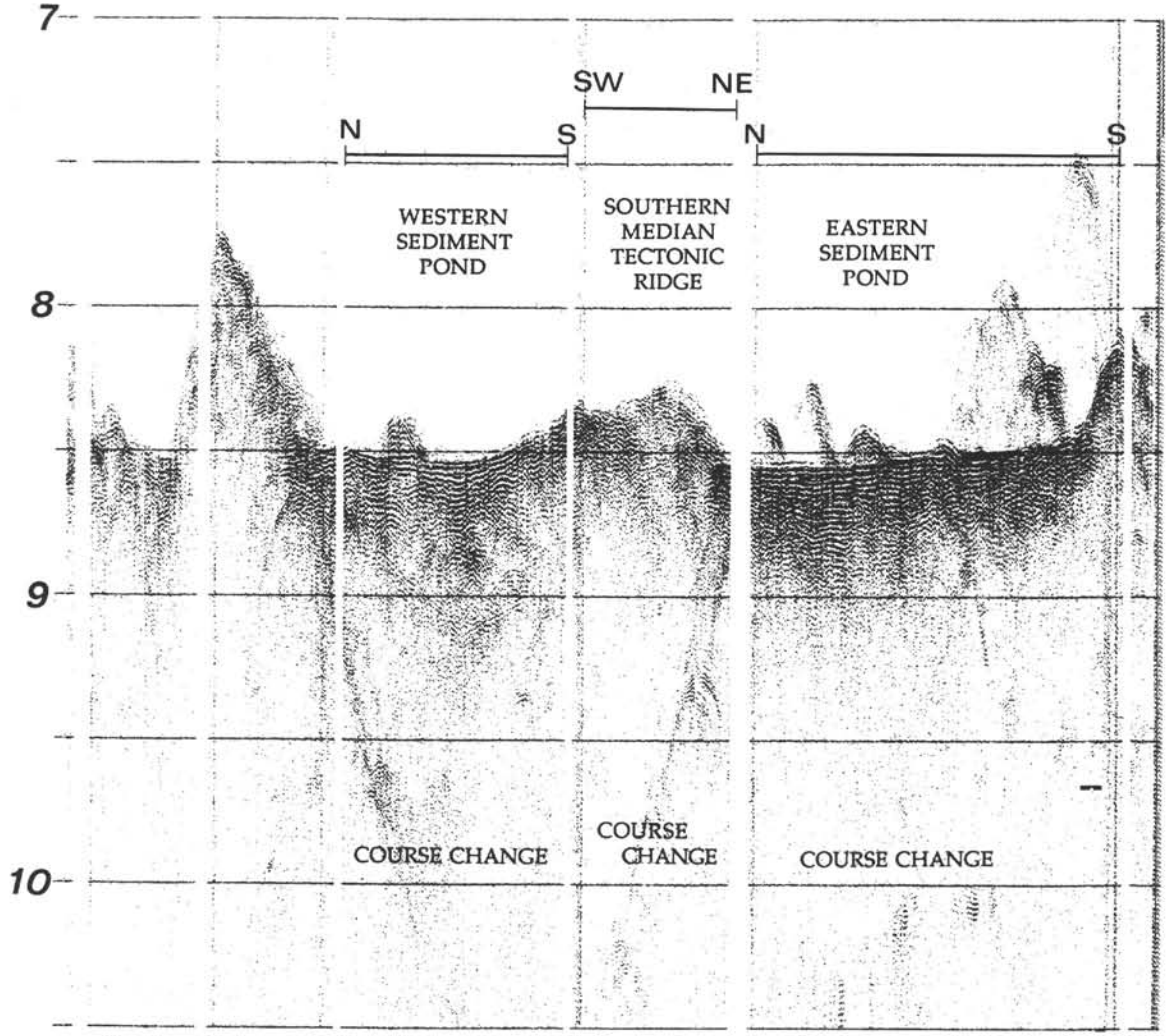

Figure 9. Single-channel, seismic-reflection profile across the southern median tectonic ridge and down the two flanking sediment ponds. The profile was run almost north-south down the axis of the western sediment pond, and then obliquely to the northeast across the southern median tectonic ridge and then due south down the axis of the eastern sediment pond.

middle of the transform, where it merges into the eastern wall of the fracture zone at roughly the same point that the northern median tectonic ridge disappears into the floor of the transform valley a short distance to the west. To the south, the ridge forms the eastern wall of the nodal basin and extrapolates across a small bench to the eastern limit of the neovolcanic zone, where it seems to disappear. Farther south, however, the western wall of a small sediment pond at 33°45′S, 57°05′E aligns with the lineament defined by the southern median tectonic ridge. This wall consists of the eastern end of a well-defined, hooked ridge that extends across the fracture zone valley from the southern rift mountains of the Southwest Indian Ridge.

Like the northern median tectonic ridge, the southern median ridge divides the transform valley floor into two smaller basins. The western of these is continuous with the western inactive transform valley, while the eastern is relatively small (only 2 km wide), but very linear and extends 90.8 km from where it begins near the midpoint of the transform, to a point nearly at the ridge-transform intersection to the south. Note that the sediment pond continues as a 2-km-wide bench past the southern nodal basin, clearly lying east of the inferred present-day zone of transform faulting on the Antarctic Plate, rather than the African Plate. This suggests that the eastern sediment pond in the southern half of the transform is a miniature version of the double transform valley to the north, with the inactive portion representing an old transform valley lying on the Antarctica side of the plate boundary, rather than the African side.

Like the northern median tectonic ridge, the southern median tectonic ridge is colinear with two hooked ridges that extend east down the nontransform wall of the inactive fracture zone valley from the rift mountains and curve northward into the fracture zone floor 10 and 20 km south of the neovolcanic zone. The extension of the median tectonic ridge would pass along the east facing north-south slopes at the eastward limits of the hooked ridges.

In the seismic profile across the southern median tectonic ridge (Fig. 9), the sediment reflectors in the western sediment pond overlap the median tectonic ridge and pinch out into a zone of what looks like disturbed sediment. Then, there is a relatively narrow transparent zone, followed by an abrupt change, back into thick turbiditic sediments in the eastern pond. This seismically transparent zone might be a basement ridge that is projecting up through the sediment near the surface. To the north, the median tectonic ridge was examined in detail during the borehole televiewer survey for Site 732; no convincing outcrops were seen. Rather, the ridge consisted of sand, gravel, and large boulders and coarse debris. Dredging in the vicinity recovered serpentinized peridotite, greenstone, and gabbro, while dredging at three other sites along the northern ridge recovered a mixture of gabbro, peridotite, basalt, diabase, and greenstone.

From several holes drilled at Site 732, near the crest of the ridge, sands and gravels were recovered that were identical to those in the piston cores. One short interval of sandy brown clay, interbedded with the sands and gravels in Hole 732B, was dated as mid-Pleistocene (about 0.27–0.46 Ma). The crustal age of the site inferred from the spreading rate is greater than 10 m.y.; accordingly, the turbiditic sands and gravels on the crest of the ridge were only recently deposited. It is possible that these sands and gravels, which sit almost 1.5 km above the floor of the transform to either side, may have been deposited by a recent debris flow that onlapped and overflowed the top of the ridge, but it seems unlikely. The more likely alternative is that the sandy clay was deposited on the floor of the transform valley, was then covered by turbidites from the wall of the transform, and was subsequently uplifted to its present position. This gives a minimum rate of uplift of 0.3 cm/yr over the last 460,000 years.

Present-Day Transform Slip Zone

The two median tectonic ridges are parallel, with the southern ridge offset 4.3 km to the east of the northern ridge. Both ridges define or align with the limit of the neovolcanic zones, where they intersect with the rift valleys of the Southwest Indian Ridge. Both ridges define the opposing wall of the active nodal basin: Both also align with the ends of the hooked ridges, which often define the terminus of the rift mountains along rift valleys walls spreading away from the transform. Thus, we postulate that the present-day active transform fault zone must be parallel to the two median tectonic ridges and must lie within a 4.3-km-wide zone defined by the offset of these two ridges.

Inactive Fracture Zone Valley

The inactive traces of the Atlantis II Fracture Zone are marked by deep valleys that exhibit complex morphologies. The opposing walls of this valley have strikingly different origins, one wall, the paleotransform wall, passed through the transform tectonic zone. while the other, the nontransform wall, did not. These different origins are reflected in strikingly different morphologies. Most notably, the paleotransform wall is straighter and steeper, and locally resembles the features found flanking the active transform valley. We regard these walls as extensions of the walls formed at the inside corners of the ridge-transform intersections.

Nontransform Walls

Where crust is spreading from the neovolcanic zone away from the transform tectonic zone, it is uplifted into a series of alternating ridges and valleys parallel to the trend of the Southwest In dian Ridge (Fig. 10A). These slope gently down to meet the paleotransform wall and form the inactive fracture zone valley. Numerous small seamounts, closed basins, and ridges and lineaments oriented parallel to the axis of spreading (e.g., Fig. 6) are exposed on the nontransform wall. This kind of morphology is characteristic of the terrain exposed on inner-rift valley floors and, accordingly, has been interpreted as old extensional volcanic terrain, relatively undisrupted except for a series of relatively small-throw normal faults (e.g., Pockalny et al., 1988). The two ridges immediately north of the northern rift valley have a distinct asymmetry with respect to the present-day rift valley, while sloping more steeply toward the rift valley. This morphology suggests that the ridges probably are formed of large, 20-km-wide, back-tilted crustal fault blocks.

North of these two blocks lies a relatively broad, deep basin that is flanked to the northeast by an unusual 2150-m-high oblong hill with steep sides extending 17 km into the map area from the east (Fig. 10B). The morphology of this hill is unlike that associated with the linear volcanic terrain on the other ridges and valleys and may have a tectonic origin. To the west, the basin is flanked by a north-south ridge situated in the fracture zone valley, which connects to the north to a volcanic ridge that extends east-west down from the rift mountains. Pockalny et al. (1988) proposed that nodal basins form centered on the intersection of a rift valley and fracture zone during relatively amagmatic cycles at a slow-spreading ridge and are periodically bisected and partially infilled along the neovolcanic zone during magmatic cycles. Thus, with continued spreading, the basins are continuously regenerated, split in half, and then regenerated again. This particular basin, with its anomalous geometry, may well have formed just as suggested by Pockalny et al. (1988) and may be the remnant of a nodal basin.

We do not think, however, that as a rule the morphotectonic character of either the Atlantis II or other large offset transforms, including the Kane, support this simple hypothesis. This is because nodal basins are generally centered and appear to form on the transform side of neovolcanic zones at slow-slipping fracture zones, and have their deepest points located some distance along the transform valley. Thus, as will be discussed in more detail later, we think that the nodal basins reflect a crustal weld across the ridge-transform intersection between the shallow crust and the older lithosphere, resulting in asymmetric spreading of the uppermost crust away from the transform during amagmatic periods. This created the pit on the transform side of the spreading axis. During particularly prolonged amagmatic cycles, however, such a deep may grow into and even extend across the actual intersection, to be split and partially infilled during the next magmatic cycle, as envisioned by Pockalny et al. (1988).

The rift mountains extending down from the nontransform walls are strikingly different from those formed at the inside corner highs that form the transverse ridges. Not only do they have much lower relief, but they also extend across the fracture zone valley. The ridge parallel topography of these rift mountains turns abruptly in the fracture zone valley to form *hooked ridges*. At the northern ridge-transform intersection, one such ridge curves around a nodal basin to abut the median tectonic ridge that flanks the nodal basin there (Fig. 6). To the north, a series of three or four such hooked ridges can be seen; these extend into the fracture zone valley and, in some cases, nearly abut the older wall of the fracture zone (Fig. 10). One such ridge is located some 15 km south of the present-day neovolcanic zone at the southern ridge-transform intersection as well.

Hooked ridges appear to be a characteristic, if intermittent, feature of the nontransform fracture zone walls at many fast and slow-slipping ocean transforms (e.g., Gallo et al., 1986; Fox and Gallo, 1986; Macdonald et al., 1986, Tucholke and Schouten, 1988). The ends of these ridges, where they curve into the fracture zone, are consistently on strike with median tectonic ridges in the transform, though there is a tendency for their tips to be offset slightly toward the rift valley (e.g., Fig. 6). Their formation likely reflects local perturbation of the neovolcanic zone and the master faults along the rift valley

A

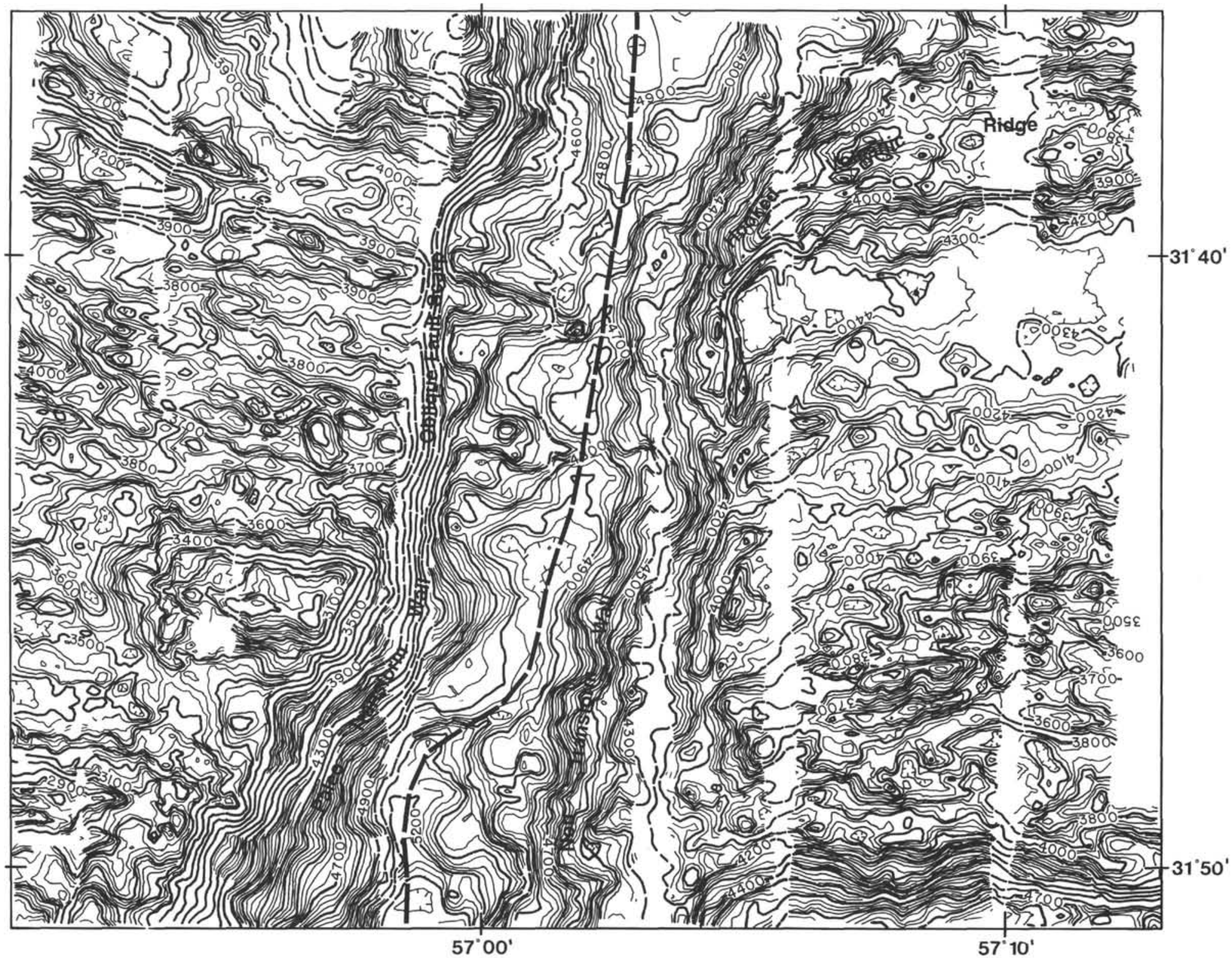

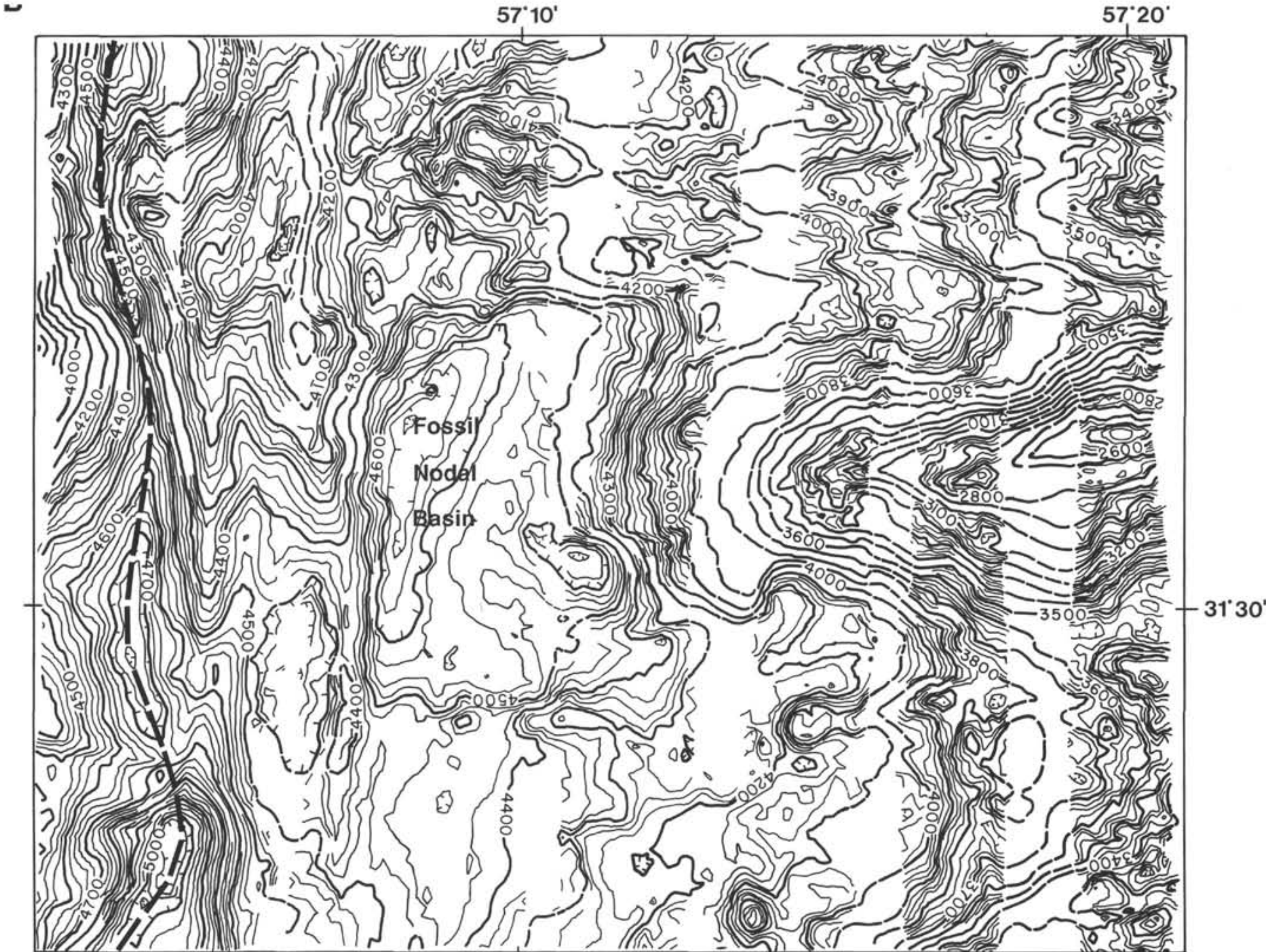

Figure 10. Hand-contoured bathymetric map of portions of the inactive northern trace of the Atlantis II Fracture Zone, where it is predominantly oriented N10°E, rather than the north-south orientation of the present-day transform slip zone. Solid lines indicate actual data, while hatched lines show inferred contours. Contour intervals include 100 m (heavy lines) and 25 m (light lines) where contour density permits. Heavy dashed lines show paleo trace of fracture zone and present day axis of the inactive fracture zone valley. **A.** Rift mountains and fracture zone valley just north of present day rift valley. Note long, straight, north-south scarp cutting the western wall of the valley at 56°58.3′E. This oblique fault has been inferred to have been caused by nontransform dip-slip faulting from differential subsidence between the more rapidly cooling younger crust to the east and the more slowly cooling older curst to the west. Note that the rift mountain topography on the western, older side of the fracture zone shows a strongly lineated tectonic grain with local closed contoured highs and lows characteristic of rifting and volcanic hills formed in a median valley oriented N80°W orthogonal to the fracture zone paleotrace and inferred spreading direction. In contrast, the topography on the younger, eastern side of the fracture zone trace, while it is also lineated with closed contoured highs and lows, is oriented east-west orthogonal to the present-day north-south spreading direction. SeaBeam tracks hand-shifted by eye to eliminate conflicts in the data. **B.** Inactive fracture zone valley and northern rift mountains just north of **A**, showing possible fossil nodal basin. Note the prominent ridge lying northwest of the basin between it and the paleofracture zone trace. This ridge may have several origins, although most likely it is composed of a fossil median tectonic ridge fragment having a volcanic hooked ridge that runs into it around the fossil nodal basin.

wall opposite the transform as they approach the transform fault. Rotation of the stress field may cause the faults to turn into the strike of the transform. Thus, they are likely to have a complex-compound origin, with the volcanic axis turning into the transform and onlapping the median tectonic ridge, combined with curvature of the major normal fault systems into the axis of strike-slip motion.

The degree to which hooked ridges have a constructional volcanic component is difficult to determine and subject to debate. Neither here nor at the Kane Fracture Zone do the active neovolcanic zones form a high constructional volcanic ridge with the extreme curvature of the Kane neovolcanic zones around the nodal basins toward the active transforms. Oblique trends and curvature of the neovolcanic zones toward the transforms have also been reported at the Oceanographer and Vema fracture zones (Williams et al., 1984; Rowlett and Forsyth, 1984; Macdonald et al., 1986; Auzende et al., 1990). In these cases, all the nodal basins lie on the transform side of the spreading center with the neovolcanic zone appearing to curve arond the basin to terminate at the far wall of the basin against the old lithospheric plate. Extreme curvature of the neovolcanic zones, and formation of a high volcanic ridge, which may actually extend into the floor of the transform, is seen at fast spreading ridges (e.g.: Lonsdale, pers. comm.; Fox and Gallo, 1989).

Dredging of two hooked ridges in the northern nontransform fracture zone valley recovered only relatively intact, weathered pillow basalts. The hooked ridge at the northern ridge-transform intersection at the Kane Fracture Zone exposes only weathered, faulted, and fissured pillow lava flows, but the data are insufficient to determine if this ridge is tectonic, constructional, or the result of some combination of these processes (Karson and Dick, 1983). Given the exclusive exposure of weathered pillow basalt on the hooked ridges, which contrasts sharply with the mixed assemblage of altered basalt and plutonic rocks commonly exposed on old transfrom walls, each hooked ridge can be taken to mark the limit of the axial neovolcanic zone and the plate boundry at the time of their formation.

Paleotransform Walls

An inactive paleotransform wall was surveyed extensively only in the northern half of the survey area. However, the southern paleotransform wall was surveyed for a short distance and has a radically different character from the active transform wall. The ridge comprising this wall plunges steeply to the south from opposite the ridge-transform intersection, with several abutments jutting into the fracture zone valley, to a low saddle nearly on the level of the fracture zone floor. A similar saddle exists on the northern paleotransform wall to the north for crust of slightly older age. The crust in these saddles geomorphologically looks like old volcanic terrain, with small seamounts and topography lineated orthogonal to the strike of the wall.

Like the southern paleotransform wall, the character of the northern paleotransform wall changes dramatically north of the ridge-transform intersection. The wall and transverse ridge become discontinuous and consist of a series of relatively low saddles and alternating highs, with much lower, though locally still steep, slopes. The surface morphology is different from the active transform walls, with well-lineated, clearly volcanic terrain that covers most of the transverse ridge, both on the highs and in the saddle points. Locally, lineated volcanic terrain can be followed as it slopes gently down from the rift mountains to the floor of the fracture zone valley (e.g., Fig. 10A). The tectonic blocks lying along the wall have much more subdued relief and typically sit only about 2.5 km above the floor of the fracture zone. The character of this wall appears to have been little affected in passing the upwelling asthenosphere at the ridge-transform intersection. First, the old wall is separated from the neovolcanic zone by a deep valley about 13 km wide and by the northern median tectonic ridge. Second, rather than uplift caused by possible effects of reheating (e.g., Gallo et al., 1986b; Tucholke and Schouten, 1988), the wall steadily decreases in height as it passes the ridge-transform intersection.

The inactive transform walls closely resemble the morphology of the northern active transform wall at the Kane Fracture Zone, described in considerable detail by Pockalny et al. (1988). Therefore, we suggest that it is a simple continuation of the transform wall into the inactive zone of the fracture zone. Thus, the change in physiographic character probably reflects a different state of stress existing at the fracture zone when the wall was formed. Therefore, we think that its physiographic features are only slightly modified from its initial formation at the southern ridge-transform intersection, other than by subsidence, mass wasting, and sedimentation.

One feature that we do think reflects modification of the paleotransform wall as it passed the northern neovolcanic zone is a steep scarp on the paleotransform wall that downdrops the volcanic terrain on the left of the bathymetric map in Figure 10A. This scarp cuts obliquely across the local strike of the paleotransform wall and is nonorthogonal to the prominent west-northwest-lineated volcanic ridges. It is parallel, however, to the present-day north-south orientation of the Atlantis II transform slip zone. Accordingly, we interpret this feature as resulting from late dip-slip normal faulting that was produced by coupling of the rapidly subsiding younger plate to the east and the more slowly subsiding old lithospheric plate to the west. The effects of such a couple between old and young crust has been reported as a general feature at other fracture zones (e.g., DeLong et al., 1977; Karson and Dick, 1983; Sevringhaus and Macdonald, 1988).

From a point just south of the ridge-transform intersection, the western transform and paleotransform walls have a strikingly different trend from the present-day slip-zone of the Atlantis II Fracture Zone for crust older than 17 m.y. This trend is roughly N10°E for about 150 km and is on strike with an additional SeaBeam crossing of the paleotransform wall farther north. Locally, in this zone, the trend of the wall diverges to N18°E. This suggests that a significantly different, and somewhat variable, spreading direction existed in the past. In the high-resolution SeaBeam map of a portion of the paleotransform wall (Fig. 10A), the crust lying on the west side of the fracture zone has the characteristic morphology of lineated volcanic crust that was generated at a slow-spreading ridge. Crust of considerably younger age across the fracture zone is similarly lineated, but oriented east-west up to the fracture zone, orthogonal to the north-west trend of the modern transform fault, and parallel to the present-day spreading axes, and then turns sharply to form hooked volcanic ridges that align with the present-day trend of the Atlantis II transform slip-zone. The lineated crust west of the fracture zone trends W18°N, orthogonal to the N18°E trend of the inactive transform wall. Such lineations are generally thought to be parallel to the paleospreading axes (e.g., Pockalny et al., 1988), and the consistent differences we see across the fracture zone in Figure 10 support the use of the trend of the northern inactive transform wall to infer a different spreading direction for the Southwest Indian Ridge prior to 17 Ma.

The implied spreading direction change at 17 Ma on average is about 10° and should have placed the fracture zone into extension (Menard and Atwater, 1968). This should have dramatically affected the state of stress in the transform and might account, in part, for the difference in character of the transform and paleotransform walls.

RESULTS OF DREDGE SURVEY

Introduction

Thirty-seven successful dredge hauls were conducted during the site survey. Twenty-four dredge hauls were made along the walls of the transform and the median valley at the ridge-transform intersection (10 on the eastern side of the transform and 14 on the western side). From these hauls, we recovered 42.1% altered peridotite, 23% gabbro and dunite, 11.6% diabase, 13.1% metabasalt and greenstone, and only 10.2% unmetamorphosed pillow basalt. In all, 3203 kg of rock was dredged, and all these samples were cut, split, weighed, and catalogued on board the ship. Five dredge hauls previously were collected from the transform during Atlantis II Cruise 93, Leg 5, along the Atlantis II transform (Engel and Fisher, 1975). Locations, initial water depth at the start of the dredge station, and lithological proportions for each dredge haul from the *Robert Conrad* are given in the Appendix (backpocket) and shown in Figure 11. While the original stratigraphic position of dredge samples is uncertain as a result of downslope slumping and mass wasting, their position on a lithospheric flow line relative to the ridge axes is well constrained. Combining magnetic anomaly data with dredge locations, the age of the samples can be estimated fairly accurately (Table 1).

All dredges conducted in the rift valley and nontransform zones were successful; however, only 24 of 36 dredge hauls attempted on the walls of the transform were successful. Three rock dredges were lost, and nine were brought up empty. Major dredge hang-ups occurred during virtually every dredge haul on slopes having angles greater than 22°, and frequently as many as 20 or 30 "bites" occurred where the dredge obviously hung up momentarily on outcrop without breaking anything off, indicating that outcrop was abundant, even where the dredges were empty. Shifting from the steeper walls of the transform to those having slopes of around 20° dramatically improved dredging conditions and recovery. On these gentler slopes, major bites were rare, and the dredge often returned full, with few indications of outcrop. This dramatic difference in dredging conditions suggests that the gentler slopes have been largely covered by slump deposits and talus ramps.

Such extremely difficult dredging conditions are highly atypical of Southwest Indian Ridge fracture zones, where previously the first author conducted four other major dredging cruises. Out of approximately 68 dredges attempted previously on the walls of 14 Southwest Indian and American-Antarctic Ridge fracture zones, only two dredges were lost and 60 contained rock, mostly altered peridotite, which is a success ratio of 88%. By contrast, the success ratio for the Atlantis II transform was 66% and would have been much less had we not switched to the gentler slopes.

We do not attribute this difficulty to physiographic differences, because the slopes dredged at other transforms were morphologically similar to those at the Atlantis II, but rather to a much larger abundance of gabbro exposed on the walls of the Atlantis II transform.The senior author previously encountered similar unfortunate conditions only at the ridge-transform intersection at the Kane Fracture Zone, where *Alvin* dives and camera tracks confirmed the presence of massive outcrops of gabbro. We regard as established fact that gabbro is much tougher, if not nearly impossible, to break off an outcrop with an ordinary rock dredge than peridotite or basalt. Generally, peridotite is highly altered and weathered, which makes for poorly cohesive outcrops, while basalt usually occurs as loosely aggregated piles of pillow lavas or as highly fractured diabase. Outcrops of gabbro, seen along scarps in fracture zones, are generally very massive, have widely spaced joints, and are generally only slightly weathered (OTTER, 1984).

Lithologic Distribution and Associations

The distribution of different rock types in the survey region is not uniform across the region. From two dredge hauls at the tips of hooked ridges in the rift mountains of the Southwest Indian Ridge on the nontransform wall, exclusively basalt was recovered, as well as from three dredge hauls from the neovolcanic zones situated along the axial ridges in the rift valleys (Fig. 12A). In striking contrast, from 24 dredge hauls along the transform, 2400 kg of rock was recovered consisting mostly of peridotite (43%), gabbro (24%), and lesser amounts of pillow basalt fragments (20%) and diabase (13%) (Fig. 12B). By dredging the prominent northern median tectonic ridge, we recovered a chaotic mixture of serpentinized peridotite, gabbro, and metamorphosed basalt and diabase fragments in four dredge hauls. Thus, plutonic rocks constitute two-thirds of the total rock dredged from the transform, which is slightly less than the proportion found for 14 other Southwest Indian and American-Antarctic Ridge transforms (Dick, 1989). At the latter, however, peridotite constitutes 63% of the recovery, whereas gabbro was rare (only about 8%). This, combined with the difficulty encountered in dredging gabbro, leads us to suggest that gabbro may actually be more extensively exposed than peridotite in the Atlantis II transform.

The transform dredge hauls were made at all levels on the walls up to their crests (Fig. 11, Appendix, backpocket). As can be seen from Figure 13A, no evidence exists for a pseudostratigraphic cross section of the crust on these walls, as reported for some fracture zones in the Indian and Atlantic oceans (Engel and Fisher, 1975; Bonatti and Honnorez, 1976). Rather, when the dredge hauls are plotted in histograms by increasing depth, one can see that the most diabase and basalt was dredged below 5000 m, and the most gabbro and peridotite at depths above 4000 m. Nor did we find any consistent association of rock types to imply ordered stratigraphic sections, or the absence of layer 3 in some regions. Instead, the different rock types seem to be associated randomly with each other, while only one-third of the dredge hauls contained only one rock type (most commonly gabbro or peridotite). The only thing that one could argue from the associations of rock types in dredge hauls is that large outcrop areas that expose gabbro or peridotite exclusively are common, whereas basalt occurs randomly mixed with plutonic fragments. This suggests that coherent outcrop areas of pillow basalt must be rare if present within the transform tectonic zone.

In Figure 13B, a histogram plot shows the basaltic rocks recovered from the transform. Only 6% is unaltered basalt. By contrast, more than 13% basalt with slight to moderate greenschist facies alteration was found, while metadiabase and diabase make up 12%. Thus, even where basaltic rocks were dredged, they generally appear to represent deeper sections of layer 2 (Table 2). In contrast, the basalts dredged in the axial valleys and in the rift mountains along the nontransform walls show at most surficial weathering, often consisting of large blocks of pillows which fit together, suggesting that we dredged intact or largely coherent pillow lava flows, rather than the shattered fragments dredged on the transform walls, where there is no morphologic evidence of pillow flows. Thus, one may conclude that over large sections of the transform tectonic zone, which extends from the floor of the transform valley to the crest of the transverse ridge, the shallow basaltic

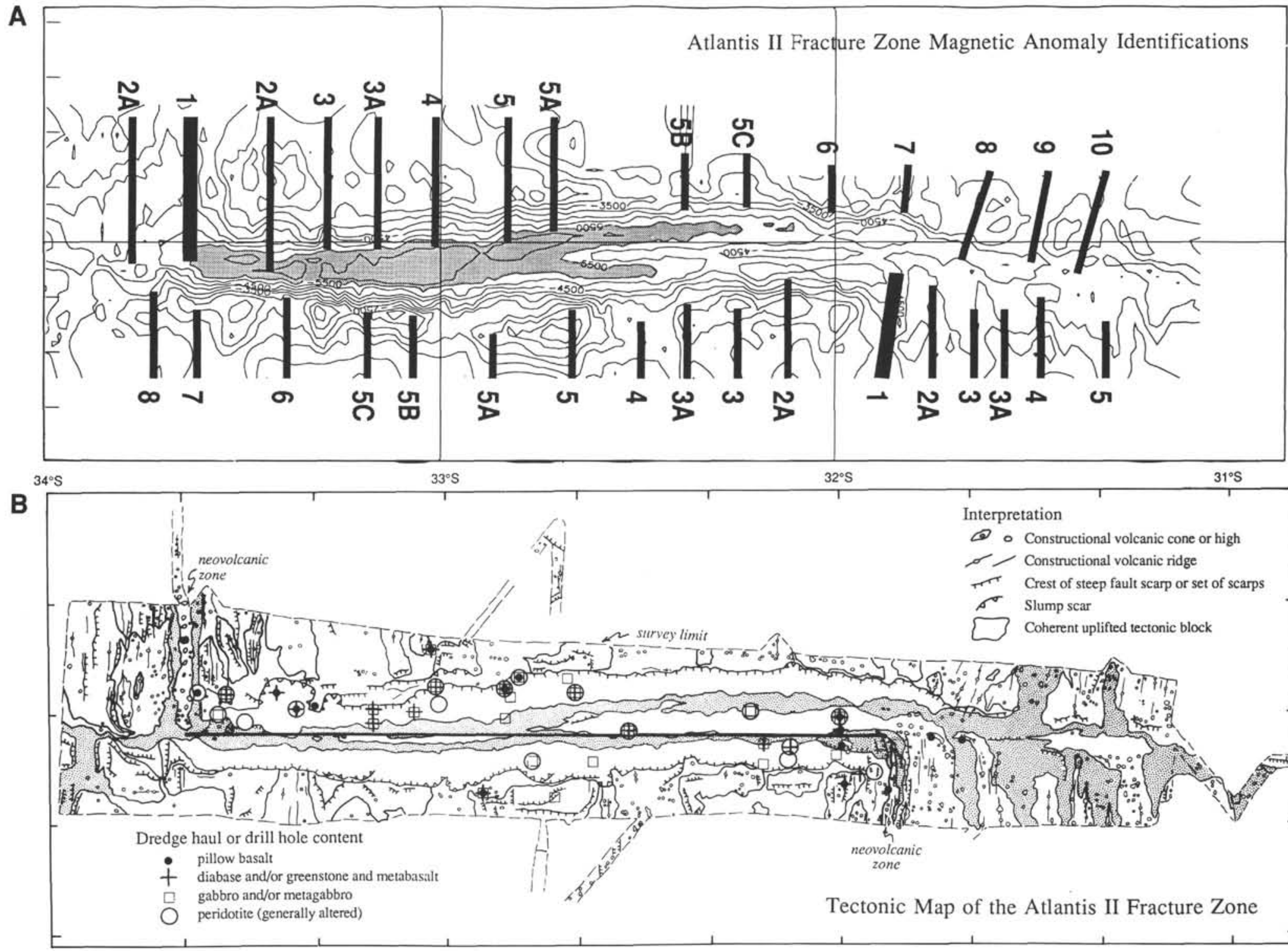

Figure 11. **A.** Computer-gridded and contoured bathymetric map of the Atlantis II Fracture Zone, showing magnetic anomaly identifications and locations. **B.** Tectonic map based on the interpretation of the physiography of the Atlantis II Fracture Zone, showing the location and contents of the principal dredge hauls. Major sediment ponds are stippled. Inferred axis of present-day transform slip shown by heavy straight line. A comparison of these two sections shows that the magnetic anomalies may have extended across regions where only gabbros and serpentinized peridotites have been dredged (e.g., anomalies 2A, 5). Up to 11 Ma, the anomalies may extend onto the floor of the transform. Coherent anomalies, however, are absent on the transform floor for crust older than anomaly 5A. This latter region we postulated as the remains of an old transtensional basin, formed within the fracture zone during plate readjustment to a spreading direction change at 17 Ma. Location of successful dredges shown by symbols, as indicated in legend. Note the absence of inferred volcanic features on the walls of the transform and locally along their crests, as compared to the nontransform walls of the trace of the fracture zone.

Table 1. Results and locations of dredge heads from three cruises.

Dredge number	Start depth (mbsf)	Location	Latitude (degrees)	Longitude (degrees)	Pd	Pd myl	Total Pd	Dunite	Gabbro	Meta-gabbro	Diabase	Meta-diabase	Basalt	Meta-basalt	Green-stone	Total (kg)
Robert Conrad Cruise 27, Leg 9 (Site-survey cruise)																
RC27-9-1	3940	Axial volcanic S rift valley	S33.655	E56.781	0	0	0	0	0	0	0	0	3.9	0	0	3.9
RC27-9-3	4250	Small axial hi N rift	S31.882	E57.233	0	0	0	0	0	0	0	0	372	0	0	372
RC27-9-4	3880	Hook R.#l N FZ ext.	S31.760	E57.073	0	0	0	0	0	0	0	0	77.2	0	0	77.2
RC27-9-5	4260	Hook R.#2 N FZ ext.	S31.695	E57.078	0	0	0	0	0	0	0	0	53.4	0	0	53.4
RC27-9-6	4160	Corner, N RTI	S31.915	E57.178	36.2	0	36.2	0.5	0	0	0	0	0	0	0	36.7
RC27-9-8	3110	Corner, N RTI	S31.994	E57.176	0	0	0	0	0	0	0	0	0	0	3.6	3.6
RC27-9-9	2023	Rift Mtn smt. N RTI	S31.981	E57.210	0	0	0	0	0	0	40.6	0	104.1	0	0	144.7
RC27-9-10	5296	N RTI transform wall	S32.006	E57.106	0	0	0	0	83	17	0	0	0	0	1.25	101.25
RC27-9-11	4893	Median tectonic ridge	S31.990	E57.057	0	0	0	0	0	0	0	17.6	0	102.9	0	120.5
RC27-9-12	5360	N Transform volcano	S32.003	E57.090	0	0	0	0	0	0	0	0	166.6	0	0	166.6
RC27-9-13	4864	Median tectonic ridge	S32.002	E56.998	2.4	0	2.4	0	3	0	1.8	0	2.3	0	0	9.5
RC27-9-14	4883	W Wall FZ N RTI	S32.025	E56.975	0	0	0	0	0	0	0	0	0	0	0	0
RC27-9-18	4899	Transform E wall	S32.118	E57.100	58.4	0	58.4	0	0	0	0	0	0	43	0	101.4
RC27-9-19	3427	Transform E wall	S32.114	E57.138	0	0	0	2.5	0	0	0	0	0	0	0	2.5
RC27-9-21	3142	Transform E wall	S32.187	E57.172	0	0	0	0	1.2	6.1	0	0	0	0	0	7.3
RC27-9-22	5116	Transform E wall	S32.207	E57.102	0	0	0	0	19.8	0	0	0	0	1	0.2	21
RC27-9-23	5133	Median tectonic ridge	S32.226	E56.989	1.6	0	1.6	0	25.4	0	0	0	0	0	0	27
RC27-9-24	4225	Transform E wall	S32.417	E57.147	0	0	0	0	0	0	0	0	0	0	0	0
RC27-9-25	5370	Median tectonic ridge	S32.537	E57.064	330.8	0	330.8	0	1.6	0.9	0	27.8	0	40.9	6.3	408.3
RC27-9-26	4440	Transform E wall	S32.629	E57.150	0	0	0	0	0.7	0	0	0	0	0	0	0.7
RC27-9-27	2492	Transform E wall	S32.900	E57.234	0	0	0	0	9.3	0.2	0.84	0	0.59	0.84	0	11.77
RC27-9-30	4382	Transform E wall	S32.782	E57.134	192.8	0	192.8	0	18.1	0	0	0	0	0	0	210.9
RC27-9-34	5509	Transform W wall	S33.019	E57.001	134.1	0	134.1	14.5	0	0	0	0	0	0	0	148.6
RC27-9-35	4180	Transform W wall	S33.009	E56.961	61.9	0	61.9	1.5	2.8	0	0	33.6	0	24	0.6	124.4
RC27-9-36	3816	Transform W wall	S32.693	E56.907	0	0	0	0	21.8	1.9	0	0	0	0	0	23.7
RC27-9-37	5652	Transform W wall	S32.653	E56.963	72.5	0	72.5	0	0.1	9.2	0	2.9	0	4.7	0	89.4
RC27-9-38	2548	Crest trans. W wall	S33.032	E56.807	0.65	0	0.65	0	0	0	1.95	23.18	2.59	61.43	1.4	91.2
RC27-9-40	4659	Transform W wall	S33.192	E56.994	0	0	0	0	28.6	23.6	40	9.3	0	13.2	5.3	120
RC27-9-41	3049	Bench @top W T wall	S33.333	E56.981	0	0	0	0	0	0	0	0	16.5	0	0	16.5
RC27-9-42	3843	Transform W wall	S33.406	E56.959	0	0	0	0	0	0	86	0	43.7	0	0	129.7
RC27-9-43	4395	Corner, S RTI	S33.558	E56.940	5.3	0	5.3	0	10.1	0	0.2	0	0	0	0	15.6
RC27-9-44	4830	Corner, S RTI	S33.628	E56.931	1.5	0	1.5	0	0	0	0	0	108.7	0	0	110.2
RC27-9-45	5495	Wall of S RTI	S33.572	E57.016	16.3	20	36.3	0	49.3	2.8	0	0	0	0	0	88.4
RC27-9-46	5675	W wall S nodal basin	S33.501	E57.029	14.7	0	14.7	0	0	0	0	0	0	0	0	14.7
RC27-9-47	4653	Transform W wall	S33.383	E57.017	4.7	0	4.7	0	0	0	3	2.4	75.6	48.95	0	134.65
RC27-9-48	5782	Transform W wall	S33.184	E57.030	0	0	0	0	176.3	0	6.4	32.7	0	0	0.5	215.9
RC27-9-49	6050	High on S transf. floor	S33.167	E57.077	0	0	0	0	0.7	0	0	0	0	0	0	0.7
				Totals	**933.9**	**20.0**	**953.9**	**19.0**	**451.8**	**61.7**	**180.8**	**149.5**	**1027.2**	**340.9**	**19.2**	**3203.9**
Atlantis II, Cruise 93, Leg 5 (R.L. Fisher, pers. comm., 1990)																
AII93-5-1D	4315	Transform W wall	S32.837	E56.948	Yes				Yes	Yes						
AII93-5-2D	3200	Transform W wall	S32.813	E56.887	Yes				Yes	Yes			Yes			
AII93-5-3D	3765	Transform W wall	S32.845	E57.015					Yes		Yes		Yes			
AII93-5-4D	6035	Transform W wall	S32.850	E56.923					Yes	Yes						
AII93-5-5D	1500	Transform E wall	S32.718	E57.235					Yes	Yes						
JOIDES Resolution (*Init. Repts.*)																
Site 732	4910	Median tectonic ridge	S32.547	E57.055	19.6%				20.5%	1.8%	15.2%		33.9%		6.3%	97.3%
Site 733	5231	Transform W wall	S33.082	E56.990						Yes			Yes			
Site 734	3745	Transform E wall	S32.113	E57.130	Yes					Yes				Yes		
Site 735	1271	E transverse ridge	S32.723	E57.267					Yes	Yes	<1%	<1%				

Pd = peridotite; Pd myl = peridotite mylonite; RTI = ridge transform intersection; T = transform; SMT = seamount; FZ = fracture zone.

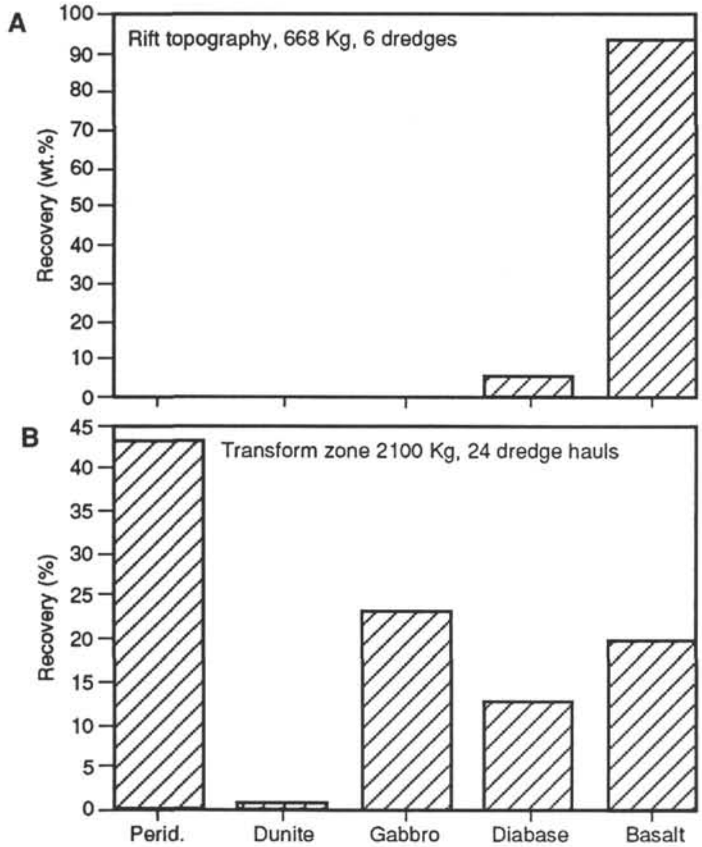

Figure 12. Histograms of total recovery (wt%) by rock type. **A.** Nontransform regions having rifted volcanic morphotectonic character. **B.** Transform tectonic zone.

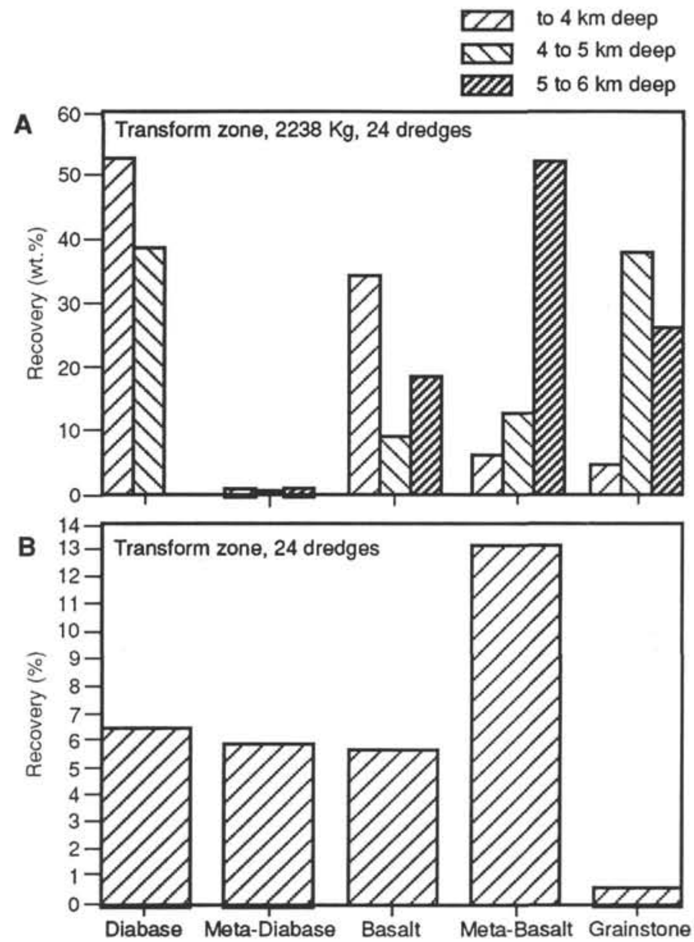

Figure 13. Histograms (wt%) showing breakdown of dredged rocks by water depth from the transform tectonic zone and showing a breakdown of basaltic rocks by type.

carapace, which normally constitutes layer 2a, is absent. This carapace is present and preserved relatively intact, however, in crust that spreads from the accretionary axis on the opposite lithospheric flow line to form the nontransform wall.

Petrologic and Geochemical Characteristics

Basalts

Shown in Figure 14 is a breakdown of basalts that were dredged from the survey area. Overall, aphyric pillow basalt was the most commom, with plagioclase phyric the next most abundant. Minor amounts of plagioclase phyric and olivine-plagioclase phyric basalts also occur. More primitive olivine phyric basalts are rare. When the dredge hauls from the rift mountains and rift valley outside the transform are considered by themselves (Fig. 14B), however, they are consistently more phyric than basalts from the transform walls (Fig. 14C). Thus, there is the suggestion that basalts exposed along the transform walls, which would represent the distal ends of a spreading segment, are consistently aphyric compared to rift valley basalts. Unfortunately, the statistics are not sufficient to draw a firm conclusion.

Shown in Table 3 are averaged multiple-spot electron microprobe analyses of glasses from the survey area performed at the electron microprobe facility of the Massachusetts Institute of Technology using natural mineral and glass standards. Chemically, the basalts are sub-alkaline mid-ocean ridge basalts (Fig. 15) that range from evolved ferrobasalt (Mg/Mg + Fe = 0.42, 3.44 wt% TiO_2) to moderately primitive MORBs (Mg/Mg + Fe = 0.61, 1.71 wt% TiO_2). Clearly, these are distinguished from typical MORBs, however, by their extraordinarily high soda contents at a given Mg/(mg + Fe) ratio and silica content (Figs. 15 and 16), compared with basalts from the Southwest Indian and other ocean ridges.

Dick et al. (1984) showed that liquidus trends defined by individual basalt suites shift systematically along ocean ridges with proximity to mantle hot spots, such as Bouvet and Marion. These shifts reflect, in large part, lower sodium contents in the primary melts far from mantle hot spots, and

Table 2. Atlantis II transform dredge assemblages.

Assemblage	Dredges
Peridotite	3
Peridotite and gabbro	3
Peridotite, gabbro, and diabase	1
Peridotite, gabbro, diabase, and basalt	4
Periodotite, diabase, and basalt	2
Peridotite and basalt	3
Gabbro	5
Gabbro and diabase	1
Diabase and basalt	1
Greenstone	1

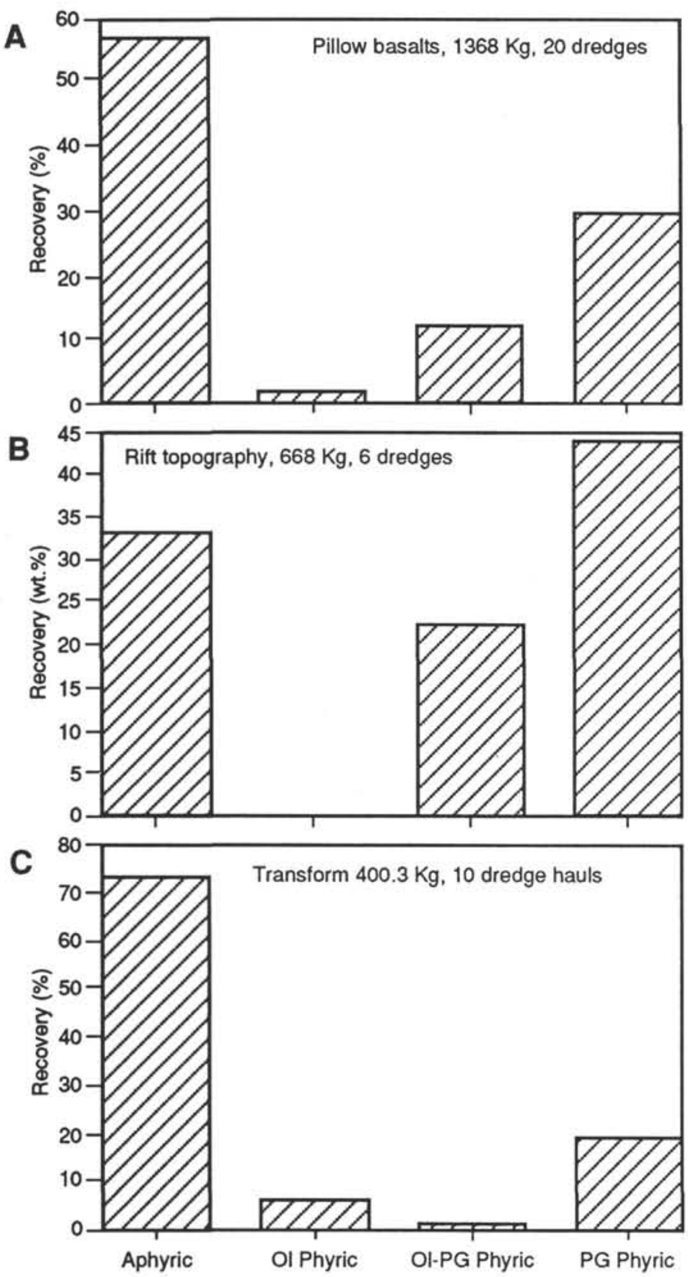

Figure 14. Histograms (wt%) showing a breakdown of basaltic rocks by variety. **A.** All samples. **B.** Rift mountains and valleys. **C.** Transform tectonic zone.

correlate with higher degrees of melting, depletion of spatially associated peridotites, and the height of the residual geoid reflecting mean ridge depth. Klein and Langmuir (1987) extensively tested this hypothesis by plotting the position of basalt liquidus trends at constant MgO in binary oxide diagrams directly vs. regionally corrected sample depths. They came to the same conclusions, but with greater regional coverage and better statistics. Thus the systematic offset of the majority of the Atlantic II Fracture Zone basalt glasses toward low Ca/(Ca+Mg) in Figure 16 can be reasonably taken to indicate a low overall degree of regional mantle melting beneath the ridge, consistent with its position far from any mantle hot spot.

Gabbros

The dredge collections include the same gabbro types found in Hole 735B: olivine gabbros, gabbros, gabbronorites, ferrogabbros, and microgabbros. Bulk rock and mineral compositions span similar ranges in the two suites. For example, (Mg × 100)/(Mg + Fe) of clinopyroxenes ranges from 60 to 89 in the dredged gabbros and from 57 to 89 in Hole 735B gabbros (Fig. 17). Although the dredged gabbros span a range of composition similar to the Hole 735B gabbros, they do not extend to quite so high iron contents and have a substantially more primitive average composition. This reflects a relative scarcity of ferrogabbro compared to the drilled section. This relationship is probably a product of the particular tectonic environment of the drill site, which penetrated a region where late magmatic iron- and titanium-rich intercumulus liquid was intruded along early shear zones formed in the solidifying gabbro section (Dick et al., Natland et al., Bloomer et al., this volume).

Preliminary results suggest that residual porosities at the time the melt was trapped (estimated from bulk rock compositions) are commonly higher (by up to 35%) in the dredged gabbros than in the drilled suite (P. Meyer et al., pers. comm., 1990). This may reflect higher cooling rates for some of the dredged gabbros because of emplacement nearer the transform.

The dredged gabbros exhibit the same high-temperature, amphibolite-facies, metamorphic assemblages as their drilled counterparts, but exhibit an even more pervasive low-temperature greenschist-facies overprint, with common retrograde assemblages of chlorite, epidote, and prehnite. We attribute the latter to late hydrothermal alteration at high levels in the fault system on which these rocks were uplifted to the seafloor. The lack of greenschist-facies alteration in the Hole 735B gabbros, in turn, results because they were drilled within a major tectonic block, far from the fault systems that bound the blocks.

Peridotites

The abundant peridotites dredged from the fracture zone were extensively point-counted, analyzed, and examined petrographically. Preliminary results were reported in Johnson et al. (1990). All the peridotites are extensively serpentinized, with 50% to 100% replacement of the primary olivine, enstatite, and diopside. Where the olivine was not altered to serpentine, seafloor weathering often reduced it to brown clay. This shows a wide range in primary modal composition lying along the overall trend for the Southwest Indian Ridge, as reported by Dick et al. (1984). The peridotites consist of olivine, enstatite, and chromian diopside, with minor amounts of chrome spinel. However, their average composition is a clinopyroxene-rich lherzolite containing relatively aluminous spinel and pyroxene, which reflects a low degree of mantle melting and depletion compared to other ocean ridge peridotites.

The peridotites are typical residual mantle peridotites, with textures ranging from protogranular to porphyroclastic to mylonitic. The protogranular textures were the earliest formed and are thought to have been produced at high-temperatures during upward flow and in the mantle. The porphyroclastic texture is thought to have been superimposed on the protogranular texture during ductile deformation and lithospheric necking in the shallow mantle beneath the rift valley. The mylonitic textures, in turn, are thought to represent shallow-level normal faulting that was associated with unroofing of the peridotites (and gabbros) and emplacement to the seafloor and into the transverse ridge.

Table 3. Multiple-spot electron microprobe analyses of glasses from survey area.

Sample number	SiO_2	Al_2O_3	FeO	MgO	CaO	Na_2O	K_2O	TiO_2	MnO	P_2O_5	Total	Mg#
RC27-9-1 -1	49.93	15.15	10.45	7.46	11.58	2.91	0.1	1.76	0.14	0.16	99.64	56
RC27-9-1-2	49.79	15.2	10.5	7.37	11.59	2.91	0.1	1.75	0.15	0.16	99.52	55.6
RC27-9-3-17	50.28	15	10.9	6.62	10.35	3.33	0.22	2.35	0.28	0.16	99.5	52
RC27-9-4-24	50.47	15.04	10.45	6.52	10.52	3.47	0.23	2.15	0.24	0.18	99.27	52.6
RC27-9-4-6	50.08	15.93	9.68	7.6	10.72	3.21	0.18	1.75	0.15	0.15	99.45	58.3
RC27-9-5-3	49.33	16.43	10.81	7.16	10.27	3.4	0.19	1.79	0.17	0.14	99.68	54.1
RC27-9-5-4	49.74	15.15	10.8	7.54	10.02	3.19	0.24	2.29	0.25	0.15	99.35	55.4
RC27-9-5-5b	49.47	14.02	12.88	5.22	9.21	3.84	0.39	3.21	0.43	0.16	98.83	41.9
RC27-9-9-9	50.31	16.06	9.19	7.57	11.03	3.13	0.22	1.75	0.18	0.08	99.52	59.5
RC27-9-9-17	50.15	14.97	11.15	6.67	9.82	3.58	0.26	2.23	0.25	0.15	99.23	51.6
RC27-9-12-6	50.27	15.91	9.97	7.01	10.13	3.64	0.23	1.88	0.27	0.17	99.47	55.6
RC27-9-12-10	50.27	15.92	10.24	7.07	10.08	3.43	0.26	1.96	0.25	0.13	99.61	55.1
RC27-9-37-57	49.76	14.33	12.31	6.36	10.28	3.16	0.25	2.39	0.25	0.15	99.25	47.9
RC27-9-37-60	49.98	13.6	12.61	6.03	10.2	3.25	0.23	2.49	0.29	0.21	98.86	46
RC27-9-38-19	51.17	15.56	10.99	6.89	10.86	2.07	0.11	1.99	0.21	0.18	100.02	52.8
RC27-9-42-2	50.16	15.53	9.91	7.85	11.02	2.76	0.15	1.63	0.15	0.12	99.28	58.55
RC27-9-42-4	49.71	16.44	10.01	8.14	10.91	2.81	0.1	1.7	0.16	0.11	100.1	59.2
RC27-9-44-10	49.48	15.26	11	7.05	10.23	3.21	0.14	2.24	0.19	0.13	98.93	53.3
RC27-9-44-11	49.57	16.03	9.97	8.29	11.04	2.86	0.13	1.72	0.15	0.14	99.9	59.7
RC27-9-44-3	49.67	15.79	9.96	8.18	10.98	2.7	0.1	1.75	0.16	0.15	99.44	59.42
RC27-9-44-4	49.51	15.73	9.96	8.3	10.9	2.93	0.1	1.72	0.17	0.16	99.47	59.76
RC27-9-44-7	49.9	15.15	10.5	7.81	10.41	3.1	0.15	2.05	0.25	0.17	99.48	57
RC27-9-47-1	49.45	14.85	11.12	7.77	10.34	3.26	0.12	2.07	0.22	0.18	99.39	55.5
RC27-9-47-4	49.37	15.01	11.6	7.79	10.23	3.06	0.14	2.19	0.18	0.15	99.73	54.5
RC27-9-47-5	50.07	15.89	10.06	8.01	11.03	2.89	0.09	1.68	0.14	0.15	100	58.6
RC27-9-47-6	49.69	15.82	10.08	7.92	11.05	2.91	0.1	1.69	0.13	0.14	99.53	58.3
RC27-9-47-8	49.68	15.81	9.97	7.91	11.09	2.87	0.1	1.68	0.14	0.14	99.38	58.6
[a]Standards												
USNM 113716	51.32	15.33	8.96	8.22	11.43	2.67	0.06	1.29	0.11	0.15	99.54	62
VGA-99	50.73	12.53	12.96	5.18	9.2	2.55	0.82	3.9	0.45	0.17	98.5	41.6
VG-2	51.14	13.9	12.03	6.75	1 0.63	2.7	0.21	1.9	0.25	0.2	99.72	50

[a]These standards are referenced in Jarosewich, E., Nelson, J.A., and Norberg, J.A., 1979. Reference samples for electron microprobe analysis. *Smithson. · Contrib. Earth Sci.*, 22:68-72.

MAGNETIC SURVEY

Character of the Magnetic Anomalies

Thirteen long lines in the survey run parallel to the transform and describe the magnetic anomaly field over a 300- × 50-km area centered on the fracture zone. Average line spacing is on the order of 4 km. These lines show well-developed linear anomalies in a direction orthogonal to the fracture zone. These anomalies lose amplitude and character toward the fracture zone (Fig. 18A).

The central anomaly can be recognized over both the western and eastern rift valleys. The amplitude of the central anomaly over the western rift valley decreases consistently as one approaches the ridge-transform intersection. Over the eastern rift valley, this attenuation is less dramatic. The central anomaly is highly skewed so that the southern minimum and the northern maximum in the anomaly coincide approximately with the southern and northern edges of the Brunhes normal magnetization (age = 0.73 Ma). The estimated skew of the central anomaly away from the fracture zone is of the order of 60°, which is in agreement with theoretical predictions that assume (1) two-dimensional sources oriented in an east-west direction, (2) the ambient magnetic field at this location (inclination = −50°, declination = −20°), and (3) a source magnetization parallel to a geocentric axial dipole field (inclination = −60°, declination = 0°). Figure 18B shows the same anomalies as Figure 18A, but with the estimated skew of 60° removed.

Toward the fracture zone, the skew of the central anomaly changes. This might be caused by the following:

1. An edge effect resulting from truncation of the Brunhes normal source at the fracture zone.
2. An asymmetric "emplacement" of the magnetic source in the vicinity of the Kane Fracture Zone.
3. Rotation of the magnetic source subsequent to its emplacement in the vicinity of the fracture zone.

Marine Magnetic Anomaly Identification

The linear magnetic anomalies north of the western rift valley and south of the eastern rift valley correlate well with one another out to 110 km from the rift valley. These anomalies can be identified as anomaly sequences 1 (central anomaly) through 5 (8.92–10.42 Ma). We used the revised geomagnetic polarity time scale of Kent and Gradstein (1986) and found an average half spreading rate of 10 km m.y.$^{-1}$ (1.0 cm m.y.$^{-1}$ for both limbs (see plot of magnetic anomaly age vs. distance in Fig. 19). Regional estimates for the Southwest Indian Ridge indicate a total spreading rate on the order of 15 to 16 km m.y.$^{-1}$ (e.g., Sclater et al., 1981). Thus, there is a suggestion that both limbs of the fracture zone should be accreting asymmetrically.

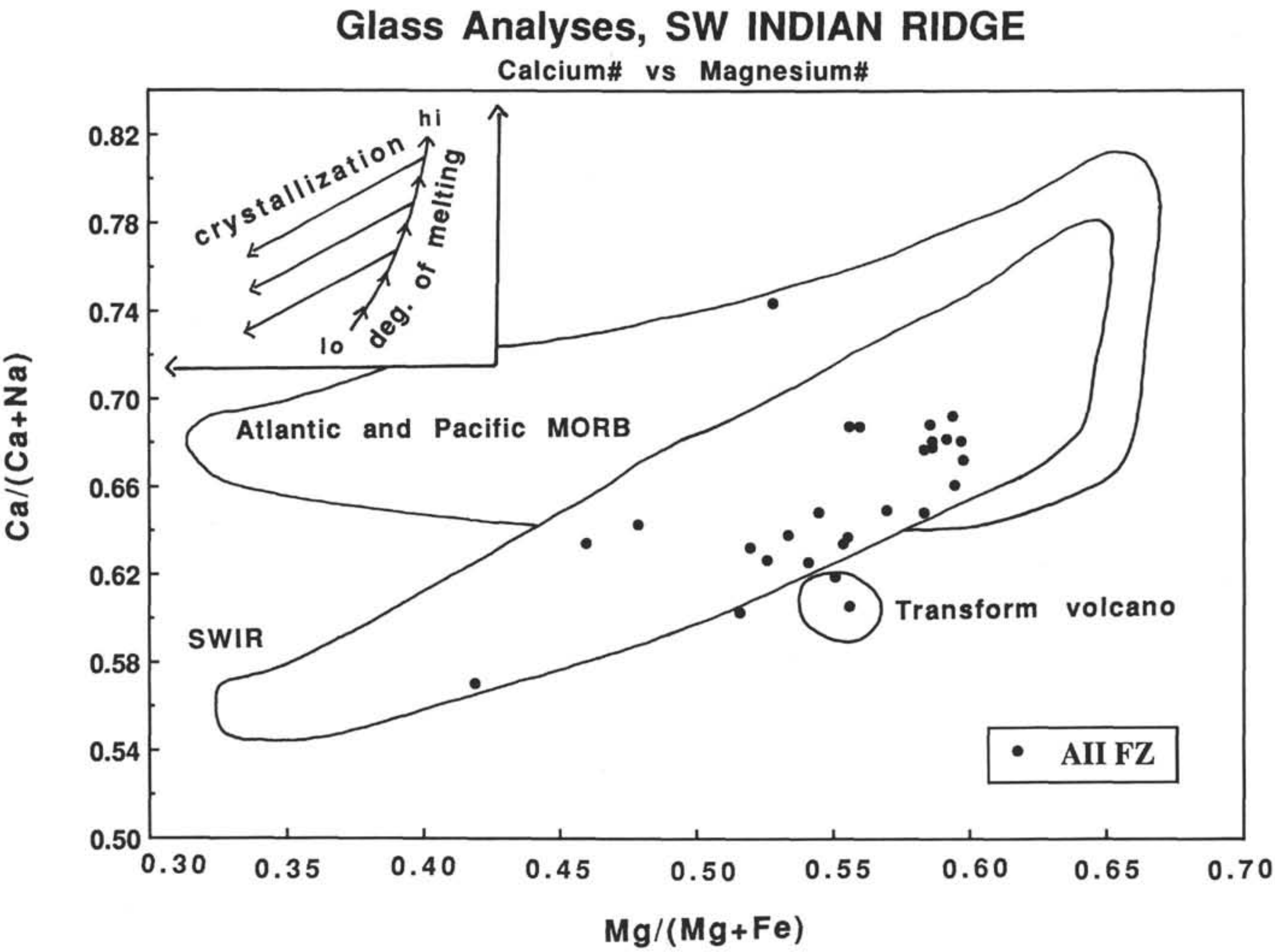

Figure 15. Plot of alkalies vs. silica for basalt glass analyses from the Atlantis II Fracture Zone and adjacent regions. Discriminant line dividing composition field of alkaline basalts (above) from that for subalkaline and tholeiitic basalts (below) shown for reference from Macdonald (1988).

Assuming that the regional estimates are correct, this implies that the anomalies north of the eastern limb (Lines 14, 15, and 16 in Fig. 18) would include anomalies 5 and 5A. Figure 19 depicts a plot of the total anomaly separation vs. age and an average total spreading rate of 15.7 km m.y.$^{-1}$).

On the individual lines, minor spreading-rate changes can be detected near anomalies 2a and 3a, but the analysis is not yet conclusive.

Identification of the older anomalies presents a serious problem. Our best-fit model (preferred model to date) for the anomalies north of the western rift valley is given in Figure 20. This model uses 9.8 km m.y.$^{-1}$ from 0 to 16.55 Ma (anomaly 5c), 5.0 km m.y.$^{-1}$ from 16.55 to 25.50 Ma (anomaly 7y; "y" = the younger edge of the normal polarity period, "o" = the older edge) and 10.8 km m.y.$^{-1}$ to 35 Ma, or older than anomalies 11 and 12.

The synthetic anomalies in Figures 20 and 21 have been smoothed with a Gaussian filter (standard deviations 2 and 4 km), simulating magnetic source emplacement and common practice when modeling anomalies over slow-spreading ridges in general and the Indian ridges in particular (e.g., Tapscott et al., 1980; Sclater et al., 1981). The lower standard-deviation simulation provides a better correlation with the younger sequence, while the high standard-deviation simulation correlates better with the older sequence. A period of very slow spreading (i.e., 5 km m.y.$^{-1}$ from 16.5 to 25.5 Ma) should confirm the findings of H. Bergh (unpubl. data, 1990), who postulates a spreading hiatus sometime between anomalies 5B and 11.

The anomalies south of the eastern rift valley, however, cannot be modeled in the same manner. Figure 21 shows our present best-fit model. The fit is reasonable out to anomaly 6, with a uniform spreading rate of 7.85 km m.y.$^{-1}$ from anomaly 6 to anomaly 3a. The fact that this should show no hiatus or period of slow spreading around anomaly 6 also makes the previous identification suspect. However, the younger anomalies (5 and younger) both south and north of the eastern rift valley are well modeled and tend to confirm the consistent accretion asymmetry over the last 10 m.y. Anomalies older than 6 do not fit at all, so that the anomaly 6 identification itself becomes suspect. Further analysis and modeling definitely will be required.

In summary, our identifications are reasonable out to anomaly 5A. Total spreading rates measured on lines across the eastern rift valley agree with regional estimates, and an average asymmetry of accretion of 10/6 (S/N) over the last 12 m.y. (5A) is well established. Identification of older anomalies remains inconclusive, although the model for anomalies north

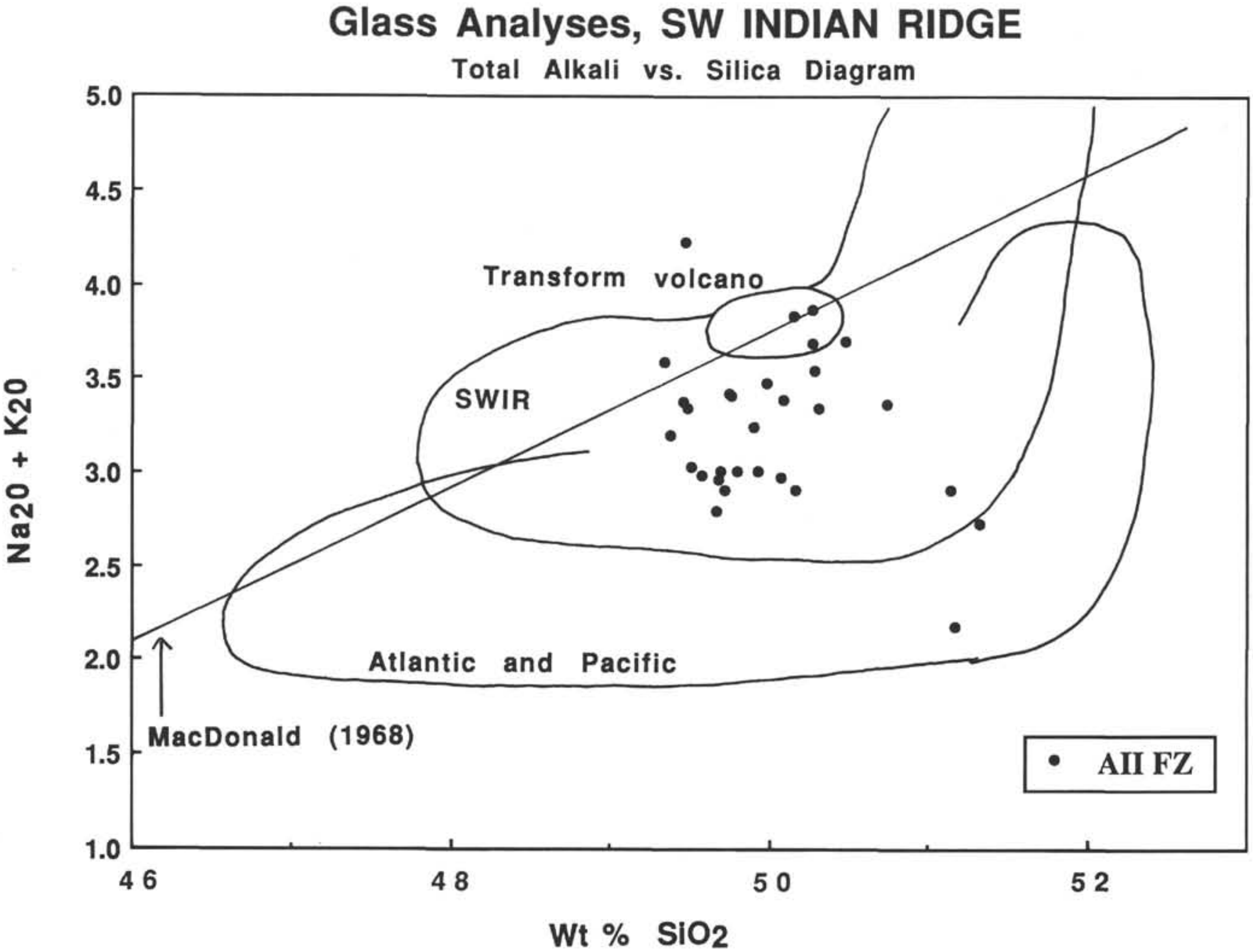

Figure 16. Plot of calcium number vs. magnesium number for basalt glass analyses from the Atlantis II Fracture Zone and adjacent ridge segments. Inset shows the relative effects of varying the degree of melting in the mantle source and fractional crystallization at shallow depths on the composition of the liquid. Increasing the degree of mantle melting produces a relatively small change in magnesium number, but a large change in calcium number because of imcompatible behavior of sodium during melting, whereas fractional crystallization produces a larger effect on the magnesium number. Thus, for a given magnesium number, a basalt having a higher calcium number is the product of higher degrees of mantle melting (Dick et al., 1984; Schouten et al., 1987; Klein and Langmuir, 1987). Thus, the Atlantis II basalts, the transform volcano in particular, are the products of relatively low degrees of mantle melting, compared to Atlantic and Pacific MORBs and to most other Southwest Indian Ridge basalts.

of the western rift valley (Fig. 20) appears good and particularly effective for simulating the distinct linear anomalies observed near the northern end of the lines that we model with anomalies 7, 8, 9, and 10.

Character of the Anomalies Near the Transform

The magnetic lineations west of the fracture zone (Lines 1, 4 through 8, and 9a) show a convincing correlation from anomalies 1 to 5. This includes Line 9A, which runs almost along the postulated transform. Lines 8 and 9A have subdued amplitudes and are over the deep fracture zone valley, where, based on the dredge results and the seafloor morphology, the extrusive carapace appears totally absent, and they are far from the truncation of this carapace.

To determine if these anomalies may have been caused by the edge effect of a truncated magnetic anomaly source layer, we determined the extent of such an edge effect. Here, we model a truncated magnetic-anomaly source layer (3–4 km depth), shown in Figures 22A and 22B. At the bottom of the figure, the magnetic polarities of the truncated two-dimensional source are depicted. Shown are 21 synthetic magnetic anomaly profiles, 2 km apart and parallel to the truncation, and perpendicular to the magnetic stripes. Synthetic Line 11 runs right along the edge. One can see that synthetic Line 9 has similar amplitudes as the lines having lower numbers, indicating that at 4 km from the edge, the magnetic lineations feel a negligible edge effect. In other words, on the side of the source, the truncation is not felt until one is 4 to 6 km from the edge. This effect is quantified in Figure 22C.

Similarly, synthetic Lines 12 and 13 (2 and 4 km from the edge) show the edge effect, but in Line 14 (at a distance of 6 km), little is left. Consequently, for a shallow source layer (in this case, between 3 and 4 km), the edge effect dies out rapidly with distance to the edge. In the case of an even shallower source layer, this occurs even more rapidly; for a deeper source layer, more slowly. Thus, we conclude that if the anomalies on Lines 9A and 8 are more than 6 km from the truncated extrusive carapace, an edge effect can be ruled out, and we must assume

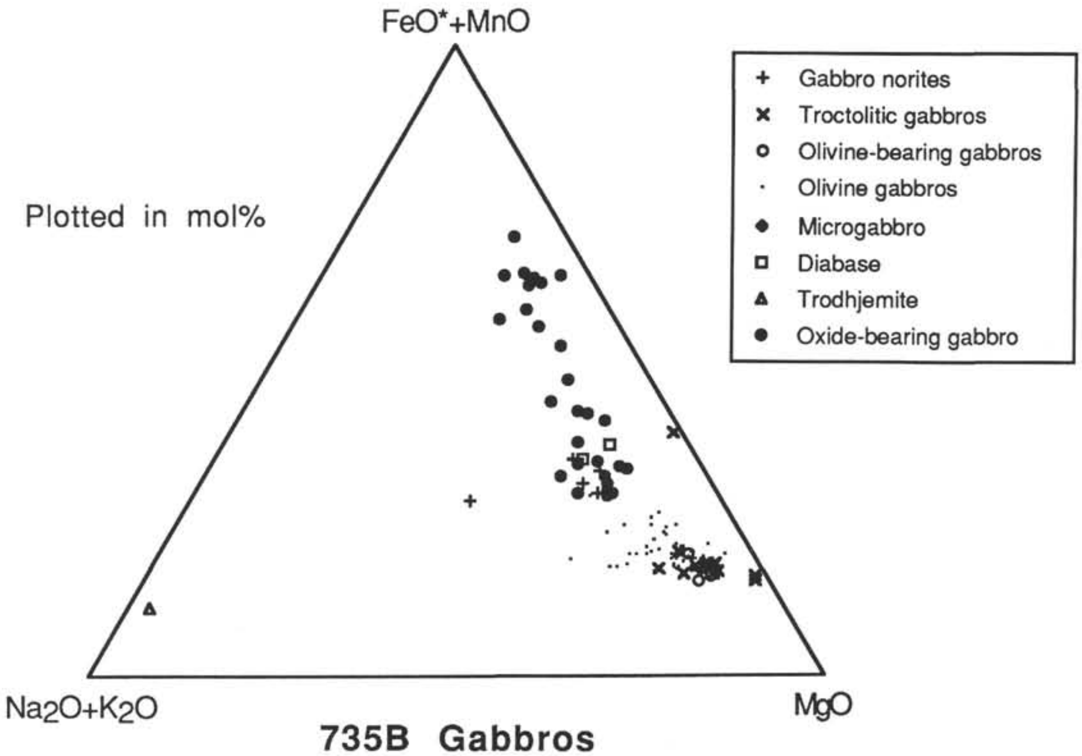

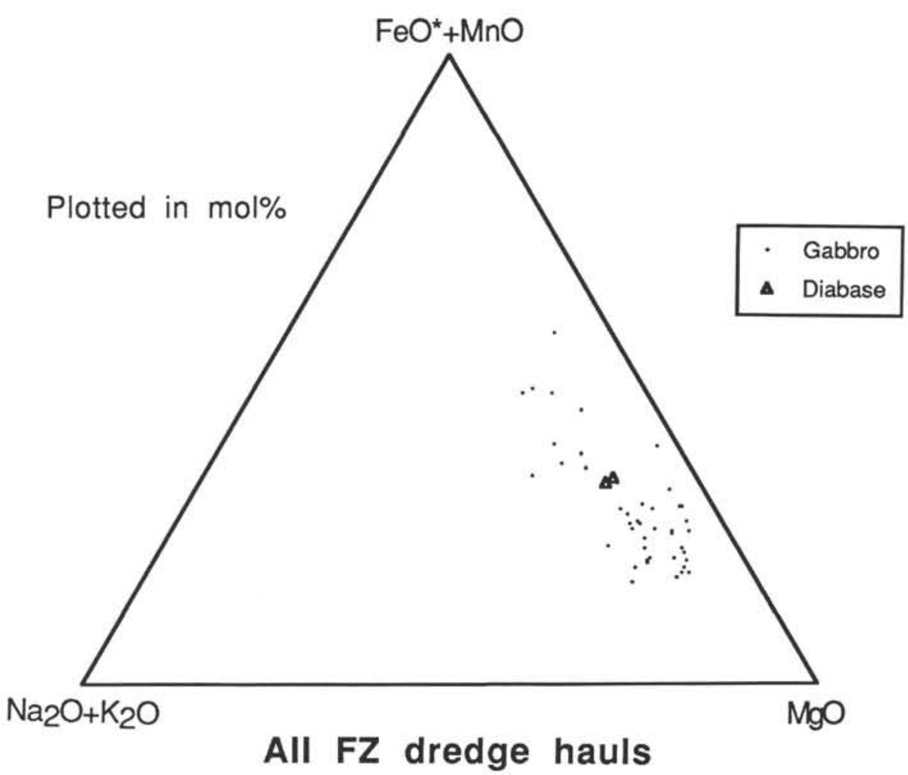

Figure 17. AFM diagrams for XRF whole-rock analyses of Hole 735B gabbros from the shipboard data and of gabbros dredged from the Atlantis II Fracture Zone during the site survey (P. Meyer, unpubl. data, 1990).

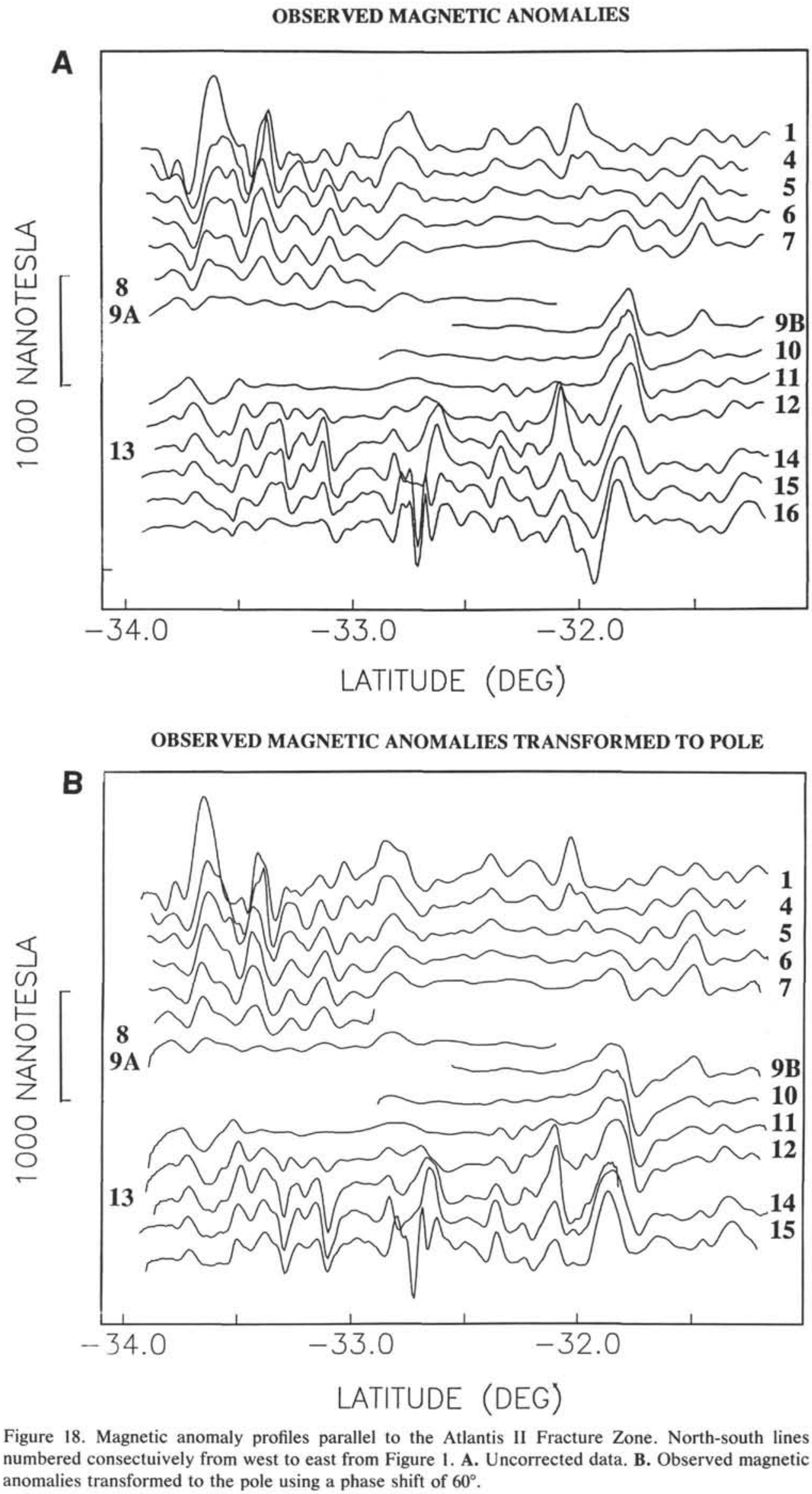

Figure 18. Magnetic anomaly profiles parallel to the Atlantis II Fracture Zone. North-south lines numbered consectuively from west to east from Figure 1. **A.** Uncorrected data. **B.** Observed magnetic anomalies transformed to the pole using a phase shift of 60°.

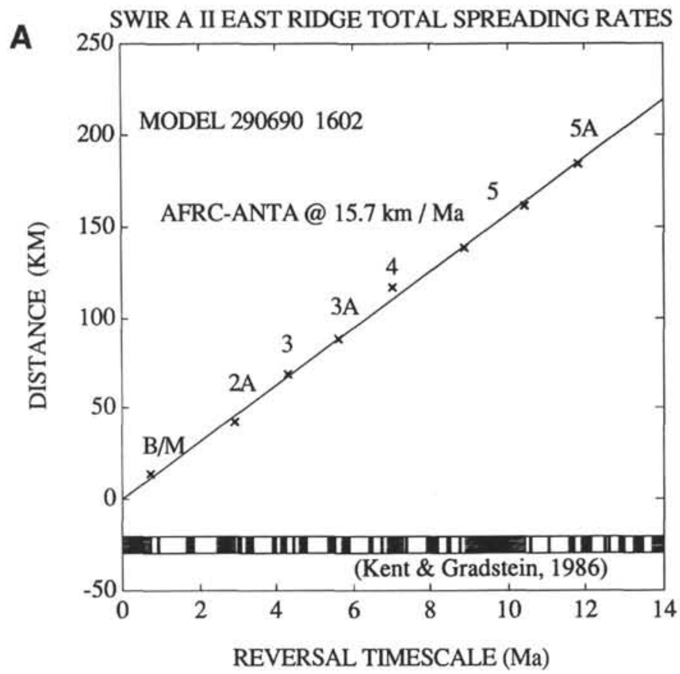

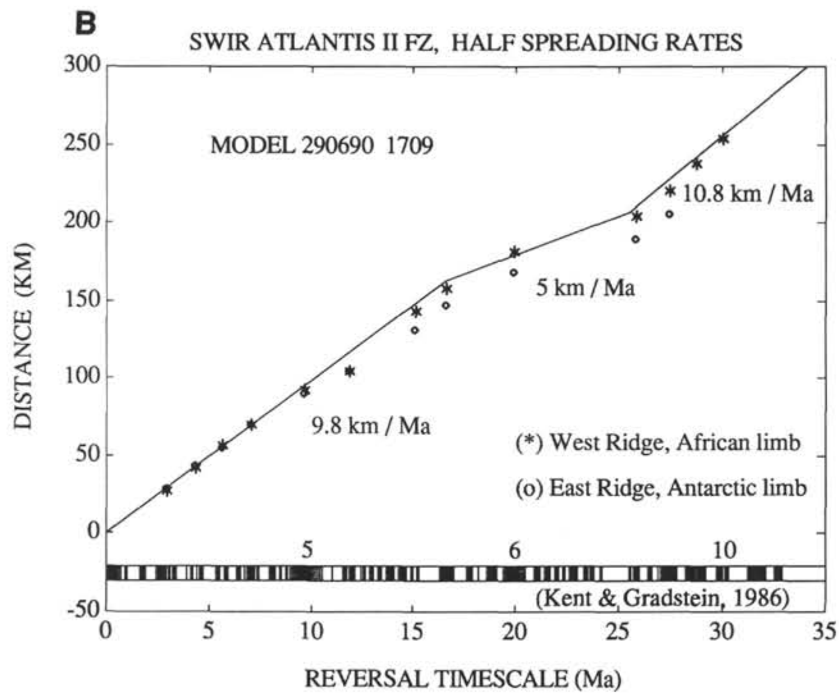

Figure 19. Magnetic anomaly age vs. distance. **A.** Atlantis II East Ridge: total spreading rates. Average age and distance between conjugate anomalies north and south of the East Ridge spreading axis indicate a total Africa-Antarctica spreading rate of ~16 km m.y.$^{-1}$. **B.** Atlantis Fracture Zone: half spreading rates. Average age and distance from the rift valley axis of the magnetic anomalies flanking the transform. Symbols explained in the figure. Solid lines and spreading rates represent the best-fit model for the anomalies north of the western rift valley shown in Figure 20. Half spreading rates of the African limb north of the western rift valley and of the Antarctica limb south of the eastern rift valley are each ~10 km m.y.$^{-1}$. Because the total Africa-Antarctica spreading rate is ~16 km m.y.$^{-1}$, both ridges must be spreading asymmetrically.

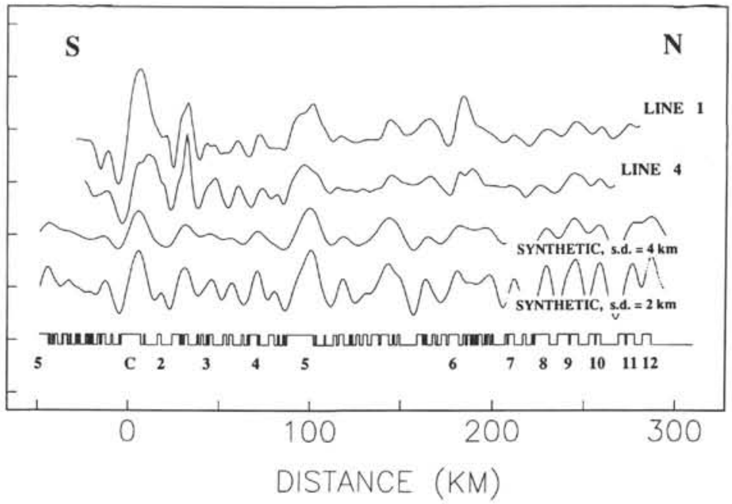

Figure 20. Best-fit model for the magnetic anomalies north of the western rift valley (Lines 1 and 4 on the African limb). Boxcar model shows the geomagnetic reversal source with anomaly numbers indicated C = central anomaly. Spreading rates for this boxcar model are presented in Figure 19B and in the text. Other source parameters for the synthetic anomalies are (1) top of magnetic layer at 3 km and bottom at 4 km, (2) magnetic anomaly skew is 60°, and (3) standard deviations (s.d.) are 2 and 4 km for Gaussian filters that simulate the emplacement process. We consider anomaly sequence C through 5 to be a reliable fit. Tick marks on the vertical axis = 500-nT intervals.

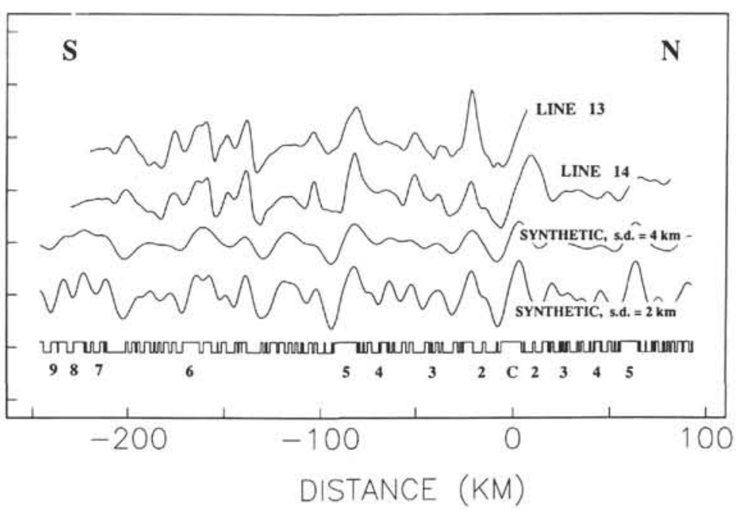

Figure 21. Best-fit model for the magnetic anomalies south of the eastern rift valley (Lines 13 and 14 on the Antarctica limb). Boxcar shows the geomagnetic reversal source with anomaly numbers indicated. C = central anomaly. Spreading rates for this boxcart model are presented in and in text. Other source parameters for the synthetic anomalies are (1) top of magnetic layer at 3 km and bottom at 4 km, (2) magnetic anomaly skew is 60°, and (3) standard deviations (s.d.) are 2 and 4 km for Gaussian filters that simulate the emplacement process. We consider anomaly sequence C through 5 to be reliable fit. Tick marks on the vertical axis = 500-nT intervals.

that the gabbroic section contains a magnetic source that records Earth's magnetic field reversals with reasonable fidelity (i.e., a narrow "magma chamber"). Such a source is consistent with the magnetic properties of the gabbro recovered from Hole 735B (Kikawa and Pariso, this volume).

Should there be a magnetic source in the fracture zone, how does it compare to the source away from the fracture zone? In Figure 23, we show magnetic Line 1 away from the fracture zone (and Line 9A for comparison), which continues upward to 4 km in steps of 1 km. If the average depth of

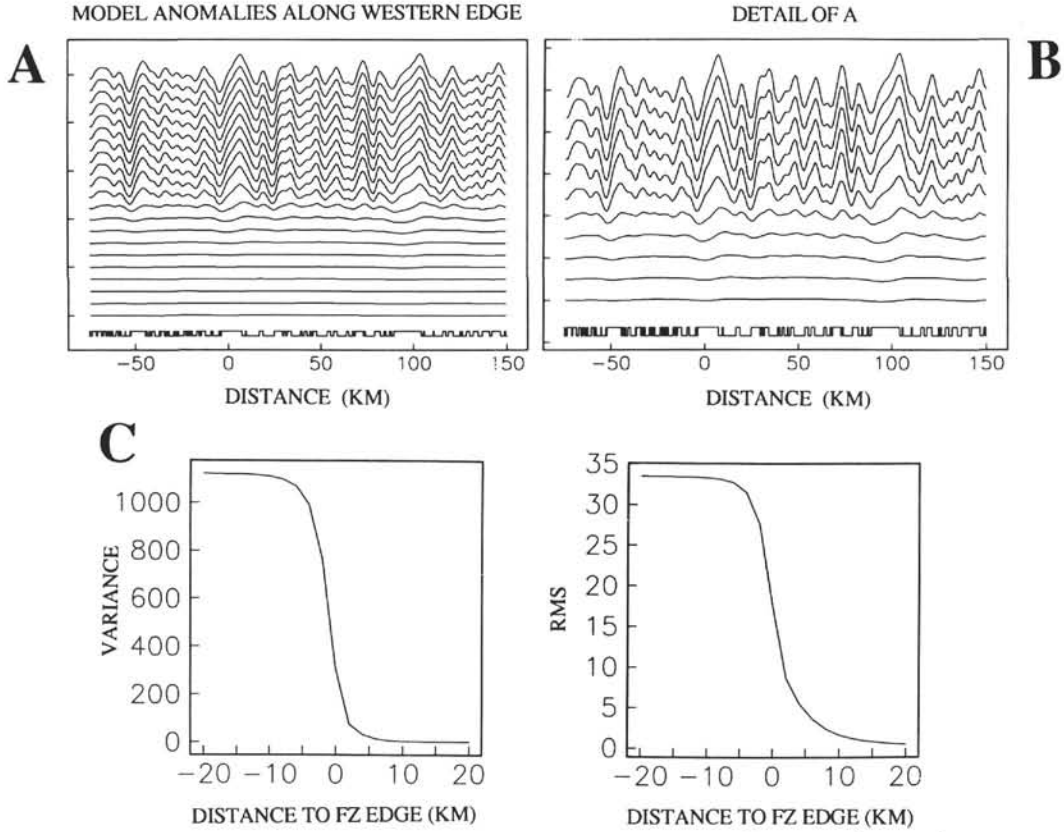

Figure 22. Forward models of magnetic anomalies caused by truncation of the magnetic anomaly source layer at the edge of a transform valley. **A.** The synthetic profiles are 2 km apart, parallel to the transform. The edge of the truncated magnetic source lies beneath the 11th profile from the top of the figure. **B.** Detail of (**A**), showing a blow-up of the synthetic profiles nearest the edge (now beneath 6th profile from the top of the figure). **C.** Variance and root-mean-square values for the profiles shown in (**B**), plotted vs. the profile distance from the edge that show the edge effect is negligible when farther away than 4 to 6 km from the edge.

the first 100 km near the ridge is 2 km, and if the average depth below Line 9A (bottom) is 6 km, then the source of Line 1 at a depth of 6 km would have produced an anomaly having a 4-km upward continuation. When comparing those lines to Line 9A, one can see that some anomalies are more pronounced and some are less. This qualitatively suggests that the magnetic source under Line 9A should be more or less of the same strength as the source under Line 1. In other words, this suggests that the absence or presence of an extrusive carapace does not matter much.

To show all this in a more straightforward fashion, we must model a three-dimensional inversion of magnetic anomalies in the presence of topography. This will eliminate the topographic effects and yield the strength and character of the magnetic source.

DISCUSSION

Plate Tectonic Evolution of the Atlantis II Fracture Zone

Magnetic anomalies east and west of the active transform give spreading rates for both transform walls of 1 cm/yr. The total spreading rate of 1.6 cm/yr for the Southwest Indian Ridge (Tapscott et al., 1980) thus requires asymmetric spreading at both the eastern and western rift valleys, with rates of 0.6 cm/yr away from the transform to complement the rates measured for the transform walls. This means that the Atlantis II transform fault is growing at a rate of 0.4 cm/yr, with a slip rate of 1.2 cm/yr, and a total age offset of 20 m.y.

Transtensional Transform Basins

The major counterclockwise shift in spreading direction of the Southwest Indian Ridge is suggested by the trace of the Atlantis II Fracture Zone, which changed from N10°E azimuth to due north-south, at 17 to 20 Ma (Fig. 11). Such a shift in plate motion places a left-stepping transform under extension (Menard and Atwater, 1968; van Andel et al., 1971), forcing reorganization of the plate boundary. This shift in spreading direction should force the spreading center axes to propagate progressively across the fracture zone valley and against the truncating lithosphere. In the case of the Atlantis II Fracture Zone, where the lithosphere into which the ridge axis attempts to propagate across the old fracture zone is old, thick, cold, and correspondingly strong, the ridge may be unable to propagate into the older lithosphere. Thus, adjustment in the plate boundary may not occur instantaneously.

A simplified model for this scenario is shown in Figure 24. Here, propagation of the ridge axes across the fracture zone stops at the old transform walls that bound older lithosphere. However, the position of these walls migrates progressively away from the propagating ridge axes as spreading continues, because their traces are oblique to the newly forming transform (Fig. 24B). This allows the ridge axes to extend continuously with time until they reach the point at which they oppose one another on a lithospheric flow line. Over the time necessary for the ridge axes to propagate to where they

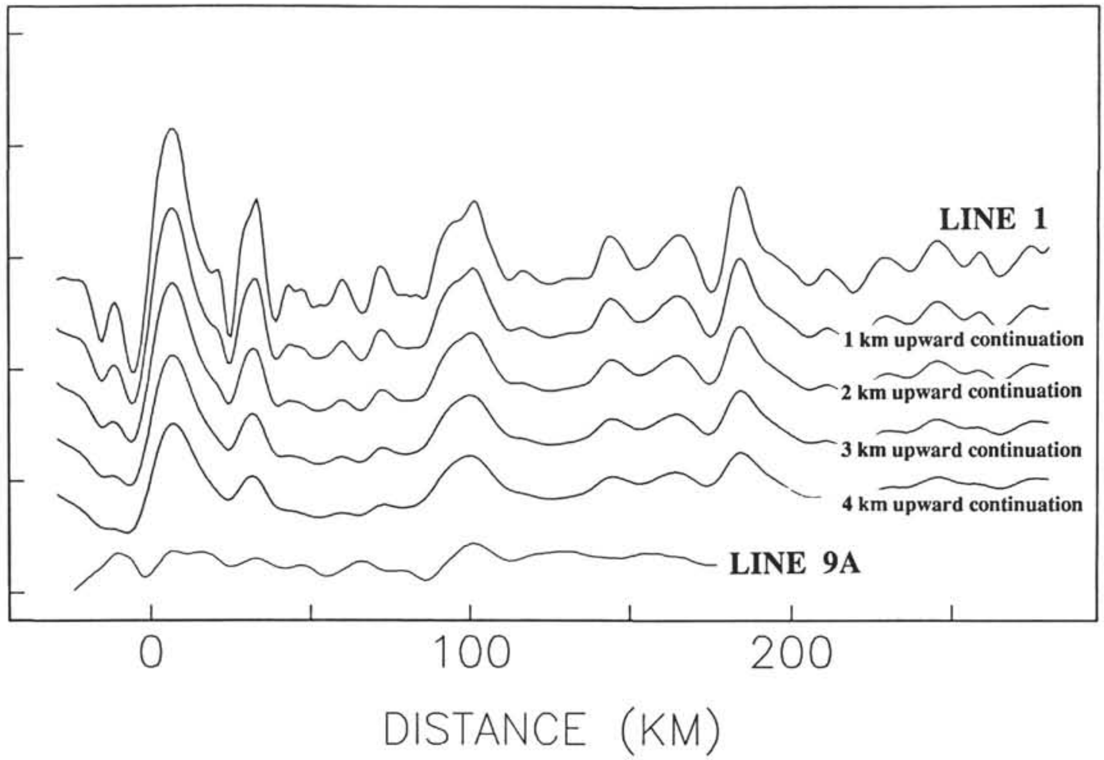

Figure 23. Magnetic anomaly Line 1, farthest from the fracture zone, upward continued to 4 km in steps of 1 km, compared with the anomalies of Line 9A, which runs near the active transform in the deepest part of the fracture zone valley. Tick marks on the vertical axis = 500-nT intervals.

are directly connected along a single strike-slip fault, extension will occur across the old transform valley to form a transtensional basin. Once extension ceases, this transtensional basin should be split by the new transform fault into two halves, which should spread in opposite directions with the opposing plates. Roest and Collette (1986) recently proposed the same explanation for formation of a tympanum-shaped basin in the 15°20′ fracture zone in the North Atlantic.

This model fits well the present-day morphology of the Atlantis II Fracture Zone. It also explains several features that previously were inexplicable. In the case of the Atlantis II transform, most of the transtensional basin created in the transform during plate readjustment has been captured by and spread to the north with the African Plate. Only a small portion of this basin, whose remnant can be seen as the eastern sediment pond in the southern half of the transform, has been captured by the Antarctic Plate. Thus, ridge propagation across the old transform zone during plate readjustment has not been equal at the northern and southern ridge-transform intersections, but may have been more pronounced at the southern. Presuming that the transform wall (which we think formed by uplift at the ridge-transform intersection) provides a trace of the ridge position with time, the pronounced curve of the western transform wall may suggest that the change in spreading direction or rate of ridge propagation across the old transform zone was not totally instantaneous, but may have occurred intermittently over some length of time. Based on the morphology of the eastern transform wall, the eastern ridge axis seems to have propagated westward in two small jumps, producing its westward-stepping character.

For an instantaneous change in spreading direction, the rate of extension across the transform should be equal to the total slip rate on the transform times the tangent of the angle between the old and new spreading directions. For the Atlantis II Fracture Zone, this is an extension rate of 0.2 cm/yr and requires formation of 23 km of new crust across the transform during the 11 m.y. that it took the simple orthogonal transform-ridge geometry to be reestablished. If the change in spreading direction were gradual, however, taking place over the entire 11 m.y. of plate accommodation, then the total extension should be greatly reduced because the extension rate across the transform is directly proportional to the angle between the old and new spreading directions. In this latter case, where the angle between old and new spreading rates is always instantaneously small, then the total extension across the transform should be negligible.

The transform floor near the ridge-transform intersections is narrow and V-shaped, and its present width can be assumed to be less than 1 km. This can be assumed, in the absence of any evidence for recent plate motion changes, to represent the normal width of a transform valley where pure strike-slip motion is occurring. In contrast, the western branch of the Atlantis II transform basin, as measured from the foot of the western wall across the northern median tectonic ridge to the present-day slip zone, and the width of the narrower, old, southern transform basin, as measured from the foot of the eastern transform wall to the slip zone, add up to a maximum of about 20 km. This is a figure very near the 23 km calculated for extension over an 11-m.y. period of plate readjustment to accommodate an instantaneous change in spreading direction.

The slope of the western transform walls flanking the large northern transtensional basin is noticeably less steep than the eastern wall flanking the narrow, southern transtensional basin, suggesting that extension across the transform was asymmetric and that, consequently, the former wall was more modified by faulting that accompanied transtension. Overall, however, these walls appear to be basically intact, with a

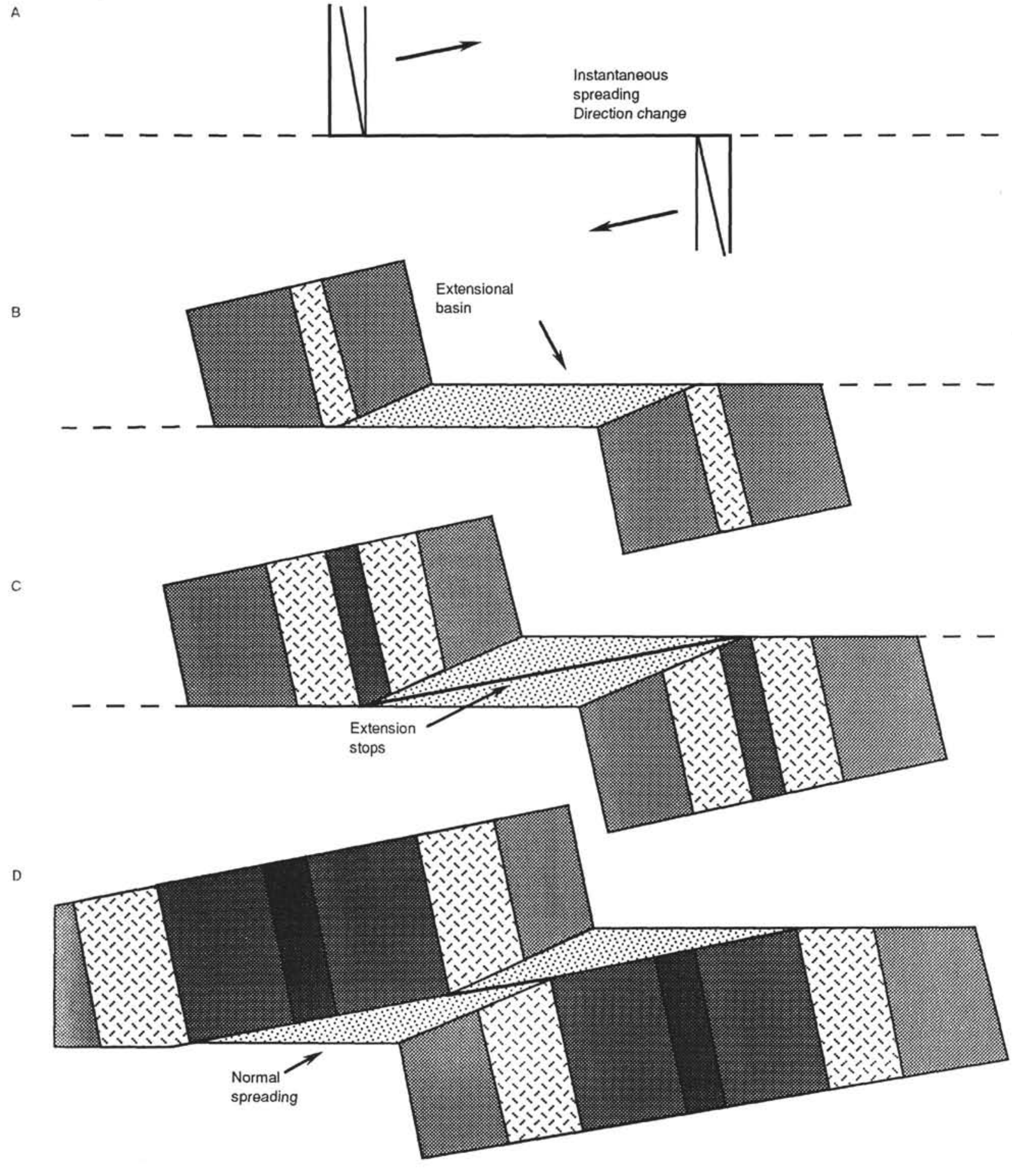

Figure 24. Formation of a transtensional basin following an extensional change in spreading direction at a hypothetical fracture zone. **A.** Instantaneous change showing reorientation of rift valley and new spreading direction (thick arrows). **B.** Extensional basin and propagation of spreading centers limited by the rate at which old lithospheric plate boundary migrates to the south and north with spreading. For an instantaneous change in spreading direction, the rate of extension orthogonal to the old transform fault is a constant. The rate of spreading across the basin is equal to the total transform slip rate times the tangent of the angle of the change in spreading direction. For the Atlantis II Fracture Zone, assuming an instantaneous change in spreading direction, the opening rate across the basin should be 0.21 cm/yr. **C.** Point at which the opposing spreading centers are aligned and a simple orthogonal geometry is established. At this point, the extension across the transform ceases. **D.** With continued spreading after extension has stopped, the transtensional basin splits in half and spreads away from the transform with the opposing plates.

geometry in cross section similar to the transform walls near the ridge-transform intersection formed long after the change in spreading direction. Thus, most of the extension appears to have occurred across the narrow zone at the floor of the old transform. This might create a zone of highly extended and thinned crust and probably may result in direct solid-state emplacement of mantle to the seafloor. The crust and mantle rocks in this zone probably should be heavily sheared and tectonized.

A significant feature of the magnetic anomalies mapped during the site survey (and shown in the tectonic map in Fig. 11) is that they can be traced down both the eastern and western transform walls and across the transform valley floor up to the inferred zone of transform-slip from anomalies 1 to 2A. The termination of these anomalies fits with the morphotectonically inferred slip zone and constrains the present position of the transform fault. However, some of the older magnetic anomalies can be traced from the rift mountains over the transverse ridges to the foot of the transform wall, but not across the sediment ponds or the median tectonic ridge to today's slip zone. In the model above, however, the sediment ponds represent the two halves of the transtensional basin that formed during plate readjustment. The crust beneath these basins should have undergone continuous faulting, extension, penetration of seawater, hydrothermal alteration, and mantle diapirism over the 11-m.y. period of plate readjustment. Such a process should obliterate any coherent magnetic anomalies previously existing in the old transform crust and create a zone of relatively low, net magnetization. This might explain the two nonsymmetric magnetic quiet zones over the sediment ponds and median tectonic ridges. Thus, we can use magnetic anomalies to constrain the time at which plate readjustment stopped and the new transform fault was created. This time, when the fracture zone stopped evolving and assumed its present simple geometry, should be between anomalies 5 and 2A.

Median Tectonic Ridges

The transtensional spreading described above also explains another enigmatic feature: median tectonic ridges. We suggest that these ridges are composite structures that were produced by repeated serpentinite diapirism along the transform slip zone through the floor of the fracture zone along the zone of strike-slip faulting. At 32°22′S, a series of three small oblong highs are each oriented at about 20° from the strike of the fracture zone and connect to form a zigzag ridge that may have been produced by serpentinite diapirism along conjugate faults. These faults were probably produced by a shear couple in the transform slip zone across a resistant block. Other marine geologists who have examined median tectonic ridges have proposed essentially this same hypothesis (e.g., Miyashiro et al., 1968; Bonatti and Honnorez, 1976; Macdonald et al., 1986; Pockalny et al., 1988). However, these ridges are not universally well developed at ocean transforms, and no explanation previously existed for why they did not run the length of the transform valley, but rather appear to terminate within it.

Examination of SeaBeam data for the Oceanographer and Atlantis fracture zones in the North Atlantic shows that both of these lack large median tectonic ridges, even though they lie near, and have offsets similar to, the Kane Fracture Zone. However, both of these zones are right-lateral offsets of the ridge axis, while all the fracture zones we examined having median tectonic ridges (e.g., the Vema, Kane, and Atlantis II) are left-lateral offsets. The same change in spreading direction that should place a left-lateral offset transform into extension and form a transtensional basin also places a right-lateral transform into compression. We think that this is the critical difference to explain the presence or absence of median tectonic ridges in the transform valley.

In our model, the crust in a transform is extensively thinned during plate readjustment and formation of an amagmatic transtensional basin as a result of an extensional spreading direction change. As a result, the mantle is probably present at shallow depth, and water should have ready access to it during faulting and shearing in the transform. Thus, hydrothermal alteration and serpentinization of the mantle should be extensive. Because serpentinization of peridotite is not a constant volume process, and can involve an expansion of up to 30% to 40% (Macdonald and Fyfe, 1985), the median tectonic ridges have been interpreted as pressure ridges that form parallel to the fracture zone axis during serpentinization of the mantle in areas of transtensionally thinned crust.

As a transtensional basin is split in half by the formation of the new transform fault at the end of plate readjustment (and each half migrates in the opposite directions), it is juxtaposed against new, much thicker, less permeable crust that forms at the opposing spreading center. Because the thickness of new basaltic crust forming on the floor of the fracture zone after plate readjustment can be considerable, it is reasonable that much less serpentinization will occur within it than in the old extended crust juxtaposed against it by the transform fault. Thus, the northern and southern median tectonic ridges at the Atlantis II Fracture Zone each have formed by preferential hydration of the mantle in old extensional crust that is situated on opposite sides of the transform fault zone. This explains why a 4-km offset lies between the two ridges and accounts for their antisymmetric disposition across the fault zone. It also explains why recent uplift still may be occurring, because hydration should be an ongoing process until the two halves of the old extensional transform basin spread out of the present-day transform tectonic zone.

Low-Angle Normal Faulting, Crustal Dismemberment, and the Evolution of Transverse Ridges

Both dredging and bathymetry show a remarkable contrast in the crust that is spreading in opposite directions away from the neovolcanic zones at the Atlantis II Fracture Zone. This asymmetry is remarkably similar to that previously documented at the Kane Fracture Zone (Karson and Dick, 1983). The transform walls consist of huge blocks of unroofed plutonic rocks that have been uplifted as shallow as 700 m (such as at Hole 735B), constituting steep transverse ridges, while pillow basalts are only rarely exposed. In contrast, the nontransform walls appear to preserve a nearly intact basaltic carapace, rarely shoal to less than 3000 m, and are formed by the ridge-parallel valleys and ridges of the Southwest Indian Ridge rift mountains, gently sloping downward to meet the adjoining wall of the fracture zone. The transform walls can be interpreted as a series of steep, high-angle faults, while the nontransform walls may be simply old, uplifted rift valley floor, back-tilted to form ridge parallel ridges with valleys and having many small seamounts and volcanic features. On the floor of the transform adjacent to the neovolcanic zone, a deep nodal basin has formed that contains plutonic rubble, while in the opposite direction, in the inactive trace of the fracture zone, a relatively intact volcanic carapace is preserved and uplifted to form low rift mountains.

These observations suggest a fundamental tectonic process that locally unroofs the ocean crust and exposes its deeper levels on the transform walls (Dick et al., 1981, 1988; Dick, 1989; Karson and Dick, 1983). A possible mechanism for this might be the formation of a crustal weld between old lithosphere and new crust across the ridge-transform intersection. This weld should exist only at shallow levels because of rapidly decreasing viscosity and increasing temperature with depth at the ridge-transform intersection. This might result in

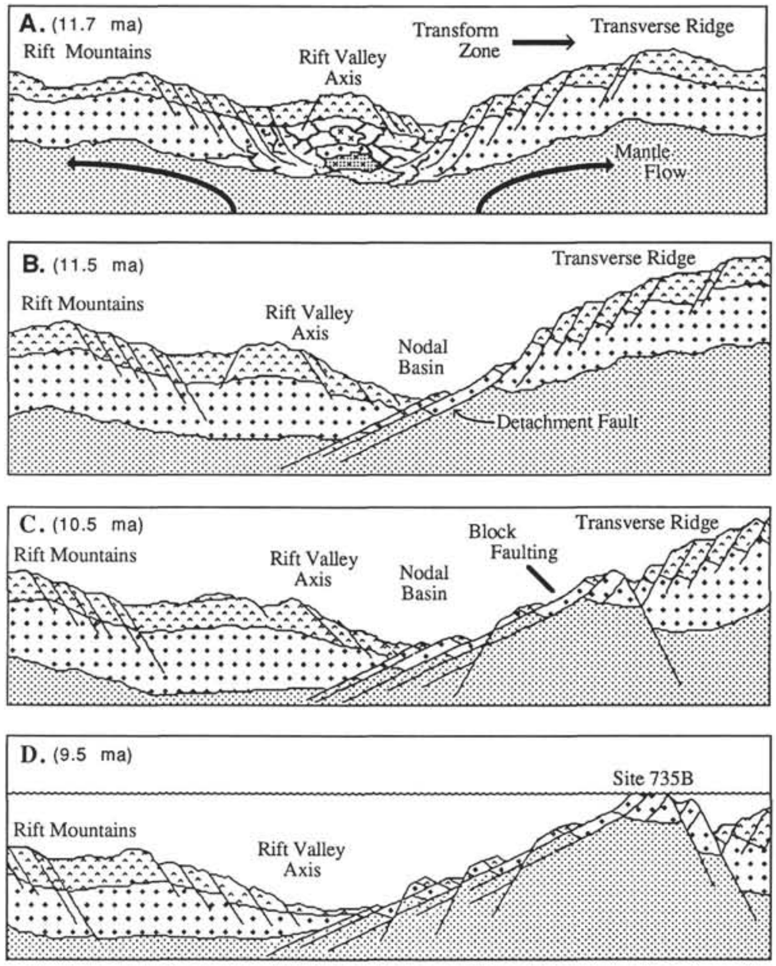

Figure 25. Temporal cross sections across the Southwest Indian Ridge rift valley drawn parallel to the spreading direction (not across the fracture zone, but parallel to it), showing the postulated tectonic evolution of the transverse ridge and Hole 735B (from Dick et al., this volume). The sequential sections are drawn at about 18 km from the transform fault. Crust spreading to the right passes into the transverse ridge and spreads parallel to the transform valley. Crust spreading to the left spreads into the rift mountains of the Southwest Indian Ridge parallel to the inactive extension of the Atlantis II Fracture Zone. **A.** Initial symmetric spreading, possibly at the end of a magmatic pulse: late magmatic brittle-ductile faulting occurs because of lithospheric necking above and in the vicinity of whatever passes for a magma chamber at these spreading rates. Hydrothermal alteration at high temperatures accompanies necking and ductile flow in subsolidus regions. **B.** At some point, the shallow crust is welded to the old, cold lithosphere to which the ridge axis abuts, causing formation of a detachment fault; and nodal basin: initiation of low-angle faulting, continued brittle-ductile faulting, and amphibolite-facies alteration of rocks drilled at Hole 735B. **C, D.** Block uplift of the rift mountains at the ridge-transform corner forms a transverse ridge enhanced by regional isostatic compensation of the local negative mass anomaly at the nodal basin. Initiation of the block uplift terminates the the extension driving cracking, and drastically reduces permeability in the Hole 735B rocks, effectively terminating most circulation of seawater and alteration. Greenschist-facies retrograde alteration continues along the faults on which the block is uplifted to account for the greenschist-facies alteration that predominates in dredged gabbros.

the formation of a relatively shallow detachment zone, where deeper, less viscous material might spread symmetrically, while the shallower rocks remained welded to the old plate. This might cause formation of a detachment fault above which the shallow levels of the crust should spread periodically away from the transform welded to the old lithosphere. The detachment fault might then locally expose the deep crust and shallow mantle, as shown in Figure 25. The effect should be greatest at the contact with the old lithospheric plate and should explain the formation of the nodal basin there.

The crustal weld should die away with distance from the ridge-transform intersection, and thus detachment faulting

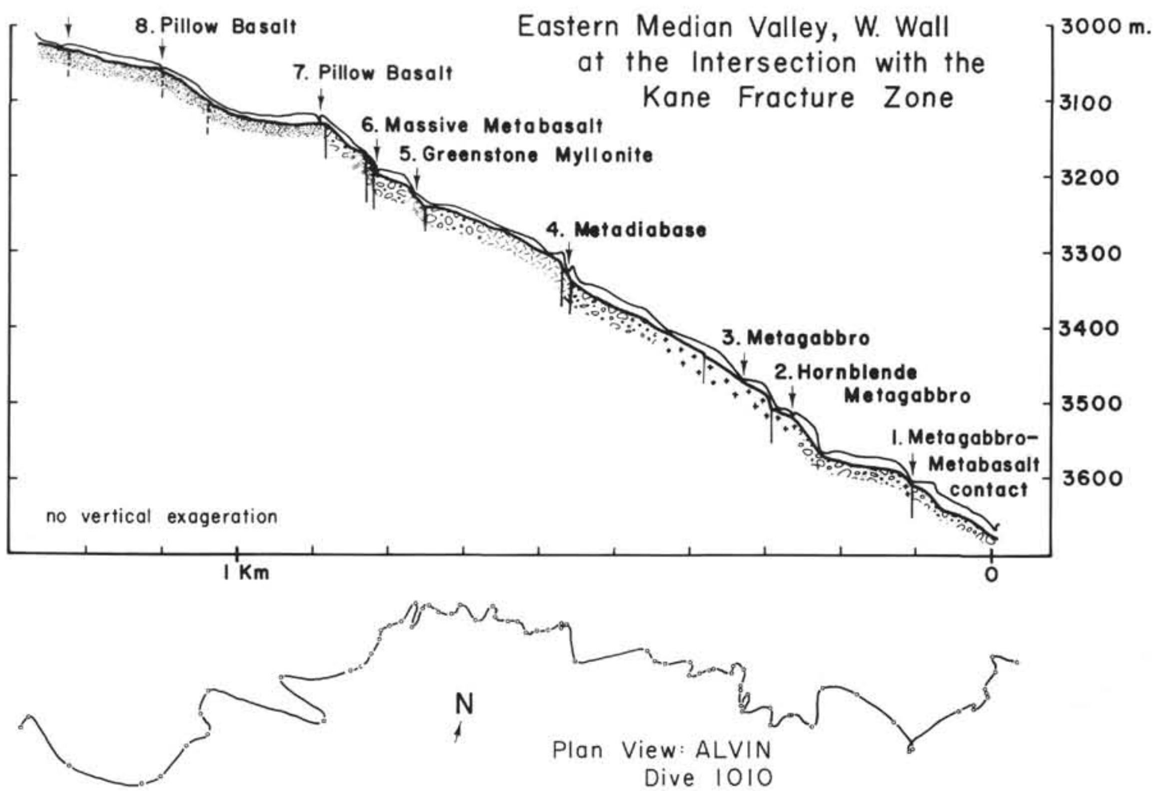

Figure 26. Cross section of the eastern rift valley wall of the Mid-Atlantic Ridge at its intersection with the Kane Fracture Zone transform valley (modified from Karson and Dick, 1983, and based on *Alvin* dive 1010). The cross section shows near-continuous outcrop and a slickensided dip-slip surface exposing gabbro anddiabase from station 2 to station 6, offset by small throw high-angle normal faults. The high-angle fuaults are associated with the uplift of the inside corner high into the transverse ridge, while the low-angle dip-slip surface represents the foot wall of the detachment fault on which the plutonic rocks were exposed.

should progressively expose shallower levels of the ocean crust with distance from the intersection. Subsequent uplift of such a section into a transverse ridge might then explain the pseudostratigraphic sections exposed on the walls of many transforms as a result of detachment faulting at the ridge-transform intersection that progressively exposed deeper levels of the crust and mantle near the plate boundary. As noted by Francheteau et al. (1976), simple normal faulting on the walls of transforms accompanying uplift is inadequate by itself to expose an entire crustal section because this mechanism requires fault throws of up to 6 km, where only much smaller fault throws have been documented.

The crucial aspect of this model is the existence of low-angle normal faults at ridge-transform intersections, as shown in Figure 25B. We point out that the dip of the predominant mylonitic foliation in Hole 735B is nearly 30°, and may have been produced by such faulting. Moreover, Dick et al. (1981) documented a 500-m-long, low-angle fault surface at the eastern Kane Fracture Zone ridge-transform intersection that lies in the slope of the hillside and that projects down the bounding wall of the nodal basin to beneath the adjacent neovolcanic zone (e.g., Fig. 26). Figure 25B was drawn on the basis of the Kane Fracture Zone results, because the eastern intersection of the Kane Fracture Zone and the northern ridge-transform intersection of the Atlantis II Fracture Zone are physiographically nearly identical. Because of a difference in interpretation among co-authors, this interpretation of a low-angle fault surface was not included by Karson and Dick (1983), but was presented separately by Dick et al. (1981).

The mechanism that forces the uplift of the great transverse ridges has been a long-standing puzzle. Initially, scientists thought that this uplift was isostatically driven because of the formation of a great mass of low-density serpentinite resulting from circulation of water into the mantle along the transform fault. Gravity studies of transverse ridges (Louden and Forsyth, 1982; Abrams et al., 1988) and the Atlantis II Fracture Zone (J. Snow et al., unpubl. data, 1990), however, have shown that these ridges are composed of relatively high-density material and are not locally isostatically compensated. Following several talks we previously presented (Dick et al., 1981, 1988), we postulate that some of the excess uplift along transverse ridges is produced as a result of uplift and crust-alflexure that accompanies regional isostatic compensation of the large, local, negative mass anomaly created by formation of the nodal basin at the ridge-transform intersection (Fig. 27). This should provide a neat explanation for why the highest density material is found on the crests of the highs along the transverse ridges and the lowest density material at the saddle points, because the excess uplift should only occur following the unroofing of deep levels of the crust and mantle.

In addition to the unroofing of the plutonic section and formation of the nodal basin (crustal dismemberment), other forces that created this local negative mass anomaly may include (1) viscous head loss in the ascending mantle near fracture zones (Sleep and Biehler, 1970); (2) the transform edge effect (e.g., Detrick and Purdy, 1980; Fox et al., 1979, Fox and Gallo, 1986), which causes preferential cooling of the asthenosphere underlying the ridge-transform intersection and

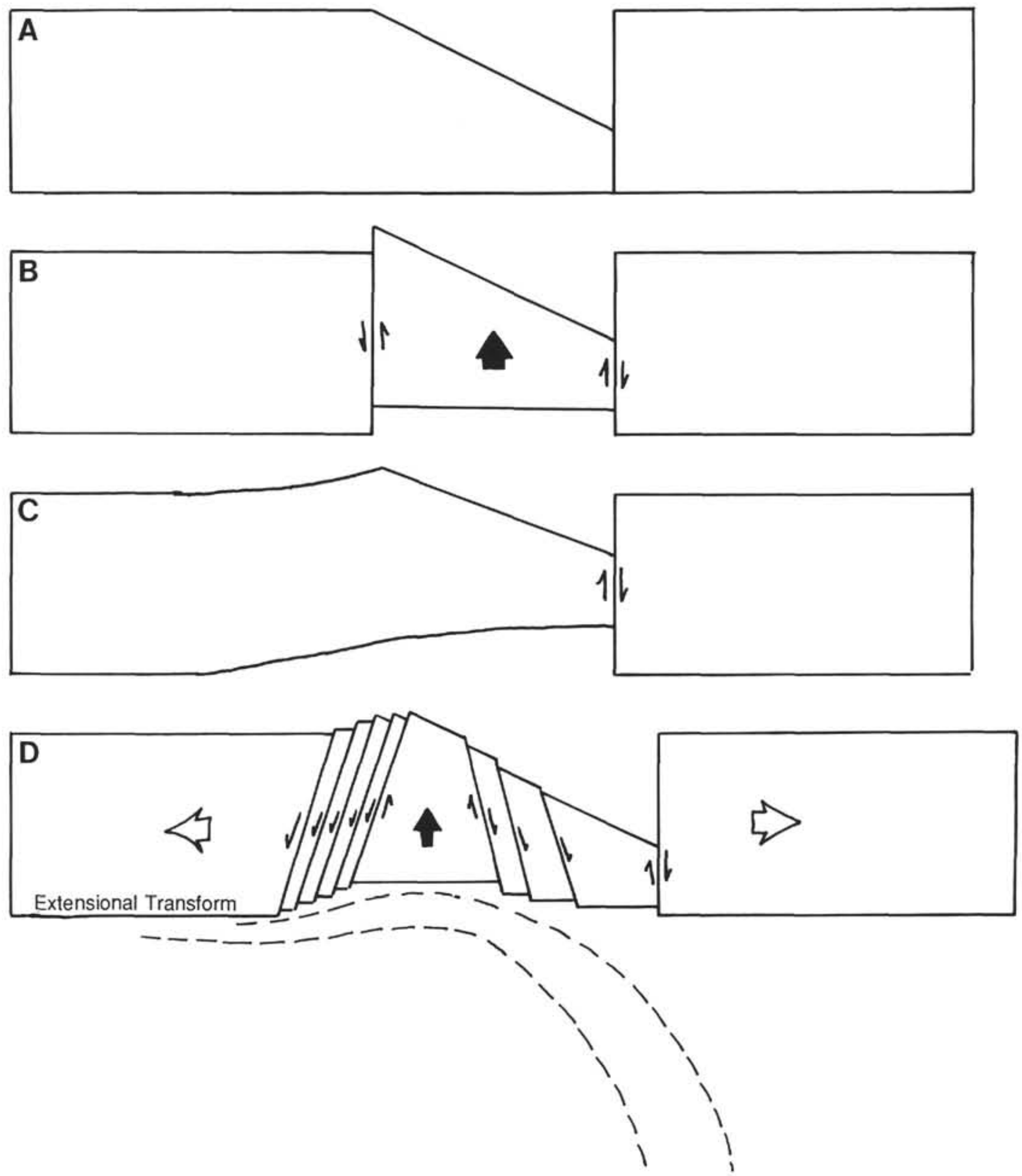

Figure 27. **A.** Simple block model drawn down the rift valley of a simplified ridge axis across the ridge-transform intersection and the old adjacent lithospheric plate showing excess crustal thinning as a result of formation of a nodal basin and an initially thinner crust near the transform fault. **B.** Simple block model for regional isostatic compensation of the negative mass anomaly shown in **A. C.** Flexural model for regional compensation of the negative mass anomaly shown in **A. D.** Combined flexure and block fault model for regional accommodation of the mass anomaly in **A**, where some component of extension across the fracture zone exists. Dashed lines are hypothetical isotherms.

contributes to a decrease in the magnetic budget and the creation of thinner crust; and (3) thinning of the crust at the distal end of a volcanic segment near a transform (Francheteau and Ballard, 1983; Dick, 1989).

These forces may reasonably account for excess uplift of up to 1 to 2 km, and are entirely adequate to explain the local relief along the crests of the transverse rdges. They are, however, insufficient to account for the up to 6 km of uplift required to form the transverse ridges as a whole, where high-density mantle peridotites are emplaced to water depths of less than 2 km. Some other dynamic force, as yet unidentified, will be required to explain this. The ocean crust east of Hole 735B appears to be anomalously deep when referenced to the age-depth curve. This suggests excess subsidence of the transverse ridge and crustal flexure to form a "moat" nearby. This and excess subsidence of the transverse ridge at the Vema Fracture Zone (Bonatti et al., 1983) strongly suggest formation of the ridge by dynamic forces at the ridge-transform intersection that placed an excess nonisotatic load on the lithosphere.

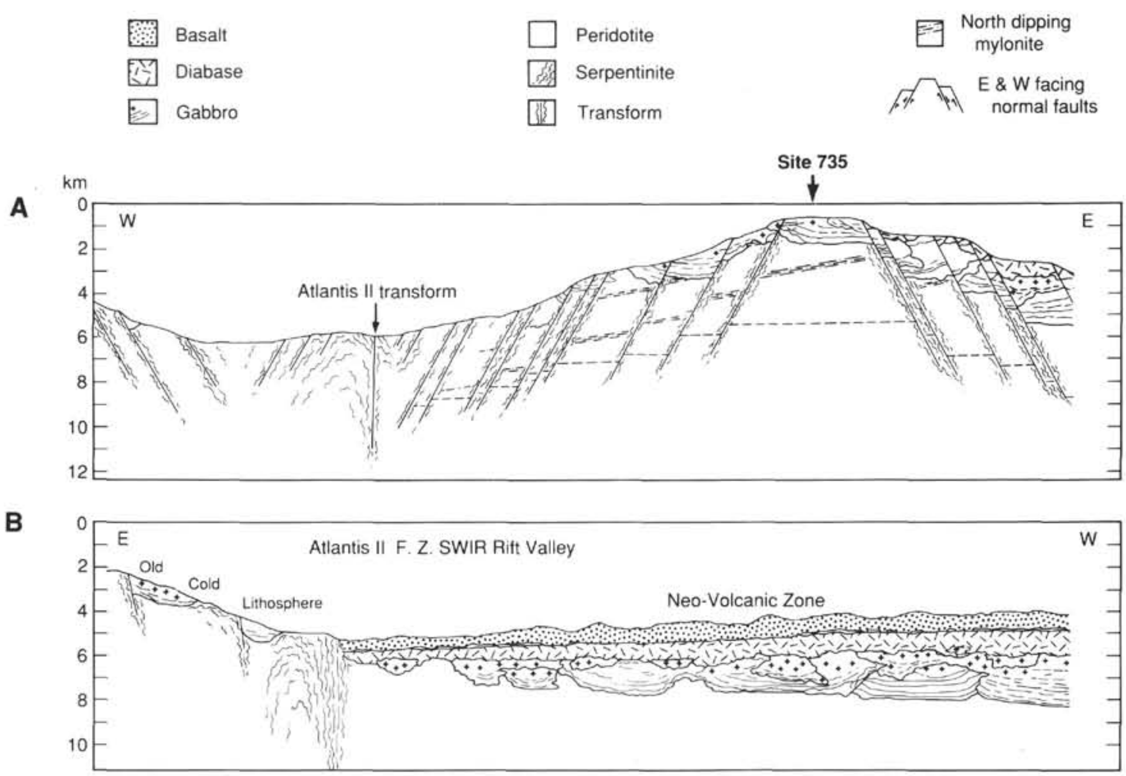

Figure 28. **A.** Balanced cross section drawn across the eastern transverse ridge at Site 735, with major normal faults inferred from major breaks in the slope of the transform wall. Lithologies inferred from scattered dredges and drilling. **B.** Bathymetric profile of the present-day southern Southwest Indian Ridge rift valley reversed for comparison to **A**. This profile is assumed here to represent the initial primary igneous stratigraphy and bathymetry for the section drawn in **A** prior to unroofing, uplift, and formation of the transverse ridge. Geologic section is inferred for a highly segmented ridge (based on Dick, 1989). Section **A** represents adjustment of this geology on the inferred fault sets and fitting of the present-day exposure of rocks on the transverse ridge.

Tectonic Setting of Site 735

Site 735 is located approximately 93 km south of today's axis of the Southwest Indian Ridge and 18.4 km from the inferred axis of transform faulting on the floor of the Atlantis II Fracture Zone. The site is situated on a shallow platform, informally named the Atlantis Bank, in about 700 m of water at the crest of the eastern wall of the Atlantis II Fracture Zone (Fig. 8). The platform, about 9 km long in a north-south direction and 4 km wide, is one of a series of elevated blocks that are connected by saddles to form a long, linear ridge parallel to the transform. An extensive 200- × 200-m borehole televiewer survey in the vicinity of the hole conducted from the *JOIDES Resolution* showed flat exposures of foliated and massive gabbro locally covered by sediment drifts. An inferred geologic cross section through the site and across the transform is shown in Figure 28, which can be compared to the simple block tectonic model (Fig. 27). The balanced section was drawn by assuming that the transform was still under extension at the time of uplift, using high-resolution SeaBeam bathymetry to infer the location of major fault sets; dredge results and drilling to infer a rough distribution of lithologies; and zero age bathymetry from the western rift valley to infer the initial pre-uplift conditions (inverted for comparison in Fig. 24B).

The strike of the foliation seen on the seafloor around Hole 735B appears to parallel the ridge axis to the north and orthogonal to the fracture zone in the televiewer survey. Some controversy about this exists, however, as attempts to orient foliated gabbros from the drill hole using magnetic inclination for obtaining paleonorth suggest oblique and even transform-parallel orientations for the strike of the foliation (Cannat and Pariso, this volume). However, we note that the orientation of the foliated peridotites exposed on St. Paul's Rocks is parallel to the Mid-Atlantic Ridge and orthogonal to St. Paul's Fracture Zone. St. Paul's Rocks is situated, with respect to St. Paul's Fracture Zone and the Mid-Atlantic Ridge, in a tectonic position identical to that of Hole 735B at the Atlantis II Fracture Zone. Tectonically, one can much easier explain the low-angle dipping foliations by ridge parallel and ridge oblique dip-slip faulting than by some unknown transform parallel mechanism. However, resolving this ambiguity is key to interpreting the results of drilling at Hole 735B and should be a principal objective of any future site survey in the region.

Given Hole 735B's position, the relatively constant spreading direction over the last 11 m.y., and the inferred strike of the foliated gabbros, it must represent crust formed beneath the median valley some 15 to 19 km away from the transform ridge intersection about 11 m.y. ago, which was subsequently uplifted 5 to 6 km into the transverse ridge (Fig. 26). Because the predicted segmentation length for a ridge spreading at less than 1 cm/yr is about 30 km (Schouten et al., 1985), the drilled section may represent the remains of a fossil magma chamber that was formed and unroofed near the midpoint of a volcanic segment by transform tectonics. Thus, the gabbros drilled in Hole 735B crystallized well away from the transform plate boundary, and its igneous stratigraphy probably represents what some have called "normal" ocean crust.

ACKNOWLEDGMENTS

We thank Captain Pat Roberge, the officers, and the crew of the *Conrad*, who performed superbly and made life enjoyable at sea. In addition, F. Beecher Wooding handled cruise preparation and deck operations at sea for the dredging program and was responsible for much of the curatorial work at sea. The success of the cruise greatly benefited from his participation. Linda Angeloni helped draft figures, manufactured thin sections, and aided in analyzing data. Jeff Fox provided considerable help, guidance, and patience as the principal reviewer of this manuscript, which was deeply appreciated by the authors.

REFERENCES

Abrams, L. J., Detrick, R. S., and Fox, P. J., 1988. Morphology and crustal structure of the Kane Fracture Zone transverse ridge. *J. Geophys. Res.*, 93:3195–210.

Atwater, T. M., and Mudie, J. D., 1968. Block faulting on the Gorda Rise. *Science*, 159:729.

Auzende, J.-M., Bideau, D. Bonatti, E., Cannat, M., Honnorez, J., Lagabrielle, Y., Malavieille, J., Mamaloukas-Frangoulis, V., and Mével, C., 1990. The MAR-Vema Fracture Zone intersection surveyed by deep submersible *Nautile*. *Terra Nova*, 2:68–73.

Ballard, R. D., and van Andel, Tj.H., 1977. Project FAMOUS: morphology and tectonics of the inner-rift valley at 36°50′N on the Mid-Atlantic Ridge. *Geol. Soc. Am. Bull.*, 88:507–530.

Bonatti, E., and Honnorez, J., 1976. Sections of the Earth's crust in the equatorial Atlantic. *J. Geophys. Res.*, 81:4104–4116.

Bonatti, E., Sartori, R., and Boersma, A. 1983. Vertical crustal movements at the Vema Fracture Zone in the Atlantic:Evidence from dredged limestones. *Tectonophysics*, 91:213–232.

Collete, B. J., 1986. Fracture zones in the North Atlantic: morphology and a model. *J. Geol. Soc. London*, 143:763–774.

Delong, S. E., Dewey, J. F., and Fox, P. J., 1977. Displacement history of oceanic fracture zones. *Geology*, 5:199–202.

Detrick, R. S., and Purdy, G. M., 1980. The crustal structure of the Kane Fracture Zone from seismic refraction studies. *J. Geophys. Res.*, 85:3759–3777.

Dick, H.J.B., 1989. Abyssal peridotites, very slow spreading ridges, and ocean ridge magmatism. *In* Saunders, A. D., and Norry, M. J. (Eds.), *Magmatism in the Ocean Basins*. Geol. Soc. London, Spec. Publ., 42:71–105.

Dick, H.J.B., Bryan, W. B., and Thompson, G., 1981. Low-angle faulting and steady-state emplacement of plutonic rocks at ridge-transform intersections. *EOS, Trans. Am. Geophys. Union*, 62:406.

Dick, H.J.B., Fisher, R. L., and Bryan, W. B., 1984. Mineralogic variability of the upper most mantle along mid-ocean ridges. *Earth Planet. Sci. Lett.*, 69:88–106.

Dick, H.J.B., Kirby, S. H., Cannat, M., and Leg 118 Scientific Party, 1988. Tectonic evolution of a half kilometer section of layer 3 drilled near the Atlantis II Fracture Zone. *EOS, Trans. Am. Geophys. Union, 69:305*.

Engel, C. G., and Fisher, R. L., 1975. Granitic to ultramafic rock complexes of the Indian Ocean ridge system, western Indian Ocean. *Geol. Soc. Am. Bull.*, 86:1553–1578.

Fisher, R. L., Dick, H.J.B., Natland, J. H., and Meyer, P. S., 1986. Mafic/ultramafic suites of the slowly spreading Southwest Indian Ridge: PROTEA exploration of the Antarctic Plate boundary, 24°E–47°E. *Ofioliti*, 11:147–178.

Fisher, R. L., and Sclater, J. G., 1983. Tectonic evolution of the Southwest Indian Ocean since the Mid-Cretaceous: plate motions and stability of the pole of Antarctica/Africa for at least 80 myr. *Geophys. J. R. Astron. Soc.*, 73:553–576.

Fox, P. J., and Gallo, D. G., 1984. A tectonic model for ridge-transform ridge plate boundaries: implications for the structure of oceanic lithosphere. *Tectonophysics*, 104:205–242.

———, 1989. Transforms of the eastern central Pacific. *In* Winterer, E. L., Hussong, D. M., and Decker, R. W. (Eds.), IThe Geology of North America: Eastern Pacific Ocean and Hawaii, Vol. N: Boulder CO (Geol. Soc. Am.), 111–124.

———, 1986. The geology of the North Atlantic transform/plate boundaries and their aseismic extensions. *In* Tucholke, B. E., and Vogt, P. R. (Eds.), *The Geology of North America: The Western North Atlantic Region*, Vol. M: Boulder CO (Geol. Soc. Am.), 157–172.

Francheteau, J., and Ballard, R. D., 1983. The East Pacific Rise near 21°N, 13°N, and 20°S: inferences for along-strike variability of axial processes of the mid-ocean ridge. *Earth Planet. Sci. Lett.*, 64:93–116.

Francheteau, J., Choukroune, P., Hekinian, R., Le Pichon, X., and Needham, H. D., 1976. Oceanic fractures do not provide deep sections in the crust. *Can. J. Earth Sci.*, 13:1223–1235.

Gallo, D. G., Fox, P. J., Madsen, J. A., Macdonald, K. C., and Forsyth, D. W., 1986,. Fast-slipping ridge-transform intersections: morphotectonic evidence for thermal rejuvenation of old lithosphere by ridge axis processes. *EOS, Trans. Am. Geophys. Union*, 66:1092.

Gronvold, K., 1988. Krafla lavas and lava composition within a fault swarm. *Symp. Geol. Geochem. Evidence for Segmentation of Continental and Oceanic Rifts*: Woods Hole (Woods Hole Oceanographic Inst.), 17.

Hamelin, B., and Allegre, C. J., 1985. Large-Scale regional units in the depleted upper mantle revealed by an isotopic study of the Southwest Indian Ridge. *Nature*, 315:196–199.

Johnson, K.T.M., Dick, H.J.B., and Shimizu, N., 1990. Melting in the oceanic upper mantle: an ion microprobe study of diopside in abyssal peridotites. *J. Geophys. Res.*, 95:2661–2678.

Karson, J. A., Thompson, G., Humphris, S. E., Edmond, J. M., Bryan, W. B., Brown, J. R., Winters, A. T., Pockalny, R. A., Casey, J. F., Campbell, A. C., Klinkhammer, G., Palmer, M. R., Kinzler, R. J., and Sulanowska, M. M., 1987. Along-axis variations in seafloor spreading in the MARK area. *Nature*, 328:681–685.

Karson, J. A., and Dick, H.J.B., 1983. Tectonics of ridge-transform intersections at the Kane fracture zone. *Mar. Geophys. Res.*, 6:51–98.

———, 1984. Deformed and metamorphosed oceanic crust on the Mid-Atlantic Ridge. *Ofioliti*, 9:279–302.

Kent, D. V., Honnorez, B. M., Opdyke, N. D., and Fox, P. J., 1978. Magnetic properties of dredged oceanic gabbros and the source of marine magnetic anomalies. *Geophys. J. R. Astron. Soc.*, 55:513–537.

Kent, D. V., and Gradstein, F. M., 1986. A Jurassic to recent chronology. *In* Tucholke, B. E., and Vogt, P. R. (Eds.), *The Geology of North America: The Western North Atlantic Region*, Vol. N: Boulder, CO (Geol. Soc. Am.), 45–50.

Klein, E., and Langmuir, C. H., 1987. Global correlations of ocean ridge basalt chemistry with axial depth and crustal thickness. *J. Geophys. Res.*, 92:8089–8115.

le Roex, A. P., Dick, H.J.B., Erlank, A. J., Reid, M., Frey F. A., and Hart, S. R., 1983. Geochemistry, mineralogy and petrogenesis of lavas erupted along the Southwest Indian Ridge between the Bouvet Triple Junction and 11°E. *J. Petrol.*, 24:267–318.

Louden, K. E., and Forsyth, D. W., 1982. Crustal structure and isostatic compensation near the Kane Fracture Zone from topography and gravity measurements: I. Spectral analysis approach. *Geophys. J. R. Astron. Soc.*, 68:725–750.

Macdonald, A. H., and Fyfe, W. S., 1985. Rate of serpentinization in seafloor environments. *Tectonophysics*, 116:123–135.

Macdonald, K. C., 1977. Near-bottom magnetic anomalies, asymmetric spreading, oblique spreading, and tectonics of the Mid-Atlantic Ridge near 3°N. *Geol. Soc. Am. Bull.*, 88:541–555.

Macdonald, K. C., and Atwater, T. M., 1978. Evolution of rifted ocean ridges. *Earth Planet. Sci. Lett.*, 39:319–327.

Macdonald, K. C., Castillo, D. A., Miller, S. P., Fox, P. J., Kastens, K. A., and Bonatti, E., 1986. Deep tow studies of the Vema Fracture Zone 1. Tectonics of a major slow slipping transform fault and its intersection with the Mid-Atlantic Ridge. *J. Geophys. Res.*, 91:3334–3354.

McKenzie, D., 1984. The generation and compaction of partially molten rock. *J. Petrol.*, 25:713–765.

Menard, H. W., and Atwater, T., 1968. Changes in the direction of seafloor spreading. *Nature*, 219:463–467.

Mutter, J. C., and North Atlantic Transect Study Group, 1985. Multichannel seismic images of the oceanic crust's internal structure: evidence for a magma chamber beneath the mesozoic Mid-Atlantic Ridge. *Geology*, 13:629–632.

Norton, I. O., and Sclater, J. G., 1979. A model for the evolution of the Indian Ocean and the break-up of Gondwanaland. *J. Geophys. Res.*, 84:6803–6830.

O'Hara, M. J., 1968. Are any ocean floor basalts primary magma? *Nature*, 220:683–686.

OTTER, 1984. The geology of the Oceanographer Transform: the ridge-transform intersection. *Mar. Geophys. Res.*, 6:109–141.

———, 1985. The geology of the Oceanographer Transform: the transform domain. *Mar. Geophys. Res.*, 7:329–358.

Parmentier, E. M., and Forsyth, D. W., 1985. Three-dimensional flow beneath a slow-spreading ridge axis: a dynamic contribution to the deepening of the median valley toward fracture zones. *J. Geophys. Res.*, 90:678–684.

Patriat, P., 1986. *Réconstitution de l'évolution du systeme de dorsales de l'ocean Indien par les methodes de la Cinematique des Plaques. Territoire des Terres Australes et Antarctiques Françaises, Mission de Récherche:* Paris (Inst. de Physique du Globe).

Pockalny, R. A., Detrick, R. S., and Fox, P. J., 1988. The morphology and tectonics of the Kane Transform from SeaBeam bathymetric data. *J. Geophys. Res.*, 93:3179–3194.

Reid, I., and Jackson, H. R., 1981. Oceanic spreading rate and crustal thickness. *Mar. Geophys. Res.*, 5:165–172.

Roest, W. R., and Collette, B. J., 1986. The Fifteen Twenty Fracture Zone and the North American-South American plate boundary. *J. Geol. Soc. (London)*, 143:833–843.

Rowlett, H., and Forsyth, D. W., 1984. Recent faulting and microearthquakes at the intersection of the Vema Fracture Zone and the Mid-Atlantic Ridge. *J. Geophys. Res.*, 6:143–158.

Ryan, M. P., 1987. The elasticity and contractancy of Hawaiian olivine tholeiite and its role in the stability and structural evolution of subcaldera magma reservoirs and rift systems. *U.S. Geol. Surv. Prof. Pap.*, 1350(2):1395–1447.

Schouten, H., Klitgord, K. D., and Whitehead, J. A., 1985. Segmentation of mid-ocean ridges. *Nature*, 317:225–229.

Schouten, H., Dick, H.J.B., and Klitgord, K. D., 1987. Migration of mid-ocean-ridge volcanic segments. *Nature*, 326:835–839.

Sclater, J. G., Fisher, R. L., Patriat, P., Tapscott C., and Parsons, B., 1981. Eocene to recent development of the Southwest Indian Ridge, a consequence of the evolution of the Indian Ocean Triple Junction. *Geophys. J. R. Astron. Soc.*, 64:587–604.

Sclater, J. G., Dick, H.J.B., Norton, I. O., and Woodroffe, D., 1978. Tectonic structure and petrology of the Antarctic Plate boundary near the Bouvet Triple Junction. *Earth Planet. Sci. Lett.*, 37:393–400.

Searle, R. C., and Laughton, A. S., 1977. Sonar studies of the Mid-Atlantic Ridge and Kurchatov Fracture Zone. *J. Geophys. Res.*, 82:5313–5328.

Severinghaus, J. P., and Macdonald, K. C., 1988. High inside corners at ridge transform intersections. *Mar. Geophys. Res.*, 9:357–367.

Sleep, N., and Biehler, S., 1970. Topography and tectonics at the intersection of fracture zones with central rifts. *J. Geophys. Res.*, 75:2748–2752.

Snow, J., Dick, H.J.B., and Hart, S. R., 1987. Preliminary results from a transform volcano, Atlantis II Fracture Zone, Southwest Indian Ridge. *EOS, Trans. Am. Geophs. Union*, 68:408.

Solomon, S. C., 1989. Just how do ocean ridges vary? Characteristics and population statistics of ocean ridges. *In Drilling the Oceanic Lower Crust and Mantle:* Woods Hole (Woods Hole Oceanographic Institution), 89-39:73–74.

Tapscott, C. R., Patriat, P., Fisher, R. L., Sclater, J. G., Hoskins H., and Parsons, B., 1980. The Indian Ocean Triple Junction. *J. Geophys. Res.*, 85:4723–4739.

Tiezzi, L. J., and Scott, R. B., 1980. Crystal fractionation in a cumulate gabbro, Mid-Atlantic Ridge, 26°N. *J. Geophys. Res.*, 85:5438–5454.

Tucholke, B. E., and Schouten, H., 1988. Kane Fracture Zone. *Mar. Geophys. Res.*, 10:1–39.

van Andel, Tj.H., Von Herzen, R. P., and Phillips, J. D., 1971. The Vema Fracture Zone and the tectonics of transverse shear zones in oceanic crustal plates. *Mar. Geophys. Res.*, 1:261–283.

Whitehead, J. A., Dick, H.J.B., and Schouten, H., 1984. A mechanism for magmatic accretion under spreading centers. *Nature*, 312:46–148.

Williams, C. A., Louden, K. E., and Tanner, S. J., 1984. The western instersection of Oceanographcer Fracture Zone and the Mid-Atlantic Ridge. *J. Geophys. Res.*, 6:143–158.

Wolfe, E. W., 1988. The Puu Oo eruption of Kilauea: magma transport, storage, differentiation, and eruption in a Hawaiian shield volcano. *Trans., Symp. Geol. Geochem. Evidence for Segmentation of Continental and Oceanic Rifts:* Woods Hole (Woods Hole Oceanographic Institution), 40.

Date of initial receipt: 31 August 1990
Date of acceptance: 14 September 1990
Ms 118B-156